

# **Functional Characterization of Microtubule Associated Proteins in ES Cell Division and Neuronal Differentiation**

**Dissertation**

**zur Erlangung des akademischen Grades**

**Doctor of Philosophy  
(Ph.D.)**

**vorgelegt**

**der Fakultät Mathematik und Naturwissenschaften  
der Technischen Universität Dresden**

**von  
Özlem Demir, MSc.**

**geboren am 11.06.1982 in Istanbul, Türkei**

**Angabe Datum: 30.09.2014**

**Tag der Verteidigung: 02.02.2015**

**Gutachter: Prof.Dr. Jonathon Howard  
Prof.Dr. Francis Stewart**

Die Dissertation wurde in der Zeit von September 2010 bis September 2014 am  
Max-Planck-Institut für Molekulare Zellbiologie und Genetik angefertigt.

# ABSTRACT

Microtubules are tubular polymers that are involved in a variety of cellular processes such as cell movement, mitosis and intracellular transport. The dynamic behavior of microtubules makes this possible because all of these processes require quick responses. Embryonic stem (ES) cells were first isolated from mouse embryos and they have two unique characteristics; they can be kept undifferentiated for many passages with a stable karyotype and they can be differentiated into any type of cells under appropriate conditions. The pluripotency of ES cells, their ease of manipulation in culture, and their ability to contribute to the mouse germ-line provides us a model of differentiation both in vitro and in vivo. In my thesis I focused on the cell division and neuronal differentiation of ES cells and developed two methods to understand the effects of microtubule dynamics in spindle assembly and chromosome segregation and to reveal the roles of different Microtubule Associated Proteins (MAPs) in the neuronal morphology formation.

In the first part, we developed a live-cell imaging method for ES cells to visualize, track and analyze the single cell behavior in a cell population over a time period. So far many techniques have been adapted and combined for imaging of cell lines, mainly for the cancer or immortalized ones. However, because ES cells are very prone to apoptosis, tend to form spheres and hard to stably label, it is quite tricky to image them in culture conditions. In our system, we combined the BAC-based gene expression with wide-field deconvolution microscopy for ES cells that are plated onto the laminin-511 coated surface and kept in CO<sub>2</sub> independent culture conditions. This combined technique does not interfere with the growth of cells and keeps them healthy up to 24 hours on the microscope stage.

In the second part, we analyzed the effects of MAPs chTOG, EB1, Kif18A and MCAK in the overall spindle morphology and mitotic progression in mES cells. For this purpose, we utilized our stable TUBB-GFP and H2A-GFP cell lines along with our live-cell imaging set-up to reveal the effects of the above-mentioned proteins and the interplay among each other. By using RNAi method we either

single or co-depleted the genes by siRNAs and measured the spindle length and width in RNAi conditions. We further analyzed the mitotic progression in H2A-GFP cell line in terms of the metaphase timing and the percentage of chromosome segregation errors. Our results showed that, EB1 depletion did not cause any significant changes in the overall spindle morphology or in the metaphase timing. However, the co-depletion of EB1 with chTOG partially rescued the sichTOG specific mini-spindle phenotype. siKif18A produced longer spindles without any change in the spindle width. Surprisingly, the co-depletion of antagonistic chTOG and Kif18A proteins had additive effects on the spindle dynamics and on mitotic progression in a way that spindle assembly was severely disrupted by the absence of these two proteins and as a result of this, both metaphase timing and chromosome missegregation levels increased significantly. These results overall indicate that MAPs have important roles in the regulation of dynamic instability and these proteins have an interplay among each other to be able to control the morphology of the spindle as well as the correct segregation of chromosomes into daughter cells.

In the last part, I will introduce you a new ES cell based differentiation and morphology model, which brings the advantages of high resolution imaging capacity, control over development and easy genetic manipulation and culturing. We have generated Tet-induced shRNA cell lines against chTOG, Kif18A and MCAK, which are also stably expressing TUBB-GFP. These labeled cells were mixed with unlabeled wild-type mES cells before differentiation at 1:1000 ratio and then they were differentiated into mouse cortical cells and spinal motor neurons. Our results showed that, all of the three genes could be successfully knocked-down by shRNA after 48 hours of Tet induction. After mixing the labeled and unlabeled cells, single neurons could be imaged at high resolution and their skeletons could be generated afterwards. The RNAi studies in shchTOG cell line showed that, the knock-down of this gene in early differentiation interferes with the neuronal differentiation.

# ACKNOWLEDGEMENTS

After 28 years of living and studying in the same city, coming to Dresden was a real adventure for me and many people deserve a thank-you for making this adventure meaningful. First of all, I would like to express my deepest appreciation to Joe for accepting me to his lab and to make start this amazing experience. I thank my TAC members Tony Hyman, Elly Tanaka and Federico Calegari for their guidance's and precious comments on the project.

I would like to thank my doctorate committee members, Prof.Dr. Jonathon Howard, Prof.Dr. Francis Stewart, Prof.Dr Rolf Jessberger, Prof.Dr. Gerhard Roedel and Prof.Dr. Anthony Hyman for reviewing my thesis and examining me.

I would like to thank all the past and present members of the Howard Lab and our lovely secretary Antje. There was a very high level of intellectual environment in the lab and this really led to the development of very interesting and new ideas. I want to especially thank Xin Liang, Sujoy Ganguly and Hugo Bowne-Anderson for our Neuron Club and sharing their ideas about the project. A big thanks goes to Ina Poser for ES cell lines and BAC constructs and for her advices and helps on the BACs, ES cells and imaging, basically everything. I would be really in trouble without her trouble shootings. I am very grateful to Heike, Marit and Andrea for keeping everything running in labs. I thank Horatiu Fantana, Alex Bird, Amr-El-Labban and Yusuke Toyoda for sharing their ideas about the spindle project. I thank our LMF facility and especially Dan White for introducing me into microscopy. And finally thanks to Nicolas Berger for his helps in the ES cell culture. Without the helps and guidances of our PhD office, this period would be really very hard. I want to thank Dr. Birgit Knepper-Nicolai and all of the members of the PhD office for their amazing job.

I want to also thank my summer student Zivojin Jevtic for his helps to the project and friendship outside. Our cultural exchange during his stay in Dresden was really very funny.

For the non-scientific part of Dresden, there are too many people to. Here I have found the chance of going back to the old days with our Dance Anatolia team. I want to thank our teachers Oya and Faikcan for their efforts and for putting the spirit of dance into us and our team Turkay, Ahu, Ali, Zeynep, Zeliha, Muge, Fatih, Aytac, Baris, Katrin and Sabine for all those funny moments during trainings and shows and for their friendship outside as well.

I want to thank Cidem Abla and the Seremet family, Aylin, Cagdas, Aslihan, Huseyin, Sibel, Ozgun and Berat for their friendships.

The best side (and probably the only one) of Joe's move to Yale was the entrance of Baran to my life. I want thank him for being an amazing friend, for all those dinners, drinks, trips, photo sessions and heart-to-heart talks. As I have always said, Dresden is especially beautiful with you. Thank you for all...

I want to thank old and new crews of Macsiki. First of all, Pekiner brothers Aydin and Gokmen, were really like my older brothers here. In my every problem, they were the first doors that I have knocked. I really appreciate them and want to thank them for their helps and understandings. Ahmet was the hero of my thesis-writing period. Without his joyful chats and delicious food, I could not find the energy to move my fingers. I really thank him for all.

There were also out-of-Dresden heroes of this PhD period. I want to thank Melis, Seda, Burcu, Basak, Oya, Unal, Ugur and my dear professor Isil Kurnaz, for their trust and continuous support on me.

Ve son olarak tum aileme desteklerinden ve sabirlerinden oturu tesekkur etmek istiyorum. Aramizdaki 2000 km'ye ragmen kalplerinin benim icin attigini ve her zaman yanimda olduklarini hissettirdikleri icin...

This study was supported by FP7-Mitosys Grant and Max Planck Society.

Ozlem Demir, Dresden 2014

# CONTENTS

<b>1. Theoretical Background</b> .....	<b>1</b>
<b>Microtubule Structure</b> .....	<b>1</b>
<b>Dynamic Instability and Control of Length</b> .....	<b>2</b>
<b>Microtubule Nucleation</b> .....	<b>4</b>
<b>Post-translational Modifications on Tubulin</b> .....	<b>5</b>
<b>Microtubule (+) end Tracking Proteins</b> .....	<b>6</b>
CLIP Family.....	7
EB Family.....	7
CLASP Family.....	9
<b>Microtubule Disassembling Proteins</b> .....	<b>10</b>
Kinesin-13 Family.....	11
Kinesin-8 Family.....	12
<b>Microtubule Assembling Proteins</b> .....	<b>13</b>
TOG Family.....	13
<b>2. Materials and Methods</b> .....	<b>15</b>
<b>Methods</b> .....	<b>15</b>
Mouse Embryonic Stem Cell Culture.....	15
Cell Counting.....	15
Freezing of ESC.....	16
Thawing of ESC.....	16
BAC TransgeneOmics.....	16
BAC DNA Isolation.....	17
Cloning of shRNA plasmids.....	17
Generation of Stable mES Cell Lines.....	18
Immunofluorescence Staining.....	19
Preparation of Protein Lysates.....	20
Western Blot Analysis.....	20
Live Cell Imaging.....	21
RNA Interference.....	22
Differentiation of mES Cells into Spinal Motor Neurons.....	22
Generation of Cortical Neurons from mES cells.....	24
<b>Materials</b> .....	<b>25</b>
Solutions.....	27

<b>3. Live-Cell Imaging of Mouse ES Cells.....</b>	<b>28</b>
<b>Introduction.....</b>	<b>29</b>
<b>Results.....</b>	<b>35</b>
<b>Discussion.....</b>	<b>43</b>
<b>4. Effects of MAPs in the ES Cell Spindle Assembly and Mitotic Progression .....</b>	<b>47</b>
<b>Introduction.....</b>	<b>48</b>
<b>Results.....</b>	<b>51</b>
<b>Discussion.....</b>	<b>65</b>
<b>5. Generation of an ES Cell Model to Study the Spatio-temporal Determinants of Neuronal Morphology.....</b>	<b>70</b>
<b>Introduction.....</b>	<b>71</b>
<b>Results.....</b>	<b>74</b>
<b>Discussion.....</b>	<b>81</b>
<b>6. Summary.....</b>	<b>84</b>
<b>7. Bibliography.....</b>	<b>86</b>

# LIST OF FIGURES

<b>Figure 1.1:</b> Dynamic instability of microtubules.....	<b>3</b>
<b>Figure 1.2:</b> Structures of +end tip tracking proteins.....	<b>10</b>
<b>Figure 3.1:</b> The procedure of BAC recombineering.....	<b>33</b>
<b>Figure 3.2:</b> Western Blotting controls.....	<b>36</b>
<b>Figure 3.3:</b> The localization of chTOG-GFP in mitosis.....	<b>37</b>
<b>Figure 3.4:</b> The localization of Kif18A-GFP.....	<b>38</b>
<b>Figure 3.5:</b> The live-cell imaging of chTOG-GFP cell line.....	<b>38</b>
<b>Figure 3.6:</b> The live-cell imaging of Kif18A-GFP cell line.....	<b>39</b>
<b>Figure 3.7:</b> Short-term live-cell imaging of TUBB-GFP&H2A-mCherry mES cell line.....	<b>41</b>
<b>Figure 3.8:</b> Long-term imaging of TUBB-GFP and H2A-mCherry cell line at early (5) and late (15) passages.....	<b>42</b>
<b>Figure 4.1:</b> Different microtubule populations in spindle.....	<b>49</b>
<b>Figure 4.2:</b> Spindle length sizes in different cell types.....	<b>50</b>
<b>Figure 4.3:</b> RNAi knockdown of chTOG, Kif18A, MCAK and EB1 genes.....	<b>51</b>
<b>Figure 4.4:</b> Spindle morphologies after single and double gene knock-downs.....	<b>53</b>
<b>Figure 4.5:</b> Spindle length (L) and width (W).....	<b>54</b>
<b>Figure 4.6:</b> Changes in the spindle length after gene knock-downs.....	<b>56</b>
<b>Figure 4.7:</b> Spindle assembly defects in sichTOG_siKif18A cells.....	<b>57</b>
<b>Figure 4.8:</b> Spindle width after gene knockdowns.....	<b>59</b>
<b>Figure 4.9:</b> Aspect ratio of ES cells after RNAi treatment.....	<b>60</b>
<b>Figure 4.10:</b> Metaphase alignment time between NEBD and Anaphase-onset.....	<b>62</b>
<b>Figure 4.11:</b> Lagging chromosomes and chromosome bridge errors in cell division.....	<b>63</b>
<b>Figure 4.12:</b> Percentage of chromosome segregation errors in ES cells after RNAi treatment.....	<b>64</b>
<b>Figure 5.1:</b> Stages of polarization in neuron cultures.....	<b>72</b>
<b>Figure 5.2:</b> The Tet-inducible gene expression system.....	<b>75</b>
<b>Figure 5.3:</b> The control of Tet-R expression in different stable clones.....	<b>76</b>
<b>Figure 5.4:</b> The depletion of MAPs in stable cell lines after Tet-induction.....	<b>77</b>
<b>Figure 5.5:</b> The specificity of GFP and Tau markers.....	<b>78</b>
<b>Figure 5.6:</b> The cellular morphology of cortical neurons.....	<b>78</b>
<b>Figure 5.7:</b> The dendritic morphology of SMNs.....	<b>79</b>
<b>Figure 5.8:</b> Depletion of chTOG impairs the neuronal differentiation.....	<b>80</b>



# LIST OF TABLES

<b>Table 2.1:</b> Antibody list used in immunofluorescence stainings.....	<b>20</b>
<b>Table 2.2:</b> Antibody list used in Western Blotting analysis.....	<b>21</b>

# ABBREVIATIONS

ADFNK	Advanced DMEM/F12 and Neurobasal medium
ANOVA	Analysis of Variation
APC	Adenomatous polyposis coli
ATP	Adenosinetriphosphate
BAC	Bacterial Artificial Chromosome
BDNF	Brain Derived Neurotrophic factor
BSA	Bovine Serum Albumin
CAP-Gly	Cytoskeleton-associated protein-glycine-rich
CBA	Chicken Beta Actin
chTOG	Colonic and hepatic tumor over-expressed gene
CLASP	Cytoplasmic linker associated protein
CLIP	CAP-GLY domain containing linker protein
CMV	CytoMegalovirus
CTT	C-terminal tail
DAPI	4',6-diamidino-2-phenylindole
DDM	Default defined medium
DMEM	Dulbecco's Modified Eagle's medium
DMSO	Dimethyl sulfoxide
EB	Embryoid Body
EB1	End Binding1
ECL	Enhanced Chemiluminescence
EF1	Elongation Factor 1
FBS	Fetal Bovine Serum
GDP	Guanosinediphosphate
GDNF	Glial Derived Neurotrophic Factor
GFP	Green Fluorescent Protein
GTP	Guanosinetriphosphate
HEPES	(4-(2-hydroxyethyl)-1-piperazineethanesulfonic acid)
ICM	Inner Cell Mass
LAP	Localization and Affinity Purification

LIF	Leukemia Inhibitory Factor
MAP	Microtubule Associated Protein
MCAK	Mitotic Centromere Associated Protein
MOPS	3-(N-morpholino) propanesulfonic acid
MT	Microtubule
MTOC	Microtubule Organizing Center
NEAA	Non Essential Amino Acids
NEB	Nuclear Envelope Breakdown
PBS	Phosphate Buffered saline
PC12	PheochromaCytoma12
PCR	Polymerase Chain Reaction
PTM	Post-Translational Modification
RA	Retinoic Acid
RIPA	Radioimmunoprecipitation assay buffer
SAC	Spindle Assembly Checkpoint
Shh	Sonic Hedgehog
shRNA	Short Hairpin RNA
SMN	Spinal Motor Neuron
TBR1	T-box brain protein 1
TIP	Tip Interacting Protein
TOG	Tumor Overexpressed Gene
TUBB	Tubulin Beta
XMAP215	Xenopus Micotubule Associated Protein 215

# 1. Theoretical Background

Microtubules are tubular polymers that are necessary for a variety of cellular processes such as cell movement, mitosis and intracellular transport. The dynamic behavior of microtubules makes this possible because all of these processes require quick responses. Together with actin and intermediate filaments, they form the cytoskeleton of the cell. Their major function in the cell is to give a mechanical support to the cell's cytoplasm. Microtubules are the basic structural components of the transport of organelles and vesicles by serving as a road for dynein and kinesin motors. And they generate the bipolar mitotic spindle during cell division to ensure the proper segregation of genetic material to next progeny.

After mentioning the importance of microtubules in different cellular mechanisms, I would like to introduce its structure and the biochemistry of its dynamic instability in the following section.

## **Microtubule Structure**

Microtubules are made up of alpha and beta tubulin heterodimers that bind head-to-tail to form tubulin protofilaments. The alpha and beta monomers are almost 50% identical and each of them has a molecular weight of 50 kDa (Burns, 1991). 10-15 of the protofilaments laterally associates and generates a hollow rigid tube structure with a 25 nm diameter (Chretien, 1992; Downing and Nogales, 1998). In in vitro systems many of the microtubules contain 14 protofilaments whereas in vivo they dominantly have 13 protofilaments (Evans et al., 1985). Genetic studies on the tubulin genes revealed that different isoforms of beta tubulin could affect the protofilament number in different cell types (Raff et al., 1997). The asymmetric nature of alpha/beta heterodimers causes microtubules to have polarity in the polymer structure. The minus end contains exposed alpha tubulin while the plus end having the beta tubulin. This

difference leads to different dynamic behaviors during polymerization and depolymerization reactions at the ends, faster growing ends contain beta tubulin and slow growing ends alpha tubulin. The polarity of microtubule lattice is also important in terms of the functioning of motor proteins such as kinesins and dyneins that move unidirectionally on the microtubules by hydrolyzing the ATP for energy. This property makes them excellent roads for cargo transporters.

On the lateral interactions of protofilaments different models have been proposed. According to the A-type lattice, alpha and beta monomers interact with each other in lateral associations, whereas in B-type lattice there are alpha-to-alpha and beta-to-beta interactions in the lattice, except at the seam. The first studies on the lattice structure suggested the presence of A-type lattice with a helical polymerization (Amos and Klug, 1974) but the later ultra structural analysis of motor-decorated microtubules showed that the real lattice is a B-type lattice with a seam (Mandelkow et al., 1986, Kikkawa et al., 1994). This fact also changed the general view of helical polymerization to the sheet growth of protofilaments that later close into a helical tube.

As mentioned earlier, microtubules show the dynamic behavior by their alternating growth and shrinkage. To explain this characteristic two mechanisms have been proposed: dynamic instability and treadmilling. Dynamic instability that is first proposed by Mitchison and Kirschner, 1984, involves the addition and loss of tubulin dimers at the same end of microtubules. On the other hand, with treadmilling tubulin addition occurs at the plus end while the end minus end losses the dimer (Margolis and Wilson, 1978).

### **Dynamic Instability and Control of Length**

Dynamic instability is based on the hydrolysis of GTP (Hyman et al., 1992). Tubulin subunits that are bound to GTP can be added into the growing protofilament. After incorporation, GTP hydrolysis occurs at the beta-tubulin site and hydrolyzed phosphate (Pi) is released. When GTP hydrolysis is slower than the microtubule incorporation rate, there will be an area at the plus tip that

is composed of GTP containing tubulin dimers. This GTP enriched site is called the GTP cap that serves as a stabilizer of GDP containing microtubule body. The exact size of the GTP cap is not clear and different studies have shown that it may range from a single GTP (Drechsel and Kirschner, 1994) up to 40 (Voter et al., 1991).

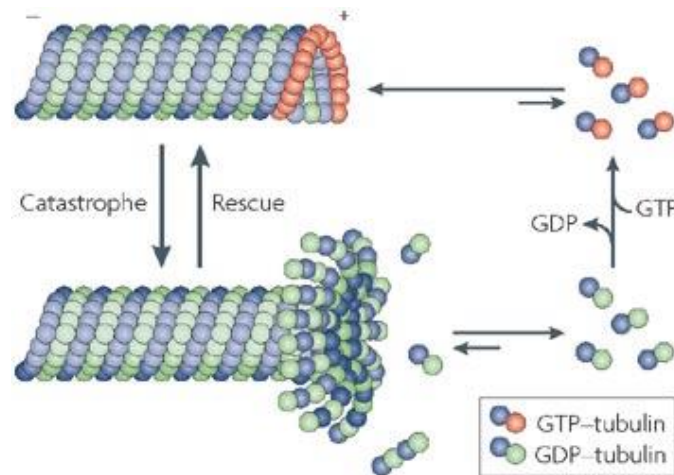


**Figure 1.1: Dynamic instability of microtubules.** Microtubule is a cylinder with outer diameter 25 nm formed by 13 laterally bound protofilaments built by heterodimers of globular  $\alpha$ - and  $\beta$ -tubulin subunits arranged in a head-to-tail manner. Polymerization and depolymerization of microtubules are driven by hydrolysis of GTP on  $\beta$ -tubulin monomer. GTP exchange is necessary for the switch between phases of growth and shrinkage separated by catastrophe (growth to shrinkage transition) and rescue (from shortening to growth). Adapted from Cheeseman and Desai, 2008)

Dynamic instability (Figure 1.1) is defined by four parameters: growth velocity (the rate of polymerization), shrinkage velocity (the rate of depolymerization), rescue frequency (the transition from depolymerization to polymerization) and catastrophe frequency (the transition from polymerization to depolymerization) (Walker et al., 1988). The growth velocity is mainly affected by the soluble tubulin concentration and the rate of GTP-tubulin association to the plus end. However, shrinkage velocity does not depend on the tubulin concentration and driven by the dissociation rate of GDP-tubulin. For this reason, as the free tubulin concentration increases the microtubule polymerization rate also increases and the catastrophe frequency decreases. However this relationship between growth rate and catastrophe frequency is not as simple as it seems, some additional factors regulate these rates in vivo according to the needs of the cell. Additionally, it is certain that the catastrophe frequency is uncoupled from the

polymerization rate, similar catastrophe frequencies occur at MT plus ends in different conditions that increase the polymerization rate (O'Brien et al., 1990).

Development of in vitro systems made it possible to study the microtubule dynamics with minimal components. These components are mainly purified tubulin and microtubule binding proteins (Kinoshita et al., 2013; Li et al., 2012; Zanic et al., 2013). According to the analysis carried out in these systems revealed the growth velocity of MTs as 1-5  $\mu\text{M}/\text{min}$  and depolymerization velocity as 10-50  $\mu\text{M}/\text{min}$ . Although these values are lower than in living cells, they give us the opportunity to dissect the roles of different proteins on the microtubule dynamics in a separate or collective manner.

As mentioned earlier, treadmilling was first observed in 1978 by Margolis and Wilson and it was implied that isolated brain tubulin continuously incorporated into microtubules at a constant rate without a significant change in the microtubule length. In fibroblast cytoplasm lacking centrosomes, there is a switch from dynamic instability to treadmilling depending on an increase in tubulin dimer concentration after depolymerization of the minus ends (Rodionov et al., 1999). Therefore we can say that dynamic instability and treadmilling are linked in the cell.

### **Microtubule Nucleation**

Intrinsic physicochemical properties explain much of the dynamics, pattern and function of microtubules in cells, however in vivo microtubule number, average length, connectivity and localization are thought to be modulated mostly by additional factors such as nucleators, stabilizers, destabilizers and severing enzymes. Nucleators are highly conserved regulators found at the microtubule minus ends that provide a template for protofilament organization. The most prominent one is  $\gamma$  - tubulin (Zheng et al., 1995; Moriz and Agart, 2001) which forms the complex of  $\gamma$  -TuRC ( $\gamma$  - tubulin ring complex) in animal cells that are thought to seed the tubulin arrangement required for initiating polymerization de novo. They are other factors e.g. centrosomin or ninein (Damermann et al.,

2003; Samejima et al., 2005) as well influencing the nucleation position and microtubule anchoring. Most eukaryotic cells possess nucleator-rich MTOCs (microtubule-organizing centers), including the centrosome, which act as foci for the microtubule array organization. On the other hand, secondary MTOCs also occur (Straube et al., 2003), allowing cells to seed diverse functional microtubule arrays in different cellular processes such as differentiation and cell division (Lawson and Carazo-Salas, 2013).

### **Post-translational Modifications on Tubulin**

Tubulin is among the most highly conserved of all eukaryotic genes, due its essential role. Lower eukaryotes have relatively fewer tubulin genes for example, 2 alpha - and 1 beta-tubulin in budding yeast. However, the tubulin gene family expanded considerably in vertebrates and they exist in different isotypic forms (7 alpha - and 8 beta-tubulins in humans) (Luduena and Banerjee, 2008). Almost all of the amino acid and length variation is confined to the C- terminal tail and they localize within the last 15 residues of sequences. These regions are disordered in the crystal structures and thought to be exposed to the outer surface of the microtubule. In contrast, the 400-amino-acid structural core is highly conserved (97% and 95% identity among alpha and beta vertebrate tubulin genes, respectively). beta- tubulin isotypes have the most diverse C-terminal tails and many of these tubulin isotypes are enriched in certain cell or tissue types; for example, TUBB1 in platelets and haematopoietic cells (Leandro-Garcia et al., 2012), TUBB2A/B is enriched in brain and epithelial cells (Banerjee et al., 1988), TUBB3 in specific neuronal cells (Burgoyne et al., 1988) and TUBB4 in ciliary and flagellar structures (Raff et al., 1997). Mutations in TUBB2B, TUBB3 and TUBB5 also have been linked to diseases of the human nervous system (Cederquist et al., 2012, Tuschfield et al., 2010). However, the roles of these different tubulin genes remain poorly understood.

In addition to the genetic variation, both tubulin subunits can be extensively altered by post-translational modifications (PTM), such as detyrosination/tyrosination, acetylation/deacetylation, phosphorylation and



polyglutamylation. With the exception of acetylation of a lysine residue that occurs within the lumen of the microtubule (L'Hernault and Rosenbaum, 1985), the other PTMs take place on the C-terminal tails. The very C-terminal tyrosine residue of alpha-tubulin can undergo a regulated cycle in which it is cleaved in the polymer state by an unknown carboxy-peptidase to produce 'Glu-tubulin' and then added back by tubulin tyrosine ligases (Janke and Bulunski, 2011). The presence or absence of the C-terminal tyrosine (CTT) has been implicated in the regulation of motor proteins (Peris et al., 2009) and CAP-Gly domain containing microtubule plus-end- binding proteins (Akhmanova and Steinmetz, 2008). Another well-known tubulin PTM is the addition of glutamate residues to the -carboxyl side chain of one or more glutamate residues in the CTT of both alpha and beta tubulin (Janke et al., 2005). Polyglutamylation is abundant in neurons and axonemal structures, the number of glutamate residues attached as branches are between 1 and 6 in neuronal cells and it is even higher in the cilia and flagella structures (Audebert et al., 1994; Gaertig and Wloga, 2008).

### **Microtubule (+) end Tracking Proteins**

+ TIPs consist of structurally unrelated proteins, which have the ability to recognize the MT (+) ends. Although some of them can bind along the MT lattice as well their common feature is that their high affinity for the polymerizing microtubule tips. The labeling of these proteins with fluorescent tags shows that they appear as comets in the MT tips while it is growing and disappearing when the MT starts to shrink. These +TIP proteins are known to fulfill various functions in the cell as being related to the MT dynamics. As far as we know +TIPs have a common function to track the growing MT ends, but structurally they do not share a common MT binding domain or any mechanism that they differ. Therefore +TIPs can be classified according to their sequence homologies and in this section I will try to summarize what we have learned so far from the previous studies.

## **CLIP Family**

CLIP (Cytoplasmic Linker Proteins) is the first identified +TIP tracking family that is shown to associate with the growing MT ends by Kreis lab in 1999 (Perez et al., 1999). The first identified protein has been named as CLIP170. Shortly after this discovery, a previously known brain-specific protein CLIP115 (De Zeeuw et al., 1997) was put into the same family with CLIP170 due to the shared CAP-Gly domain. This specific domain is very important because it assists the association of the protein to MTs and basic serine-rich residues surrounding this domain facilitate the binding (Hoogenraad et al., 2000). A single CAP-Gly domain of CLIP-170, together with the adjacent serine-rich region, can track growing microtubule ends (Gupta et al., 2009). CLIPs contain coiled-coil domains to mediate the homo-dimer association to form parallel structures (Akhmanova and Steinmetz, 2008). A third member of CLIP family is the p150glued. This protein is a part of dynactin complex and is involved in the regulation of microtubule-based motor systems (Schroer et al., 2004).

Tip1p, which is the CLIP170 homolog in yeast, is shown as an anti-catastrophe factor (Brunner and Nurse, 2000). On the other hand mammalian CLIPs can induce the MT rescues in mammalian cell culture cells (Komarova et al., 2002). These observations support the idea of that CLIPs are positive regulators of microtubule growth.

## **EB Family**

End binding (EB) proteins contain 3 different members EB1, EB2 and EB3 and they altogether generate a highly conserved family (Su and Qi, 2001). First EB1 was identified as being an interaction partner of APC protein in a yeast two-hybrid system (Su et al., 1995). In tissues EB1 is expressed ubiquitously and it is mostly found at higher levels than EB2 and EB3 whereas EB2 and EB3 show tissue-specific expression patterns. Particularly EB3 is abundant in neurons, but it is also found in muscle cells (Nakagawa et al., 2000).

EB proteins possess conserved structural features; they all contain a MT-binding portion containing a calponin homology (CH) domain at their N-terminal site (Akhmanova and Steinmetz, 2008). This CH domain has shown to be important and sufficient for the interaction with MT plus ends (Komarova et al., 2009). EB proteins need to dimerize to be able to bind to MTs and their dimerization site is found at the C-terminal region (Buey et al., 2011). Although all of the members of the EB family can do homo-dimerization with another protein, it was recently shown that EB1 and EB3 prefer hetero-dimerization between them (De Groot et al., 2009) while EB2 strongly prefers homo-dimerization with another EB2. These different interaction preferences indicate diverse levels of regulation of their functions.

EB1, that is the most abundant EB protein in cells, stimulates microtubule growth, facilitates rescues and inhibits catastrophes (Tirnauer et al., 2002). EB1 also inhibits catastrophes and promotes the initiation of microtubule growth in *Schizosaccharomyces pombe* (Busch and Brunner, 2004). On the other hand, in vitro studies of EB1 and Mal3 effect on the dynamics of microtubules, that are polymerized from purified tubulin show that these proteins facilitate not only rescues but also catastrophes (Bieling et al., 2007; Vitre et al., 2008) although in another contrary study of microtubule dynamics suggested catastrophe suppression by EB1 (Manna et al., 2008) and actually no effect of EB1 on the catastrophes was observed in Dixit et al., 2009. Moreover, in a recent study, dimers of EB1 promote persistent microtubule growth by suppressing catastrophes in vitro (Komarova et al., 2009).

EBs can interact with MT plus ends in both interphase and mitosis (Morrison et al., 1998; Mimori-Kiyosue et al., 2000). Their abilities to interact with other MT dynamics regulators define their functions on MT growth regulation. For example, in vitro data demonstrates that EB1 can bind to other +TIPs such as CLIP170 and this interaction synergize to increase the MT dynamics, according to the proposed mechanism by modifying the MT-stabilizing cap (Lopus et al., 2012). Furthermore, EB1 has shown to associate with CLASP proteins at the cell cortex and MT-rescue events have been increased upon this interaction (Mimori-

Kiyosue et al., 2005). EBs do not only interact with MT growth factors, but they can also load MT destabilizers to the MT plus ends. These interactions are not only important for the localization of destabilizer proteins but they are also involved in their catastrophe-inducing activities (Montenegro Gouveia et al., 2010).

EB proteins do not only interact with microtubules and its effectors. They can bind to different structures and influence a wide variety of cellular processes. EB1 is an active component of centrosome and its centrosome binding somewhat independent of its MT interaction. This can be facilitated by its C-terminal domain (Louie et al., 2004) and leads to the recruitment of gamma-tubulin to centrosomes (Askham et al., 2002). EB1 was shown to interact with spectraplakins ACF7/MACF1, most probably to establish a link between actin and microtubule cytoskeletons (Kodama et al., 2003). More than that, EB proteins are suspected to have an enormous number of interacting partners to mediate the fast MT dynamics according to the rapidly changing needs of the cell. More detailed picture of EB functions are waiting to be elucidated.

### **CLASP Family**

The largest group of +TIPs comprises large and complex, often multidomain, proteins containing low-complexity sequence regions that are rich in basic, serine and proline (basic-S/P) residues. They share the small four-residue motif Ser-x-Ile-Pro (SxIP, where x denotes any amino acid), which is specifically recognized by the EBH domain of EB proteins. CLASPs promote rescues at the shrinking microtubule plus ends by recruiting tubulin dimers (Al-Bassam et al., 2010; Maiato et al., 2005). CLASPs are found in a direct association with other plus end tracking proteins such as CLIPs chTOG and SLAIN2 to promote persistent MT growth. CLASPs are also localized at the growing microtubules but they are specifically enriched at the leading edge of migrating cells to form a link between microtubule and actin cytoskeleton (Akhmanova and Steinmetz, 2010). Additionally, CLASP is also involved in Golgi assembly and dynamics, because in CLASP depleted cells severe defects in Golgi morphology was observed (Miller et

al., 2009) most probably due to its effect on microtubule nucleation at the Golgi apparatus. This effect of CLASP on MT nucleation has been observed a while ago in nocodazole treated cells, in which the non-centrosomal microtubules nucleate at the dispersed Golgi vicinities in a CLASP dependent manner (Efimov et al., 2007) to generate a subpopulation of microtubules which are stable and acetylated. Another mammalian CLASP homologue PEG1p is important for mitochondria distribution, which facilitates the capturing of mitochondria on the growing MT, tips and immobilizes them. This feature is essential for mitochondria positioning and transport (Chiron et al., 2008).

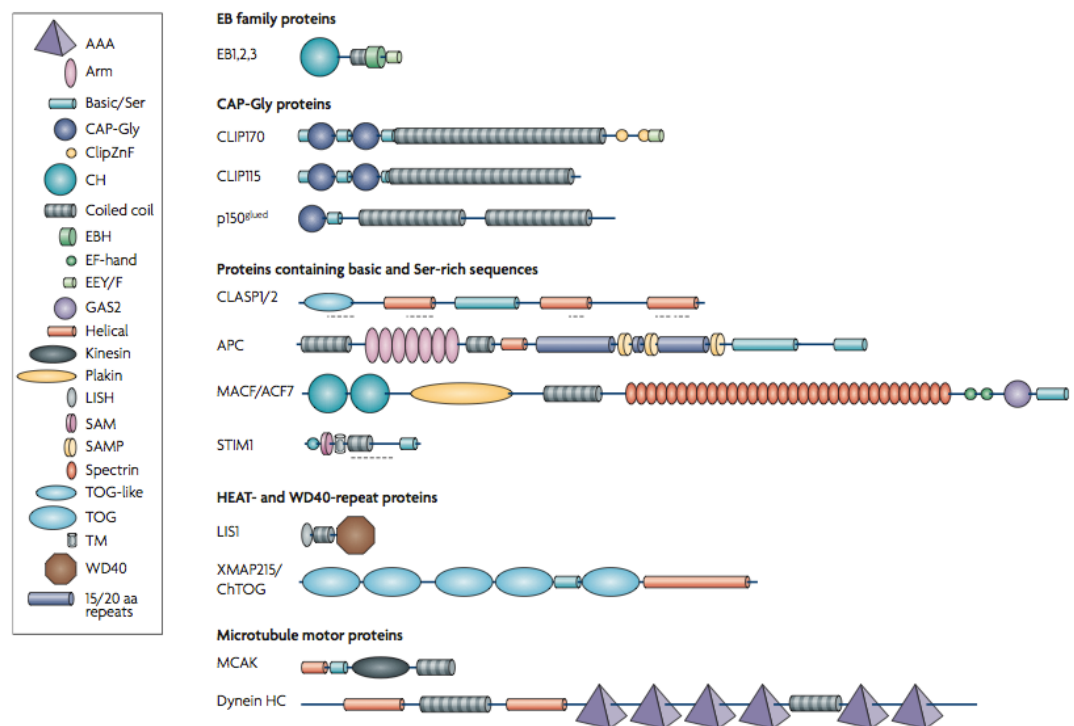


**Figure 1.2: Structures of +end tip tracking proteins .**The main plus-end tracking protein (+TIP) families have been grouped according to prominent structural elements that are involved in tracking the growing microtubule plus ends (adapted from Akhmanova and Steinmetz, 2008).

## Microtubule Disassembling Proteins

Microtubule destabilizing proteins are divided into three major classes. These are kinesin-family members, mainly kinesin-13, kinesin-14 and kinesin-8; microtubule severing enzymes, katanin and spastin; and tubulin dimer-sequestering proteins. Stathmin and RB3 (Helmke et al., 2013). Microtubule

destabilization rates determine the lifetime of microtubules and therefore these proteins have profound effects on the interphase microtubule array organization and on the spindle size and assembly.

Kinesin family proteins are important regulators of microtubule density and dynamics. Their regulation through phosphorylation, interaction partners and dynamic localization patterns show the complexity of their behavior. Microtubule severing proteins cleave the microtubules by using the energy coming from ATP hydrolysis at points within the microtubule filament (Diaz-Valencia et al., 2011) and have increased activities in mitosis and in neuronal branching. After this short introduction for microtubule destabilizers, I will discuss the functions of kinesin-8 and kinesin-13 family members that are also used in our experiments.

### **Kinesin-13 Family**

Kinesin-13 members were initially named as M kinesin family because of the position of their motor domain in the middle of the protein. Kinesin-13 is comprised of 2 subfamilies, these are: KIF24 and mammalian-specific Kif2 subfamilies. KIF24 is a ubiquitous protein that is mainly involved in intracellular vesicular trafficking and ciliogenesis (Noda et al., 2005). On the other hand, there are 2 proteins in Kif2 subfamily which are: Kif2a, Kif2b and Kif2c/MCAK. All of these three proteins have globular N-terminal domain, a central catalytic core, a positively charged neck region and a C-terminally located dimerization domain (Wordemann, 2005).

Kinesin-13 members have a wide variety of intracellular functions. There are important for vesicular transport as mentioned above (Noda et al., 2005), in neuronal branching (Homma et al., 2003) and in microtubule depolymerization during interphase and mitosis. Kinesin-13s depolymerize microtubules by inducing a conformational change in the microtubule structure upon binding to the end and this event leads to catastrophe (Desai et al., 1999). Kinesin-13s are unique depolymerizers because they can destabilize both of the microtubule

ends by using the energy coming from ATP hydrolysis while other depolymerizers usually walk along microtubules (Hunter et al., 2003). They do it in a way that forcing protofilaments into a curved conformation which is likely structural intermediate in the depolymerization process (Niederstrasse et al., 2002). Among the kinesin-13s MCAK is the best-studied family member. By diffusing along microtubules instead of walking, MCAK rapidly targets both microtubule ends (Helenius et al., 2006). Once it reached to the +TIP 14 MCAK dimers generate an ATP-hydrolyzing complex that processively depolymerize microtubules (Hunter et al., 2003). For this reason, it was proposed as a major microtubule remodeler by preventing microtubule aging via induction of random catastrophes (Gardner et al., 2012).

The plus end accumulation of MCAK is thought to be by an EB1 dependent mechanism. MCAK can interact and colocalize with EB1 at microtubule +ends and this direct association suggests that MCAK might be using the EB1 hitchhiking mechanism to bind and stay at plus ends (Lee et al., 2008). MCAK-microtubule interaction is also regulated by post-translational modifications such as Aurora B can phosphorylate EB1 at the mitotic centromere to prevent its microtubule attachment and depolymerization activity (Andrews et al., 2004). Most of these phosphorylation sites reside at the EB1 interaction site of MCAK showing that EB1 binding is very important for tip tracking of MCAK (Honnappa et al., 2009).

### **Kinesin-8 Family**

Kinesin 8 family members KIF18A in humans in mammals and Kip3 in yeast have been shown to be *in vivo* plus-end directed microtubule depolymerizers. Kip3 is a highly processive microtubule plus-end-directed motor which is a catastrophe factor *in vivo* (Gupta et al., 2006) and a microtubule depolymerase *in vitro* (Varga et al., 2006; Varga et al., 2009). Kip3 depolymerizes longer microtubules faster than shorter ones because of its accumulation at the ends of longer stabilized microtubules. Kip3 slows down the *in vitro* microtubule growth rate in a length-dependent manner, and it promotes microtubule catastrophe as

well by increasing the rate at which destabilizing effects occur (Gardner et al., 2012). A recent work by Stumpff et al. (Stumpff et al., 2008) identified Kif18A, another member of Kinesin-8 family, to be important for spatial confinement of kinetochore movements (Gardner et al., 2013).

### **Microtubule Assembling Proteins**

Microtubule assembling proteins can be divided into two groups, microtubule stabilizers and microtubule growth-promoting factors. Microtubule stabilizers consist of mainly three proteins, MAP1/MAP2, Tau and Doublecortin. These proteins do not interact with the ends of microtubules but they bind on the microtubule lattice to reduce the depolymerization by increasing the strength of longitudinal bonds between the filaments. Doublecortin favors 13-protofilament microtubules and binds between the protofilaments stabilizing the longitudinal bonds between tubulin dimers. It decreases catastrophe rate, although it does not affect microtubule growth rate.

### **TOG Family**

TOG (Tumor overexpressed gene) proteins are highly conserved microtubule dynamics regulators (Al-Bassam and Chang, 2011). XMAP215 is the first protein identified in *Xenopus*, which is involved in the promotion of rapid microtubule growth (Gard and Kirschner, 1987). Later, it has been identified that XMAP215 increases the microtubule growth rates upto 10 folds and serves as a processive microtubule polymerase (Brouhard et al., 2008), which is extremely required for fast microtubule assembly during differentiation, migration and cell division (Brittle and Ohkura, 2005). XMAP215 catalyzes this fast reaction by transiently binding to plus ends and by adding 25 tubulin dimers to microtubule one by one before dissociating (Brouhard et al., 2008). TOG proteins do not only localize at plus ends, but can also bind to microtubule lattice and free soluble tubulin. They can promote the tubulin assembly at both microtubule ends, however they do it more efficiently on plus ends (Vasquez et al., 1994).



The mammalian TOG family member is chTOG (CKAP5) and it has been shown to promote microtubule assembly both in solution and from nucleation centers (Charrasse et al., 1998). The knockdown of these proteins leads to short interphase microtubules caused by reducing growth rates and increased catastrophes (Cullen et al., 1999; Wang and Huffaker, 1997).

## **2. Materials&Methods**

### **Methods**

#### **Mouse Embryonic Stem Cell Culture**

Feeder-free mouse R1/E embryonic stem cells were cultured in DMEM high-glucose media containing 1X Glutamax 15% ESC screened and heat-inactivated Fetal Bovine Serum, 0.055 mM beta-mercaptoethanol, 1X NEAA, 1X Penicillin/Streptomycin solution and 500 µg/ml purified recombinant LIF. ES cells were maintained in a humidified chamber at 37°C and 5%CO<sub>2</sub>. Media of cells were changed in a daily base and the cells were passaged in every 2-3 days according to their confluence. Passaging was done by trypsinization (0.05% trypsin in an EDTA solution) for 3-4 minutes. Trypsin was neutralized after addition of ESC medium and cell clumps were dispersed into a single cell suspension. Afterwards 1/10 of the cells were transferred into the fresh ESC medium in a 10 cm dish.

#### **Cell Counting**

Before experiments, cells were counted and split according to their density. They were harvested and centrifuged 5 minute at 300Xg. After discarding the trypsin-containing supernatant, pellet was resuspended in 10 ml of fresh ESC medium. 10 µl of this cell suspension was mixed with 10µl of 0.4% trypan blue solution to a final volume of 20 µl. 10 µl of this mixture was loaded into the chamber of the counter slide and cells, number/ml, was counted by Cell Counter (Invitrogen).

## **Freezing of ESC**

Cells were trypsinized and collected after centrifugation. The pellet was resuspended in ESC medium at a concentration of  $2 \times 10^6$  cells/ml. An equal amount of 2X freezing medium containing 50%FBS, 20%DMSO in the complete ESC medium was added to the cell suspension. Cells were transferred into 2ml cryo-vials as 1ml/vial and then stored in the -80 freezer in the isopropanol-filled cryobox. After 48 hours cells were transferred into liquid nitrogen tanks for long-term storage.

## **Thawing of ESC**

Vials were quickly taken out of the liquid nitrogen and placed into 37C waterbath. After about 90 seconds they were transferred into 10 ml warm ESC medium in a drop-wise manner. Cells were centrifuged at 300Xg for 5 minutes. After centrifugation, DMSO containing supernatant was discarded and the pellet of cells was resuspended in 10 ml ESC medium. Cells were cultured in 10 cm dishes.

## **BAC TransgeneOmics**

Bacterial artificial chromosome (BAC) constructs containing the full-length genes, including promoter sequences and regulatory elements were chosen using the Genome Browser (<http://www.genome.ucsc.edu>). Chosen constructs were ordered from BACPAC Resources Center. Proteins were tagged at the C-terminal site with the LAP (localization and affinity purification) cassette (Cheeseman and Desai, 2005). This cassette contains Enhanced Green Fluorescent Protein (EGFP), which enables localization and immunopurification by specific antibody against GFP. BAC engineering was performed as described previously (Poser et al., 2008).

## **BAC DNA Isolation**

BAC DNA was isolated from bacteria using the Nucleobond Mini Kit (Macherey-Nagel) according to manufacturer's instructions. NucleoBondBACkits employ a modified alkaline /SDS lysis procedure to prepare the bacterial cell pellet for plasmid purification. Both chromosomal and plasmid DNA are denatured under these alkaline conditions. Potassium acetate is then added to the denatured lysate, which causes the formation of a precipitate containing chromosomal DNA and other cellular compounds. The potassium acetate buffer also neutralizes the lysate. Plasmid DNA can revert to its native supercoiled structure and remains in solution. After equilibrating the appropriate NucleoBond Column with equilibration buffer, plasmid DNA is bound to the anion-exchange resin and finally eluted after efficient washing of the column. After precipitation of the eluted DNA it can easily be dissolved in TE buffer for further use.

## **Cloning of shRNA plasmids**

The cloning of shRNA plasmids was started by designing the shRNA oligos. When designing the top and bottom strand single-stranded oligos, we considered that the top strand oligo had sequences required to facilitate directional cloning, a transcription initiation site and sequences encoding the shRNA of interest while the bottom strand oligo had sequences required to facilitate directional cloning and sequences complementary to the top strand oligo. You can find the list of shRNA oligos below.

### Mouse chTOG shRNA

5'- CACC AAT AAA GAG CAG TCG CAA A CGAA T TTG CGA CTG CTC TTT ATT -3'

5'- AAAA AAT AAA GAG CAG TCG CAA A TTCG T TTG CGA CTG CTC TTT ATT -3'

### Mouse KIF18A shRNA

5'- CACC AAG AAG AGG TGT CGA AAC A CGAA T GTT TCG ACA CCT CTT CTT -3'

5'- AAAA AAG AAG AGG TGT CGA AAC A TTCG T GTT TCG ACA CCT CTT CTT -3'

### Mouse MCAK shRNA

5'- CACCA GGA AAT CGT GTA TCG TGA A CGAA T TCA CGA TAC ACG ATT TCC -3'

5'- AAAA GGA AAT CGT GTA TCG TGA A TTCG T TCA CGA TAC ACG ATT TCC T -3'

### Luc control shRNA

5'- CACCA CGG CAA GCT GAC CCT GAA GTT CAT CGAA ATG AAC TTC AGG GTC AGC TTG CCG -3'

5'- AAAA CGG CAA GCT GAC CCT GAA GTT CAT TTCG ATG AAC TTC AGG GTC AGC TTG CCG T -3'

Single-stranded top and bottom oligos were resuspended in water to a final concentration of 200  $\mu$ M before use. Then for annealing, they were mixed at 50 $\mu$ M concentration and incubated with 1X oligo annealing buffer (Invitrogen). They were incubated at 95C for 4 minutes to open the secondary structures in oligos and then at room temperature for 10 minutes to anneal the top and bottom oligos to each other.

Once the annealing reaction was completed, 1  $\mu$ l of the 50  $\mu$ M annealing mixture was diluted to 5nM ds oligos with distilled water. The ligation of ds annealed oligos to pENTR/H1/TO vector was performed with T4 ligase. The ligation mixture was incubated at room temperature for 1 hour and then then 2  $\mu$ l of it was transformed into One Shot TOP10 competent cells (Invitrogen). Transformation was initiated by adding the ligation mixture into competent cells. After an incubation of ice for 5 minutes cells were heat shocked at 42C for 30 seconds and then returned into ice. 250  $\mu$ l SOC medium was added to cells and they were put to 37C for 1 hour. Cells were spread onto Kan+ plates and incubated O/N.

### **Generation of Stable mES Cell Lines**

R1/E cells were seeded on 6-well plates coated with 0.1% gelatin solution at 180,000 cells/well density. They were transfected next day with 4  $\mu$ l of eluted BAC DNA using Lipofectamine 2000 transfection reagent according to manufacturer's instructions. Basically, 250  $\mu$ l of Optimem was put in two different Eppendorf tubes. 4  $\mu$ l BAC DNA was added in one of the tubes and 12  $\mu$ l Lipofectamine 2000 into the other tube. They were left approximately 5 minutes for equilibration. Then they were put together to a final volume of 500  $\mu$ l,

vigorously vortexed and kept at room temperature for 20 minutes for the formation of DNA-liposome complex. Meanwhile the media of cells were replaced with 3 ml fresh ESC medium. After 20 minutes, tubes were vortexed again and added onto the cells in a drop-wise manner. Their medium containing transfection mixture was changed after 24 hours to a fresh one. After 48 hours, the selection of BAC-inserted stable ESC colonies was made to start by adding 250 µg/ml G148 to the medium.

### **Immunofluorescence Staining**

Cells were seeded on 1µg/ml laminin-511 at 50.000 cells/well in 24-well plate. Next day growing cells were washed with PBS and then fixed with ice-cold methanol at - 20C for 6 minutes. Then methanol was discarded and replaced with PBS for rehydration of samples. After 2 more washes to eliminate the residual methanol, cells were blocked in 0.2% fish skin gelatin solution, which is dissolved in PBS. Cells were incubated in this solution for 1 hour. Meanwhile, primary antibodies were diluted in blocking solution and cells were incubated with them either 1 hour at room temperature or overnight at 4C. After rigorous washes with PBS, secondary antibodies, which are diluted again in blocking solution added onto the cells and incubated at room temperature for 1hour in a light-tight chamber (Table 2.1). Cells were washed 2 times with 0.1% Triton-PBS solution and once with PBS each for 10 minutes. Finally coverslips were mounted in DAPI-Prolong Gold antifade reagent overnight and sealed. Images were acquired on the Delta-Vision Widefield fluorescence microscope system with 60X 1.4 NA oil Plan Apochromat.

**Table 2.1:** Antibody list used in immunofluorescence stainings

<b>Antibody</b>	<b>Company</b>	<b>Type</b>	<b>Dilution</b>
Anti-GFP	MPI-CBG home-made	Goat polyclonal	1:5000
Anti-beta tubulin	Sigma	Mouse monoclonal	1:100
Anti-Map2	Santa Cruz	Rabbit polyclonal	1:100
Anti-tau	Santa Cruz	Rabbit monoclonal	1:100
Anti-Tbr-1	Abcam	Mouse monoclonal	1:100

### **Preparation of Protein Lysates**

Cells were trypsinized, harvested and centrifuged for 5 minutes at 300Xg. The pellet was washed once with PBS and centrifuged again. Cell pellet was resuspended in 1X RIPA lysis buffer and then subjected to 1X freeze-thaw cycle in -80C. Then lysates were incubated on ice for 15 minutes and centrifuged at 13.000 rpm for 15 minutes at 4C. The supernatant was transferred into a new tube. Protein concentrations were determined spectrophotometrically at 595 nm by Bradford assay. Protein extracts were stored at -80C for further use.

### **Western Blot Analysis**

Total protein lysates were mixed with 3X Reducing loading buffer and incubated 5 minutes at 95C. Then quickly spun and loaded onto NuPAGE 4-12% Bis-Tris gels with NuPAGE MOPS running buffer. Proteins were separated at 150V for 1 hour and right afterwards transferred onto nitrocellulose membrane either by wet blotting or by I-Blot Dry Blotting system. The efficiency of protein transfer was checked by Ponceau S staining. Membranes were blocked in 5% milk powder dissolved in PBS for 1 hour. Then primary antibodies were diluted in blocking solution and incubated with membranes at the given concentrations and durations (Table 2.2). Membranes were washed at least 3 times with PBS-T

and then secondary antibodies were added at 1:10,000-1:30,000 dilutions. After 1 hour incubation at room temperature, membranes were washed 3 times with PBS-T each for 10 minutes and the once with PBS. Luminescence signal was developed by Pierce Supersignal West Femto substrate and afterwards blots were exposed to Amersham Hyperfilm ECL.

**Table 2.2:** Antibody list used in Western Blotting analysis

<b>Antibody</b>	<b>Company</b>	<b>Type</b>	<b>Dilution</b>
Anti-GFP	Roche	Mouse monoclonal	1:2000
Anti-TetR	MoBiTec	Rabbit polyclonal	1:1000
Anti-Kif18A	Santa Cruz	Goat polyclonal	1:1000
Anti-ch-TOG	Santa Cruz	Goat polyclonal	1:1000
Anti-MCAK	Santz Cruz	Goat polyclonal	1:1000

### **Live Cell Imaging**

For live-cell imaging of GFP-tagged mouse ES cells, first we have coated the surface of 8-well IBIDI u slides with 1 $\mu$ g/ml laminin-511 for 1hour at 37C. Then, 20.000 cells added into each well and they were incubated for 24 hours in 37C chamber. Next day they were either transfected with siRNAs or imaged directly. First, the growth medium of cells was replaced by the imaging medium, which is suited to support the growth in the absence of CO<sub>2</sub> and to reduce the effects of phototoxicity. The growth medium was discarded and the cells were washed once with imaging medium. Then 200  $\mu$ l of imaging medium was added onto the cells and they were left approximately 1 hour in an incubator for equilibration. Meanwhile, the heating of the imaging chamber in Delta-vision microscope was also turned on. After the equilibration steps of cells and the chamber were completed, cells were put on stage and appropriate fields have been selected. Then, slide was left on the stage for at least 30 minutes for an additional equilibration with the objective and immersion oil to prevent any focus drift during image acquisition caused by temperature fluctuations. After that,z-stack of optical sections of images were collected in10-12  $\mu$ m total thickness and with



5-6 sections using either 40X 1.2 NA, 63X 1.4 NA or 100X NA objectives in SoftWoRx software. Images were deconvolved by enhanced ratio method and all images were max-projected in the Fiji (ImageJ) software.

### **RNA Interference**

Cells were either plated onto gelatin-coated 6 cm dishes for Western Blotting or onto laminin-511 coated IBIDI  $\mu$ -chambers for live-cell imaging. Next day, siRNAs were diluted at 10  $\mu$ g/ml concentration in Optimem and 30  $\mu$ l of Lipofectamine 2000 was added into this solution. Then 400 ng of siRNA/well was added to imaging samples and 4  $\mu$ g/dish in Western Blot control dishes. After 48 hours, either the imaging was initiated or protein samples were collected by extraction.

Sequences of siRNAs used in the RNAi experiments are given below.

Mouse EB1: TGATTTGCCAGGAGAACGA

Mouse chTOG: AATAAAGAGCAGTCGCAAA

Mouse MCAK: GGAAATCGTGTATCGTGAA

Mouse Kif18A: AAGAAGAGGTGTCGAAACA

Non-targeting control: CAGCATACATTCAGAATGTAA

### **Differentiation of mES Cells into Spinal Motor Neurons**

Differentiation of mES cells into spinal motor neurons was carried out according to the protocol described in Wichterle et al., 2008. 1 to 2  $\times 10^6$  ES cells per 10-cm tissue culture dish was plated in 10 ml of ADFNK (differentiation) medium. Cells were evenly distributed by swirling the dish in a figure eight motion before placing the dish in the incubator.

On differentiation day 1 cultures were checked for large number of EBs—small floating aggregates of ES cells that are visible under the microscope. Dishes were swirled gently and all floating EBs were transferred into 15-ml tube. EBs

were centrifuged for 3 min at low speed ( $200 \times g$ ), room temperature. Supernatant was aspirated and gently flicked on the tube to disperse EBs. 10 ml of ADFNK medium was added and EBs were plated in a new 10-cm tissue culture dish. The dish was swirled once to evenly distribute EBs and place back in the incubator.

On day 2, EBs should be of a fairly uniform size (50- to 100- $\mu\text{m}$  in diameter) and most of them should be floating. Dishes were swirled again and EBs were collected in a 15-ml tube and they were let settle by gravity ( $\sim 15$  min) or by gentle centrifugation (3 min at  $200 \times g$ , room temperature). Medium was aspirated and EBs were resuspended in 400  $\mu\text{l}$  of ADFNK medium. Four 10-cm culture dishes were prepared, each containing 10 ml of ADFNK medium supplemented with RA at 1  $\mu\text{M}$  final concentration. Using a 200- $\mu\text{l}$  pipettor and a large-orifice yellow tip, EBs were mixed by repeated pipetting and 100  $\mu\text{l}$  of EBs were dispensed per 10-cm dish. Dishes were swirled in a figure eight motion and then returned into the incubator. Effective neuralization of EBs is achieved with RA concentrations ranging from 100 nM to 5  $\mu\text{M}$ . RA is light sensitive and aliquots should be wrapped in aluminum foil and stored in the dark. To simplify the differentiation protocol, it is possible to supplement the medium with Hh on this day 2. In particular, HhAg1.3 is relatively stable and will remain active until day 3 to 4 when it is required to ventralize EBs.

By day 3, differentiating ES cells reach the neural plate stage and can be patterned along the dorso-ventral axis. To induce motor neuron specification dishes were supplemented with Shh protein at  $\sim 200$  ng/ml, final concentration. On day 5, the medium in the dishes has to be turned to orange/yellow as an indication of proper patterning and differentiation. This old medium was replaced by the fresh ADFNK medium by taking care not to aspirate the EBs. For better survival of motor neurons the medium was supplemented with GDNF to a final concentration of 5 ng/ml. Day 6 to 7 is the peak of motor neuron differentiation. EBs were collected for further analysis of mature motor neurons.

## **Generation of Cortical Neurons from mES cells**

150,000 cells were spread onto gelatin-coated 6-cm dishes in the ES cell medium. So the cell density was 5,000 cells/cm<sup>2</sup>. Next day the ES medium was discarded and dishes were washed with warm PBS 1X. Afterwards 5 ml DDM medium was added to cells to initiate the differentiation. After 2 days, DDM was replaced with fresh DDM containing 1 μM cyclopamine. Cells were incubated with cyclopamine by changing the DDM medium in every 2 days until day 10. At day 10, medium was replaced with DDM only. Meanwhile, 15 mm coverslips or imaging chambers were coated with poly-D-lysine (50 μg/ml) and laminin (1 μg/cm<sup>2</sup>). At day 12, cells were passaged and resuspended in 5 ml DDM/N2:Neurobasal/B27 medium. For analysis of neurons at day 21, cells were seeded at 250X10<sup>3</sup> cells per well of 12-well plate in N2/B27 medium. Medium was changed in every 2 days until day 21 and then analysis continued with immunofluorescence staining (Gaspard et al., 2009).

## Materials

DMEM, 4.5g/L glucose+GLUTAMAX (Invitrogen)

DMEM:F12-GLUTAMAX (Invitrogen)

Advanced DMEM:F12 (Invitrogen)

CO<sub>2</sub>-independent medium (Invitrogen)

Neurobasal Medium (Invitrogen)

Non essential amino acids (Invitrogen)

ES cell screened FBS (Hyclone)

Knock-out serum replacement (Invitrogen)

Sodium pyruvate (Invitrogen)

Bovine Serum Albumin (Sigma)

Recombinant LIF (MPI-CBG)

Penicillin-Streptomycin (Invitrogen)

Trypsin-EDTA (Invitrogen)

G-418 (Invitrogen)

Beta-mercaptoethanol (Invitrogen)

Gelatin (porcine skin) (Sigma)

Gelatin (fish skin) (Sigma)

N2 (Invitrogen)

B27 (Invitrogen)

GDNF (R&D Bioscience)

Cyclopamine (Santa Cruz Biotechnology)

Retinoic Acid (Sigma)

Shh (R&D Bioscience)

Laminin-511 (Biolamina)

Poly-D-Lysine (Sigma)

Laminin (Roche)

Fibronectin (Roche)

Lipofectamine 2000 (Invitrogen)

Optimem (Invitrogen)  
Trolox (Sigma)  
DMSO (Sigma)  
Isopropanol (Sigma)  
Methanol (Sigma)  
DAPI (Sigma)  
Prolong-Gold antifade reagent (Invitrogen)  
NuPAGE Bis-Tris Gel 4-12% (Invitrogen)  
NuPAGE MOPS running buffer (Invitrogen)  
Ponceau S stain (Sigma)  
ECL Substrate (Pierce)  
RIPA lysis buffer (Cell Signalling Technologies)  
Milk powder  
Nucleobond Mini-Kit (Macherey&Nagel)  
10cm TC Dish (BD-Falcon)  
6cm TC Dish (BD-Falcon)  
24-well plate (Nunc)  
8-well imaging chamber (IBIDI)  
Cryovials (Nunc)  
Coverslips (12mm)  
Glass slide  
Nitrocellulose membrane (Whatmann)  
Blotting paper (Whatmann)

## Solutions

### ES Cell Growth Medium

1 bottle	DMEM 4.5g/l glucose with Sodium Pyruvate
20%	FBS
1X	100X Pen/Strep Solution
1X	100X Glutamax
1X	100X NEAA
1000u/l	LIF
1mM	Beta-mercaptoethanol

### Live-Cell Imaging Medium

1 bottle	CO <sub>2</sub> Independent Medium
20%	FBS
1X	100X Pen/Strep Solution
1X	100X Glutamax
1X	100X NEAA
1000u/l	LIF
1mM	Beta-mercaptoethanol
1uM	Trolox

### ADFNK Medium

250ml	Advanced DMEM/F12
250ml	Neurobasal medium
5.6ml	Penicillin/streptomycin
5.6 ml	100X L-Glutamine
400µl	50 mM 2-mercaptoethanol
56 ml	Knockout serum replacement

### **3. Live-Cell Imaging of Mouse ES Cells**

Live-cell imaging is a powerful tool to visualize, track and analyze the single cell behavior in a cell population over a time period. So far many techniques have been adapted and combined for imaging of cell lines, mainly for the cancer or immortalized ones. The recent developments in the stem cell biology made it necessary to optimize such conditions for embryonic stem cells to be able to study their cell biology deeper. However, because they are very prone to apoptosis, tend to form spheres and hard to stably label, it is quite tricky to image them in culture conditions. Here we describe an imaging system for mouse ES cells that is suitable for long-term live-cell imaging. This system combines the BAC-based gene expression with wide-field deconvolution microscopy for ES cells that are plated onto the laminin-511 coated surface and kept in CO<sub>2</sub> independent culture conditions. This combined technique does not interfere with the growth of cells and keeps them healthy up to 24 hours during imaging.

## **Introduction**

Embryonic stem (ES) cells were first isolated from mouse embryos (Evans and Kaufmann, 1982; Martin, 1981). They are derived from the inner cell mass (ICM) of preimplantation embryos at the blastocyst stage, but have been also isolated from earlier eight-cell stage embryos (Delhaise et al., 1996) and morulae (Sukoyan et al., 1993). ES cells have mainly two unique properties. First, under appropriate conditions, ES cells can be kept undifferentiated for many passages, while retaining a stable karyotype. Second, they can be differentiated both *in vitro* and *in vivo* into cells representing the three germ layers; ectoderm, mesoderm and endoderm. These characteristics make ES cells invaluable for studying the molecular mechanisms of pluripotency and lineage differentiation processes for regenerative therapies of a variety of human diseases (Keller, 2005). Interestingly, ES cells contribute efficiently to the developing embryo and resulting animal when injected into a recipient blastocyst stage embryo. Thus, the pluripotent state of ES cells offers unprecedented opportunities, and is harnessed when genetic modifications are engineered into ES cells to create genetically modified mice (Thomas and Capecchi, 1987).

After the initial isolation of murine ES cells over a decade ago, many studies have been carried out to dissect the regulatory mechanisms that give the ES cells their before-mentioned unique properties. Most of our knowledge of ES cell biology comes from the study of the molecular mechanisms supporting pluripotency in mouse ES cells, and more recently work performed investigating human ES cells. Mouse ES cells are usually cultured on fibroblast feeder cells, although some feeder-free cell lines have also been recently generated (Robertson, 1987). One key factor required for stem cell maintenance is Leukaemia Inhibitory Factor (LIF), a member of IL-6 cytokine family (Williams et al., 1988). Despite its essential action through the LifR/Gp130/Stat3 pathway, addition of recombinant LIF protein to cell culture media is not sufficient to isolate and propagate ES cells in an undifferentiated state, suggesting that some others external factors are required, which are likely to be present in the serum (Nichols et al., 1990), which is a necessary constituent of the culture media.



A core regulatory network of transcription factors, which act on both to promote self-renewal and inhibit differentiation, sustains the pluripotency. So far three molecular players have been found to preserve the state of pluripotency in ES cells. These are; the POU domain containing factor OCT4, the HMG domain-containing factor SOX2, and the homeobox domain containing factor NANOG. Three of them have been shown to be essential for the maintenance and propagation of ES cells and for early embryonic development in the mouse. Oct-4 inactivation is directly associated with lethality after implantation and the differentiation of ICM into trophectoderm was blocked by the loss of pluripotency (Nichols et al., 1998). Sox2-deficient mouse embryos show quite severe defects in the ICM-derived epiblast (Avilion et al., 2003). Moreover, mouse embryos lacking Nanog have no discernable epiblast at peri-implantation stages (Mitsui et al., 2003). Thus the idea that these three factors represent the core component of a network required for the maintenance of pluripotency supported by both in vivo experiments using genetically modified mice, and in vitro experiments where these factors are knocked-down or overexpressed.

The pluripotency of ES cells, their ease of manipulation in culture, and their ability to contribute to the mouse germ-line provides us a model of differentiation both in vitro and in vivo. The dynamics of their unique characteristics can be studied extensively by live-cell imaging and if ES cells are genetically marked their progeny can be live imaged in situ. Due to the recent advances in the regenerative medicine and its potential applications the field of live ES cell imaging is of great interest to the pharmaceutical and biotechnology industries, and many are now developing high-throughput screening platforms for automated analysis of intracellular localization and dynamics.

As I mentioned above, stem cells are central to the generation, homeostatic regeneration and repair of tissues. A deep understanding of stem cell behavior and its molecular control is both of the highest academic interest and essential for therapeutic application of these cells. However, our understanding of stem cell biology remains surprisingly limited due to their laborious isolations and

very fragile nature. In recent years, many laboratories have been focused on generating high-throughput methods to isolate the stem cells in bulk amounts and to establish the cell lines if applicable. After overcoming these technical issues, now people started to study the stem cell behavior in great detail. For this reason, lots of screening methods have been developed either to study the pluripotency (Loh et al., 2006; Jiang et al., 2008) or for drug tests (Caspi et al., 2009). Although these methods all give valuable conclusions they were away from tracking the behavior of single stem cells. At this point, continuous long-term single-cell observation, in contrast, can give surprisingly clear answers to long-standing questions of the fate generation in stem cells (Eilken et al., 2009; Rieger et al., 2009).

Continuous long-term imaging of stem cells must be definitely noninvasive and by the recent advances in the microscopy field supports the health of cells during live-cell imaging (Artus and Hadjantonakis 2007). In practice, however, *in vivo* stem cell observations are at present limited by technical considerations due to the requirement of immobilization of organisms on the stage for a long time. On the other hand, *in vitro* imaging allows observation of single mammalian cells for up to weeks, including the simultaneous quantification of multiple molecular properties (Spiller et al., 2010; Megason and Fraser, 2007) and with a high enough throughput to obtain statistically sound insights.

But the bad news is that there is no universal answer to how best to image cells long-term. Imaging has always been a difficult issue that is supposed to be optimized according to the questions that we ask. Moreover, we have to always keep in mind that what is good for pictures and cell tracking is bad for the cells. The best approach will depend on several factors: the biological question, the cell types to be observed and their required culture conditions, the necessary cell incubation hardware and its compatibility with imaging hardware, the available image-acquisition software and the image-processing hardware and software, and the brightness of molecular reporters (Schroeder, 2011). Imaging can be highly invasive and quickly kills cells or changes their behavior under the wrong conditions. Typical imaging optimizations that lead to cell stress include

phototoxicity resulting from long or frequent exposure to excitation light, changed the culture medium or surface, and medium evaporation or changing the gas composition owing to non-airtight incubators (Schroeder, 2011). Although problematic for imaging of any living cells, these changes will affect sensitive primary stem cells even more.

Imaging experiments involve many layers of interdependent hardware and software components that must inevitably be optimized. It will often not be the lack of a cutting-edge microscope that inhibits the success of an experiment but the lack of compatible peripheral components. These include incubation, gassing and feeding devices with the required optical quality, ease of use and robustness; flexible, robust, fast and user-friendly software for microscope and incubation control; data management and backup systems; and computers with the right software for handling and analysing the massive amounts of electronic data generated via long-term imaging. Bringing these components together requires experience, compromise and multiple rounds of incremental optimizations (Schroeder, 2011).

One powerful method to rapidly investigate gene function combines RNAi with bacterial artificial chromosome (BAC) recombination technology and is called BAC transgenomics (Kittler et al., 2005). In transgenomics a BAC carrying a third allele of the gene of interest is introduced and stably integrated into the genome of the host cell. To facilitate selection and further biochemical analysis, the BAC containing the gene of interest is modified via homologous recombination in *E. coli* employing bacteriophage enzymes (Zhang et al., 1998). Usually, a tag that contains a fluorescent marker (GFP) for localization studies in addition to other features useful for downstream applications e.g. affinity purification is fused during the recombination process. After recent technological developments, BAC recombineering has become a highly efficient and high throughput method, which can be carried out in multiple samples (Poser et al., 2008). Recombineering procedure starts first with finding a suitable BAC containing the gene of interest and suitable primers are identified using the software BAC finder([www.mitocheck.org/cgi-bin/BACfinder](http://www.mitocheck.org/cgi-bin/BACfinder))(Hutchins et al., 2010). The BAC

is then typically ordered from a resource center which normally provides the plasmid as a bacterial stab culture and all the remaining recombineering modifications are performed in *E. coli*. The advantage of using homologous recombination in *E. coli* for BAC modification is, that it alleviates the limitations of the use of restriction enzymes (Figure 3.1). Because the integration site is defined through homologous regions, which are stretches of DNA shared by the DNA molecules that recombine, a wide range of DNA modifications at any chosen position and unlimited by fragment size is easily possible (Muyrers et al., 2001). Due to the fact that homologous arms of only 35 to 60 nucleotides are sufficient for successful recombination (Poser et al., 2008), they can be generated through oligonucleotide synthesis and subsequently attached to the DNA fragment via polymerase chain reaction (PCR) resulting a linear PCR fragment, which exhibits gene-specific homology arms on both ends. In the downstream process, an antibiotic resistance easily identifies bacteria carrying the inserted cassette through drug selection.

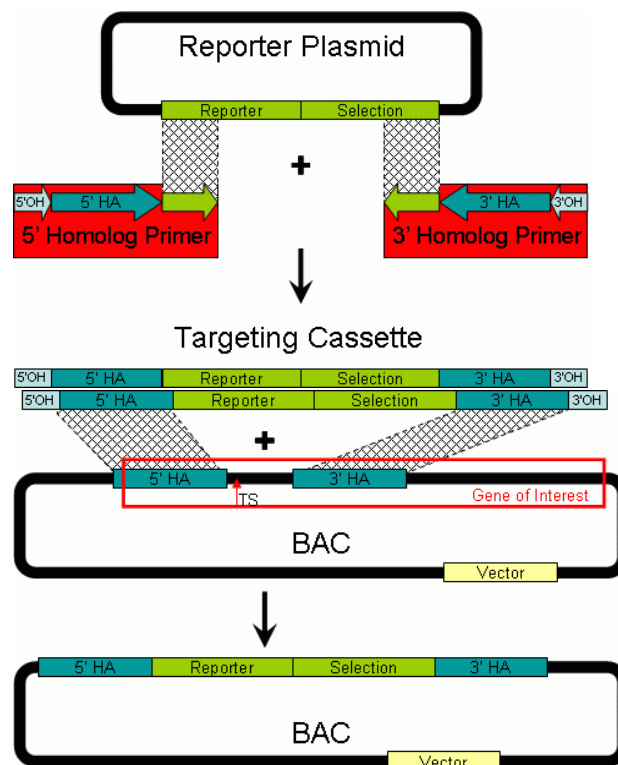


**Figure 3.1: The procedure of BAC recombineering.** Targeting cassette can be generated by PCR to introduce the region of homology (in blue), a selectable marker (e.g. Neo, Kanamycin/Neomycin resistance gene) and the reporter gene (e.g. GFP) (in green). The PCR primers used to generate the targeting construct are usually 35-60 oligonucleotides with 20-30 nucleotides corresponding to the target site sequence to introduce the homology arm and 20-30 bases from the ends of the selectable marker. The targeting cassette is electroporated into the bacterial cells that are induced to express the phage recombination genes. Recombinant clones

are selected as resistant colonies and confirmed with PCR. (adapted from [http://www.fmi.ch/groups/roska.b/eBAC/eBAC\\_help.htm](http://www.fmi.ch/groups/roska.b/eBAC/eBAC_help.htm))

Correct insertion of the tagging construct is verified by checking clones by a PCR reaction that amplifies the region around the insertion site. Afterwards, the purified BAC DNA is transfected into cultured mammalian cells, mostly via lipofection. After selection of the marker carried on the modified BAC, cell pools stably expressing the tagged transgene are used for downstream analyses (Ding et al., 2012). Because BACs are much larger (up to 250 kb and more) than conventional cDNA constructs and harbor the gene of interest in its genomic context, they also frequently contain the endogenous regulatory sequences that control the expression levels of the gene and this allows for expression of the tagged protein at near physiological levels, (Sarov et al., 2006). Additionally BAC transgenes also retain all *cis*-regulatory elements in the native configuration in addition to alternative splice isoforms, translational and miRNA controls and alternate polyadenylation sites (Ding et al., 2012). Subsequently, BACs are a more accurate way of probing protein function than traditional studies based on cDNA, which commonly use viral promoters that have problems with deregulation and overexpression (Bird et al., 2012).

## Results

After transfection of BACs of chTOG-GFP and Kif18A-GFP, we first wanted to see whether genes are producing proteins at appropriate sizes. For this purpose, we have checked the protein expression levels and protein sizes by Western blotting. Cell lysates of the stably transfected cells have been collected and they were resolved by SDS-PAGE. As the negative control, we have used the untransfected mES cells. After detection with anti-GFP antibody, we have seen that chTOG-GFP has given a band above 200 kDa band showing the expression of chTOG-GFP. On the other hand, we have also observed many other bands, which were smaller than the expected size. They are most probably alternative splicing forms or degradation products that were produced during lysate preparation. Similarly, we have seen a single band in the Kif18A-GFP cell line indicating the proper expression with its correct band size around 100 kDa. The absence of any GFP signal in the negative control further confirmed the specificity of the GFP antibody and the presence of GFP-tagged proteins in stable mES cell lines (Figure 3.2A).

Our next question was whether the expression of transgenes was affecting the pluripotency of mES cells or not. This was quite important because ES cells have a high tendency to differentiate when the endogenous and exogenous conditions are relevant. Although we keep the expression of the transgene as low as possible by adding one allele to cell at their endogenous expression levels, they could still generate different cell populations from a pluripotent stem cell. Due to this fact, we have carried out again Western blot with our cells at 10 passages after transfection with antibodies against TUBB3 and Oct-4. TUBB3 was a marker for neurons and Oct-4 for stem cells. As positive and negative controls for western blots we have used the total mouse brain lysate and we have performed the immunoblottings (Figure 3.2B). Results showed that both of our BAC-transfected cell lines and WT mES cell line were negative for TUBB3 gene, indicating that they are not transfected to neuronal lineage, which is the most easily differentiable lineage. Furthermore, our cells were still positive for Oct-4 expression, even with some increase in chTOG-GFP and Kif18A-GFP. Brain lysate

was negative for Oct-4 expression as expected. Same amount of protein loading was checked by alpha-tubulin expression.

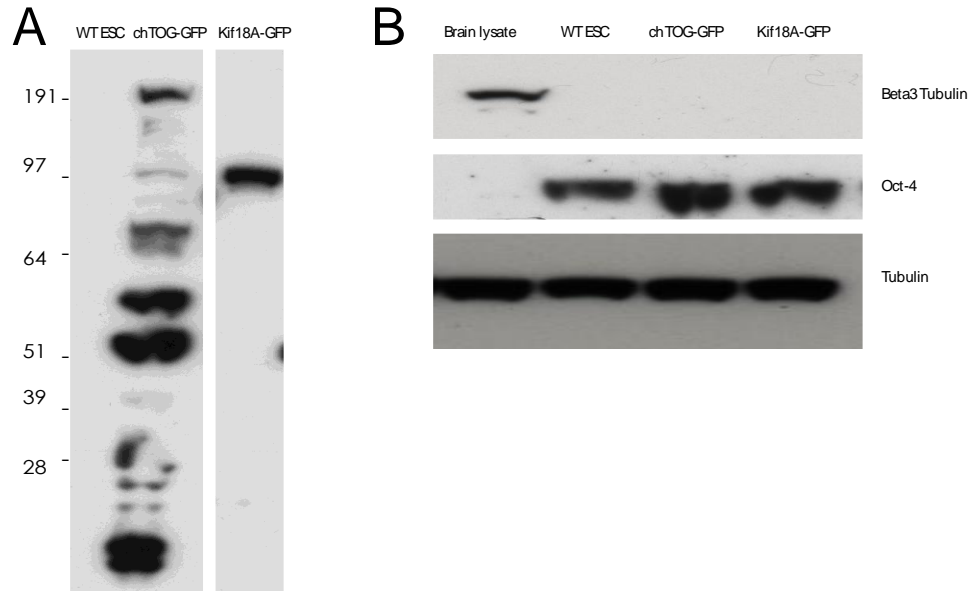


**Figure 3.2: Western Blotting controls.** A panel shows the BAC expression and B panel ES cells and differentiation marker expressions

The second step in the characterization was to check their subcellular localizations in the cell. Because chTOG is a known microtubule polymerase (Brouhard et al., 2008) and centrosome stabilizing protein (Gergely et al., 2003), it was supposed to be present on centrosomes and spindle. When we stain the fixed cells with anti-GFP, anti-TUBB and DAPI, we have seen that the GFP signal was present on centrosomes and spindle during prometaphase and metaphase (Figure 3.3). But after the anaphase onset, it shows a distributed pattern throughout the cytoplasm with some chTOG still at the poles and finally at telophase chTOG loses its specific localization and observed in cytoplasm having an almost homogenous distribution. Additionally, chTOG is totally absent at the midbody of dividing cells, showing that microtubules depolymerize during final separation of two daughter cells.

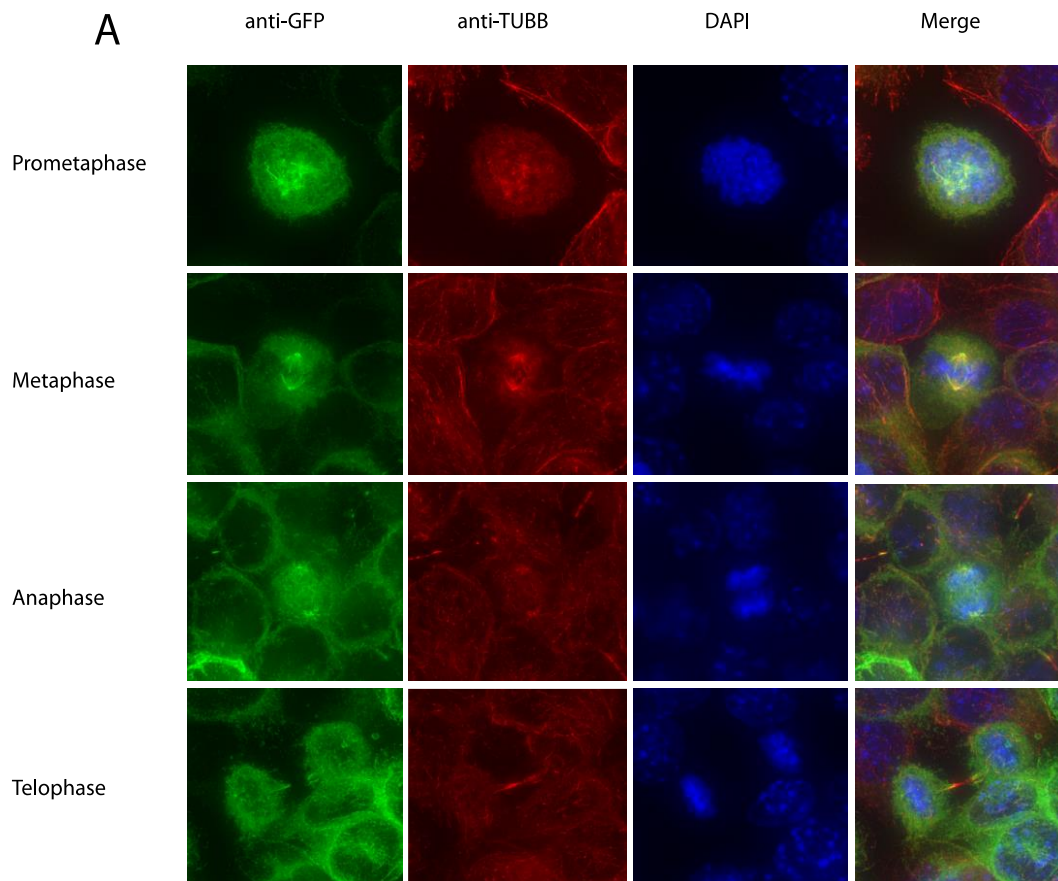


**Figure 3.3: The localization of chTOG-GFP in mitosis.** chTOG-GFP is present on the spindle microtubules starting from the very beginning of the mitosis. It intensively localizes to centrosomes and spindle in metaphase and with anaphase onset this localization disappears. In telophase it is specifically absent from the midbody and shows a cytoplasmic distribution.

On the other hand, Kif18A-GFP shows a little bit different localization patterns. It is mainly present in the nucleus of interphase cells and with the onset of nuclear envelope breakdown it starts to localize on the spindle. One interesting thing was that it is almost absent from the centrosome area by mainly localizing on the kinetochore and interpolar microtubules. (Figure 3.4)



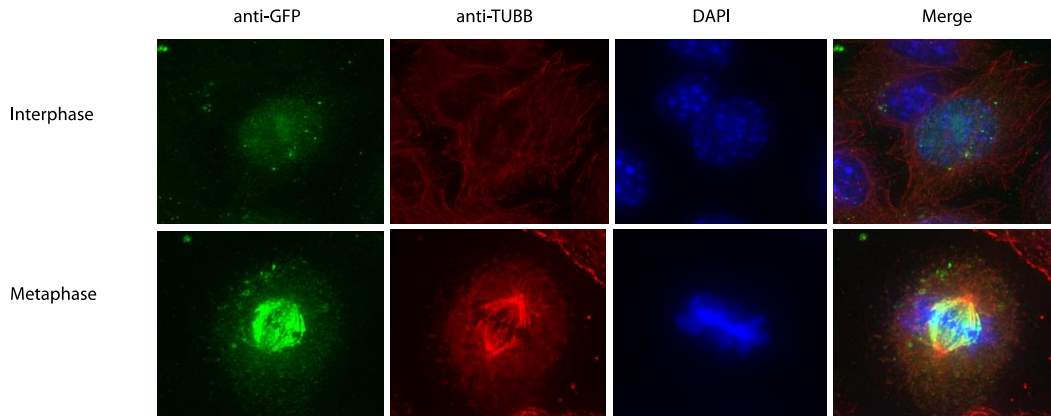


**Figure 3.4: The localization of Kif18A-GFP.** Kif18A-GFP localizes to nucleus in interphase but in metaphase it is mainly found on the spindle part excluding the centrosomes.

Our next step was to visualize these proteins *in vivo* to be able to see their dynamics during mitosis. We performed live-cell imaging of chTOG-GFP and Kif18A-GFP cell lines with high spatio-temporal resolution to confirm the staining results. We used 60X objective with 200nm/pixel spatial and 10s/frame time resolution. Our results were in agreement with immunofluorescence data indicating the strong centrosomal localization of chTOG during mitosis (Figure 3.5).

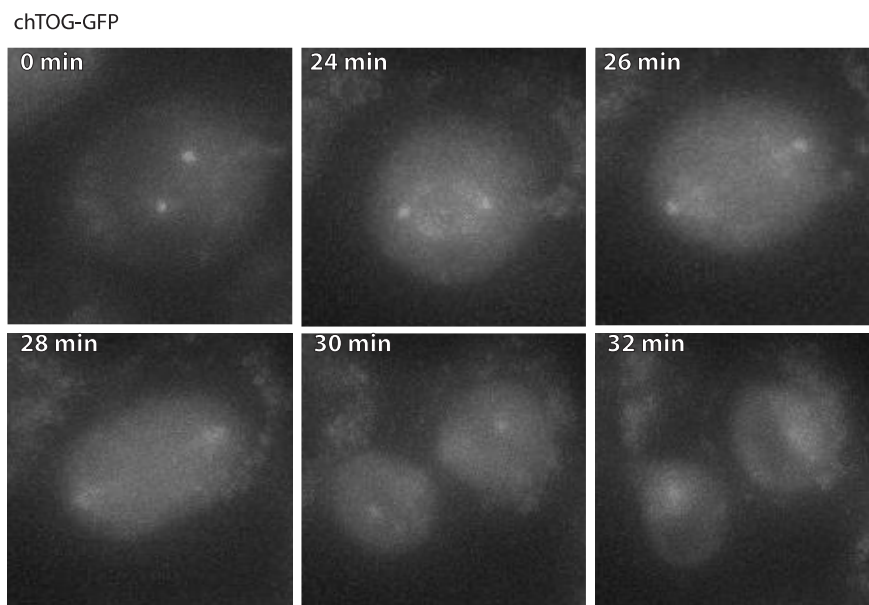


**Figure 3.5: The live-cell imaging of chTOG-GFP cell line.** Cells were imaged under 60X objective at 10 sec/frame time resolution. GFP-labeled proteins mainly localize on centrosomes during mitosis and to a lesser extent to the spindle. They are not present at midbody in telophase.

Kif18A movies were showing the presence of Kif18A on the spindle except centrosomes (Figure 3.6). Additionally, there was a kind of accumulation of Kif18A as spots at the tips of kinetochore microtubules in metaphase. This strong signal was suddenly abolished with the anaphase onset and then Kif18A started to condense on interpolar microtubules in anaphase B. This condensation resulted in a highly dense Kif18A signal in the midbody pointing that Kif18A might be involved in the regulation of microtubule dynamics, probably in depolymerization, at the final cleavage site.

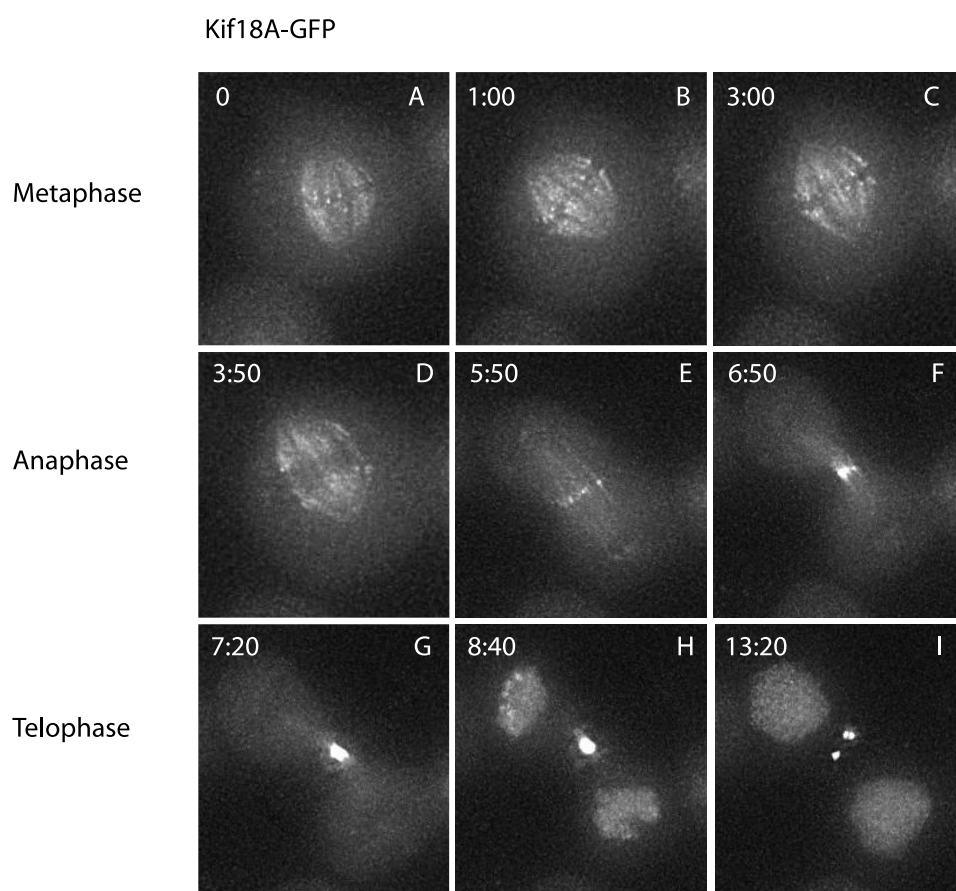


**Figure 3.6: The live-cell imaging of Kif18A-GFP cell line.** In metaphase, Kif18A-GFP is mainly found on the spindle showing accumulations at the kinetochore sites of kinetochore microtubules. With the anaphase onset this accumulation signal disappears and with the beginning of cytokinesis Kif18A starts to localize on interpolar microtubules at the cleavage site. Towards the end of cell division, it begins to translocate into nucleus and shows nuclear localization.

Next goal was to generate a system, which was suitable for the high-throughput analysis of mitosis and long-term imaging. For this purpose we have chosen to

use the TUBB as mitotic spindle and histone as the chromosome markers. We have transfected the wild-type ES cells with TUBB-GFP BAC and selected single clones with G418. On the other hand, we have cloned the H2A gene into pBUD-mCherry vector and then transfected the single clones with this plasmid and selected again with Zeocin. Then we have tested the double-labeled cell line for imaging.

First we did short-term imaging to see whether the localizations of markers were correct. By using 10sec/frame rate, we have imaged our double-labeled cell line in Delta-vision microscope and confirmed that TUBB-GFP localizes to the mitotic spindle and H2A-mCherry to the chromosomes during mitosis (Figure 3.7).

### TUBB-GFP, H2A-mCherry

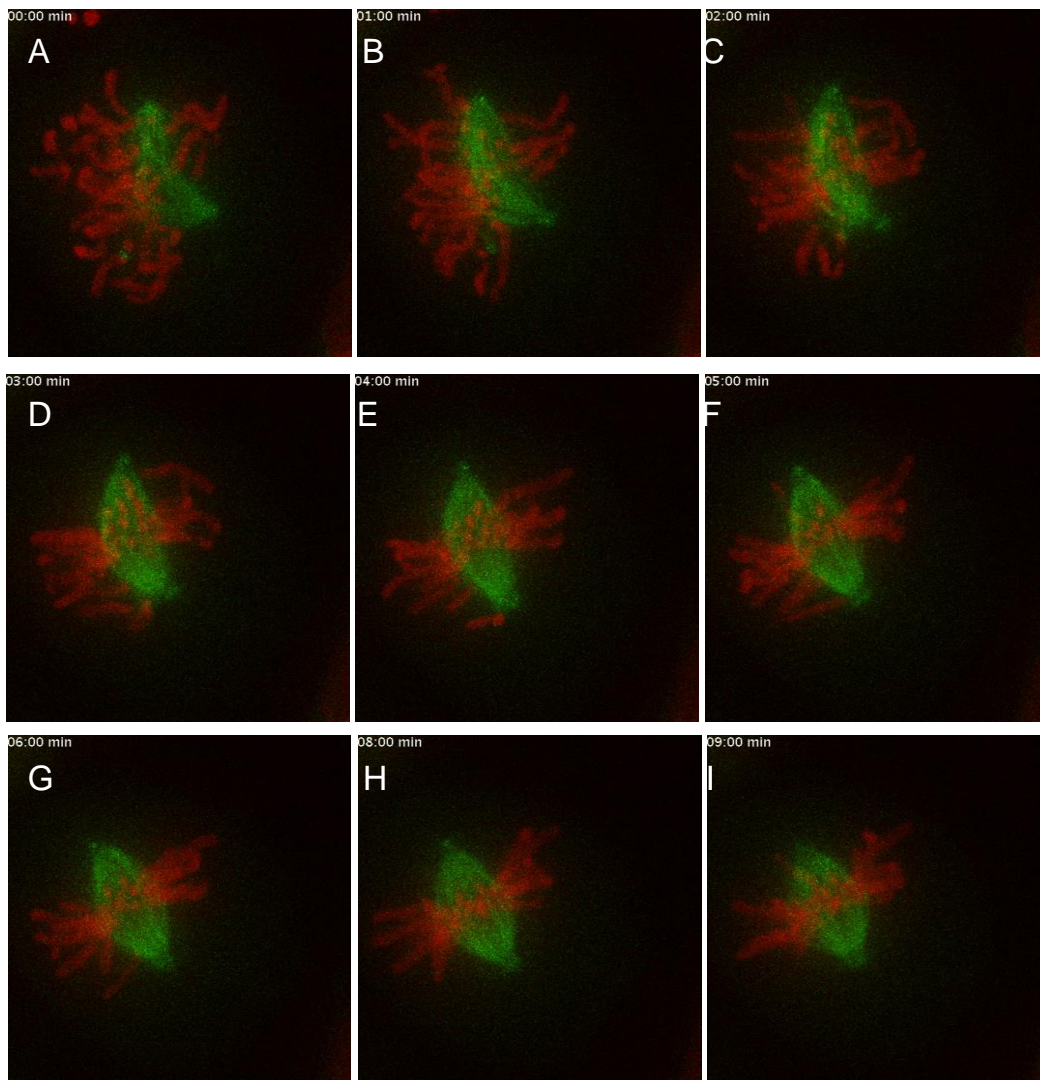


**Figure 3.7: Short-term live-cell imaging of TUBB-GFP&H2A-mCherry mES cell line.** Double-labeled cell line is imaged at 10sec/frame rate under 100X objective for 10 minutes. TUBB-GFP localizes to the mitotic spindle and H2A-mCherry to chromosomes in this dividing cell.

After this we performed long-term imaging of mES cells by decreasing the frame rate to 2 min/frame and increasing the total imaging time to 24 hours. In this set-up, we have also decreased the magnification by using a 40X objective, to be able to reduce the photo-toxicity and bleaching on samples. The exposure times for mCherry and GFP were set up as 5 ms for each and images were collected from 6 different sections in a total of 12  $\mu\text{m}$  thickness. Images were quite satisfactory in terms of their signal to noise ratio, fluorescent signal was stable

during imaging without any bleaching and cells did not show any sign of cell death (Figure 3.8).

Although this imaging set-up looked fine in different aspects, we encountered with some problems at later passages of cells. When we repeated the experiment with cells at passage 15, we have seen that most of the cells have lost their H2A-mCherry expressions, although they were still under the selective pressure of Zeocin (Figure 3.8). TUBB-GFP expression was influenced by the passage number, probably because it was controlled by its own promoter and regulatory elements.

### TUBB\_GFP&H2A\_mCherry Cell Line

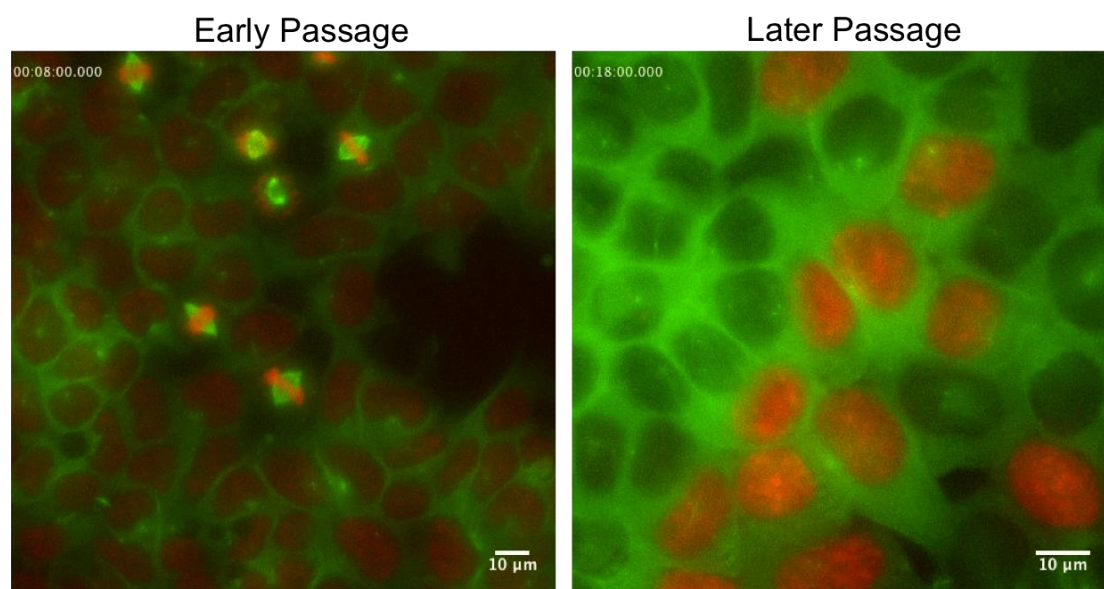


**Figure 3.8: Long-term imaging of TUBB-GFP and H2A-mCherry cell line at early (5) and late (15) passages.** In the imaging of early passage cells, 40X objective was used and imaging was carried out at 2min/frame rate for 24 hours. Late passage cells were imaged with 60X objective at 2min/frame rate for 24 hours. Images were collected from 6 optical sections in 12 uM thickness and maximum projected afterwards.

## Discussion

Embryonic stem cells are very powerful biological tools that are used in understanding development, regeneration and oncogenesis. Although there are many recent advances in the isolation, characterization, differentiation and tracking of these cells, there are some limitations in the imaging of ES cells. These limitations come from the natural characteristics of them such as genetically silencing of viral promoters, spherical-colony formation in cell culture and high levels of sensitivity to photodamage. In this chapter, I have presented you how we have tackled with these problems to be able to image ES cells at high spatio-temporal resolutions. We have solved the fluorescent labeling problem by using Bacterial Artificial Chromosomes (BAC), in which the proteins are expressed from their own endogenous promoters at their almost physiological levels. Tagging of cells by BAC gave stable protein expressions without any sign of gene silencing. The spherical shape of ES cell colonies was preventing the spatial resolution of ES cells due to their 3D feature. By using laminin-511, which is a substrate that supports the pluripotency of ES cells, we could obtain nice flat cells that were perfectly suited for imaging. Lastly, we solved the very important phototoxicity issue by combining the widefield microscopy and post-imaging techniques to enhance the signal to noise ratio. By keeping the light exposure as low as possible and absorbing the free radicals by anti-oxidants in the imaging medium, we could make survive and divide the ES cells as long as 24 hours on the stage.

BACs are very valuable tools in mediating physiological gene expression. Because the endogenous promoters of genes regulate the amount of gene product that is produced, the synthesized protein amount is somewhat always controlled or does not interfere with cellular processes. Regarding that embryonic stem cells are very prone to rapid transitions in their cellular state depending on the gene expression levels, it is necessary to strictly control the gene expression to be able to keep the cells at their pluripotent state. BAC transgenomics is highly advantageous from this respect compared to constitutively active expression constructs, because it does not favor the

production of a silenced gene in the ES cells. However, it might be also disadvantageous if the promoter of the gene of interest is heavily suppressed in ES cells. In such a case, the signal could not be detected. Moreover the use of BACs is a quite convenient way to reduce the photo damage during live-cell imaging. Because there is an uncontrolled expression from a constitutively active promoter, the amount of fluorescent reporter will also increase in the cell and during image acquisition there will be an increased amount of free radical production in the cell that will eventually lead to the oxidative stress and therefore cell death.

For the mitotic analysis of cells, we wanted to create a TUBB-GFP and H2A-mCherry expressing cell line. For double labeling of ES cells we had to choose a good promoter that is resistant to gene silencing in ES cells. This was because a cell could not be transfected by a second BAC, which can disrupt the genomic stability due to their large sizes. For this reason, we have selected the TUBB-GFP BAC labeled cell line and cloned the H2A gene into an expression vector. In Chung et al., 2002, various overexpression promoters have been analyzed in terms of their robustness in embryonic stem cells. After comparisons of the elongation factor 1 alpha (EF), chicken beta-actin (CBA) and viral cytomegalovirus (CMV) promoters, they have found that when transiently transfected, the EF and CBA promoters robustly drove reporter gene expression, while the CMV promoter was inactive. They have also demonstrated that the EF and CBA promoters effectively drove gene expression in different stages of cell development: naïve ES cells, embryoid bodies (EBs), and neuronal precursor cells. In contrast, the CMV promoter did not have transcriptional activity in either ES cells or EB but had significant activity once ES cells differentiated into neuronal precursors. These results showed that viral promoters were inefficient to express genes in ES cells, most probably due to the epigenetic suppression of gene expressions to prevent any dosage effect in further developmental stages. By taking this study as a reference, we have chosen the EF1 promoter to control the H2A expression. After the stable transfection and selection of TUBB-GFP cell line with H2A-mCherry, we could image the cells for short and long-term under microscope, however we have observed that after increasing passage number



and freeze-thawing cycles, the expression of H2A was decreasing. The cells were kept under selective antibiotic pressure, we were sure that all the cells were carrying H2A-mCherry in their genome in a stable manner. After this unsuccessful attempt to create a stable double-labeled cell line, we have concluded that even the mammalian mild-expression promoter EF1-alpha was not stable enough as the BAC system. And afterwards we decided to move on with a single BAC labeled TUBB-GFP and H2A-GFP cell lines to investigate the roles of MAPs in the spindle assembly and mitosis that will be covered in the next chapter.

Cell culture conditions during imaging are also very important parameters that need to be well optimized. It depends on the type of media, buffer system, supplements added and the use of CO<sub>2</sub> during imaging. In our system, we used CO<sub>2</sub>-independent medium instead of DMEM and supplemented it with the same components as in DMEM plus Trolox. This medium was supporting the growth of cells, even in the absence of CO<sub>2</sub>. Moreover it did not direct the cells to differentiation. There are also other CO<sub>2</sub> independent media formulations for imaging such as the use of phenol-red media medium buffered with HEPES. However, we have observed that HEPES buffer could not keep the pH stable for a long time and this situation causes of the death of the cells. Therefore we argue that HEPES-based media formulations are not convenient for long-term imaging of ES cells. Moreover, the addition of Trolox lowers the phototoxicity by its anti-oxidative functions, leading to a less stressful environment for the growth of cells.

Because mouse ES cells are growing in clusters, it is difficult to observe single cells in the colony due to their orientations. In our system, we utilize laminin-511 coating on the glass chambers that directs the cells to spread and grow as a monolayer. Laminin-511 has been shown to support the growth of human (Rodin et al., 2010) and mouse ES cells (Domogatskaya et al., 2008) and it helps to keep the cells at their pluripotent state in both mammalian systems. Because of laminin-511 increases the attachment of cells to the substrate, it produced flat cells, which were excellent for fixed and live-cell imaging. In our hands we could



successfully image the ch-TOG, Kif18A and MCAK labeled cell lines, both after methanol fixation or as live on stage with very high spatial resolutions, which can enable the analysis of their subcellular localizations.

## **4. Effects of MAPs in the ES Cell Spindle Assembly and Mitotic Progression**

The mitotic spindle is a machinery that functions in the proper segregation of chromosomes during cell division. The spindle is built up of microtubule polymers that organize into a bipolar structure and its highly specialized morphology is very important for its function. In this chapter we have analyzed the effects of +TIP binding proteins chTOG, EB1, Kif18A and MCAK in the overall morphology and mitotic progression in mES cells. For this purpose, we have utilized our stable TUBB-GFP and H2A-GFP cell lines along with our live-cell imaging set-up to reveal the effects of the above-mentioned proteins and their interplay among each other. By using RNAi method we have either single or co-depleted the genes by siRNAs and measured the spindle length and width in RNAi conditions. We further analyzed the mitotic progression in H2A-GFP cell line in terms of the metaphase timing and the percentage of chromosome segregation errors. Our results showed that, EB1 depletion did not cause any significant changes in the overall spindle morphology or in the metaphase timing. However, the co-depletion of EB1 with chTOG has partially rescued the chTOG specific mini-spindle phenotype. siKif18A produced longer spindles without any change in the spindle width. Surprisingly, the co-depletion of antagonistic chTOG and Kif18A proteins had additive effects on the spindle dynamics and on mitotic progression in a way that spindle assembly was severely disrupted by the absence of these two proteins as a result of this both metaphase timing and chromosome missegregation levels increased significantly. These results overall indicate that +TIP proteins have important roles in the regulation of dynamic instability and these proteins have an interplay among each other to be able to control the morphology of the spindle as well as the correct segregation of chromosomes into daughter cells.

## **Introduction**

Division of one cell into two daughter cells occurs through two processes, these are mitosis and cytokinesis. The mitotic spindle is the structure, which is assembled by a dynamic array of microtubules facilitate these processes to ensure the proper segregation of DNA content into newborn cells.

Spindle bipolarity is the key feature of spindle structure, which is made up mainly by the anti-parallel arrangements of microtubules. Centrosome or MTOCs are duplicated prior to the spindle formation and this provides a cue for bipolarity (Helmke et al., 2013). Microtubules can also generate bipolar spindles even in the presence of multiple centrosomes, showing a high degree of microtubule organization during spindle assembly (Godinho et al., 2009).

The mitotic spindle is built up of three different microtubule populations. They are kinetochore fibers (k-fibers), spindle (interpolar) microtubules and astral microtubules (Figure 4.1). K-fibers connect the kinetochore of each sister chromatid to the pole of the spindle. In simple organisms such as yeast k-fibers consist of a few microtubules (Winey et al., 1995) while in advanced species they are usually 20-30 (McEwen et al., 1997). K-fiber microtubules have a highly regulated dynamics during mitosis and they continue to grow and shrink even after kinetochore attachment is maintained (Guo et al., 2013). This dynamic behavior is absolutely necessary for the congression of chromosome to the metaphase plate prior to segregation (Helmke et al., 2013). A second population is spindle microtubules or interpolar microtubules. They are quite short compared to k-fibers and reside within the single half of the spindle. They function as to support the rigidity of the spindle to resist to pole-to-pole compression and it may provide a pool of microtubules to maintain k-fibers (Helmke et al., 2013). Depletion of spindle microtubules from *Xenopus* egg cell extract spindles showed that they are important in establishing the k-fiber dynamics and for maintaining the spindle size (Houghtaling et al., 2009). Astral microtubules are a subpopulation of mitotic microtubules that project outward toward the cell cortex. Although they are found in most of the spindles, they can

be absent in female meiotic spindles and in plant spindles that lack centrosomes (Helmke et al., 2013). They are basically not required for the progression of mitosis, but they are important to ensure the fidelity of the process. Astral microtubules localize to the region between the spindle pole and cell cortex and therefore its function is generally considered as determination of cell geometry. They are absolutely required for correct positioning and orientation of the mitotic spindle apparatus (Mitchison et al., 2012), and are thus involved in determining the cell division site based on the geometry and the polarity of the cells (Rankin and Wordeman, 2010).

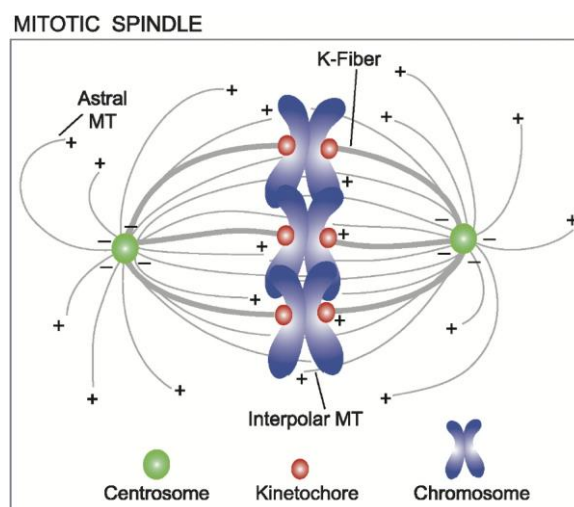


**Figure 4.1: Different microtubule populations in the spindle.** K-fibers connect the kinetochores of each sister chromatid to the pole of the spindle. Spindle or interpolar microtubules function as to support the rigidity of the spindle to resist to pole-to-pole compression and it may provide a pool of microtubules to maintain k-fibers. Astral microtubules are a subpopulation of mitotic microtubules that project outward toward the cell cortex to ensure the fidelity of the process (adapted from Kline-Smith and Walczak, 2004).

Spindle morphology is an interplay among the kinetochores microtubules, spindle microtubules and astral microtubules. MAPs that bind to and regulate the dynamics of these microtubule populations also determine its morphology. We can define the morphology as spherical, elliptical or banana-shaped according to the ratios of spindle length to its width.

Spindle length has been intensively studied over the last years because the size of the metaphase spindle is a key factor that affects the positioning of chromosomes at the centers (Bringmann et al., 2007). Furthermore, the extent of

anaphase B separation is also influenced by the length of metaphase spindle to determine the final position of spindle poles. A second mechanism related to spindle length is the formation of cleavage furrows after anaphase because there has to be a minimum spacing between asters to initiate the entry into cytokinesis (von Dassow et al., 2009). Apart from the mitotic mechanics, spindle length is constant in a given cell type (Figure 4.2) showing that deviations or disturbances from this specific spindle length size may affect the fate of cells (Dumont et al., 2007; Goshima and Scholey, 2010).

System	Cell length <sup>a</sup>	Metaphase spindle length	Postanaphase B spindle length	References
<i>S. cerevisiae</i>	8 $\mu\text{m}$	2 $\mu\text{m}$	10 $\mu\text{m}$	Straight et al. (1998); G. Goshima, personal observation
<i>S. pombe</i>	15 $\mu\text{m}$	2.5 $\mu\text{m}$	12–15 $\mu\text{m}$	Nabeshima et al. (1998)
<i>C. elegans</i> single-cell embryo	43 $\mu\text{m}$	15 $\mu\text{m}$	25 $\mu\text{m}$	Hara & Kimura (2009)
<i>C. elegans</i> meiosis I/II	45 $\mu\text{m}$	7.7 $\mu\text{m}$ /6.2 $\mu\text{m}$	5.7 $\mu\text{m}$ /5.0 $\mu\text{m}$	McNally et al. (2006); F. McNally and A. Fabritius, personal communication
<i>Strongylocentrotus purpuratus</i> (sea urchin)	30 $\mu\text{m}$	20 $\mu\text{m}$	30 $\mu\text{m}$	Foe & von Dassow (2008)
<i>Drosophila</i> embryo (cycle 11)	–	11.8 $\mu\text{m}$	16 $\mu\text{m}$	Brust-Mascher et al. (2009)
<i>Drosophila</i> S2 cell (flattened)	23 $\mu\text{m}$	10 $\mu\text{m}$ (pole to pole) or 11.5 $\mu\text{m}$ (centrosome to centrosome)	18 $\mu\text{m}$ (pole to pole)	Goshima et al. (2005b); I. Matos and H. Maiato, personal communication
<i>Danio rerio</i> (zebrafish) single-cell stage	500 $\mu\text{m}$	~35 $\mu\text{m}$ (pole to pole) or ~55 $\mu\text{m}$ (centrosome to centrosome)	~200 $\mu\text{m}$ (centrosome-to-centrosome distance at onset of cytokinesis)	M. Wuhr, personal communication
<i>X. laevis</i> meiosis II	1,200 $\mu\text{m}$	30 $\mu\text{m}$	–	Wuhr et al. (2008); M. Wuhr, personal communication

**Figure 4.2: Spindle length sizes in different cell types.** Metaphase spindle length is characteristic and predictable for any given cell type but varies considerably across cell types. In smaller cells (<200  $\mu\text{m}$ ), spindle size increased approximately linearly with cell length. In larger cells, however, the length of the spindle did not increase significantly in relation to cell length but instead asymptotically approached a maximum length of 60  $\mu\text{m}$  (adapted from Goshima and Scholey, 2010).

## Results

In this chapter, we investigated the roles of main microtubule dynamics regulators during cell division and their interplay among them. For this purpose, we set up a live-cell imaging system that was described in the part and after single or double siRNA treatments, cells were imaged for 12 hours. In our experiments we have utilized the TUBB-GFP expressing mouse ES cells line and primarily focused on 4 different genes. They are mammalian XMAP215 homologue chTOG (CKAP5), kinesin-8 protein Kif18A, kinesin-13 member depolymerase MCAK and ubiquitously expressed end-binding protein EB1. After single and double co-depletions of these genes, we have analyzed how they affect the spindle morphology and along with mitotic timing and fidelity. After post-imaging analysis, spindle length, spindle width and cell length were quantified in Fiji (ImageJ).

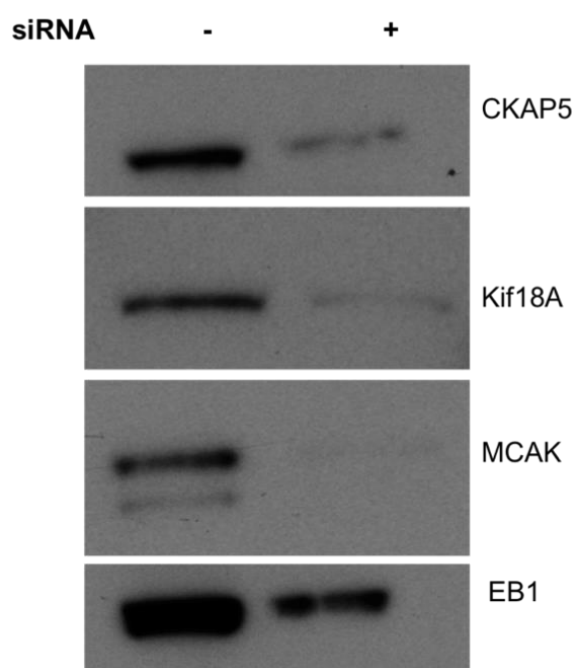


**Figure 4.3: RNAi knockdown of chTOG, Kif18A, MCAK and EB1 genes.** BAC-GFP expressing cells were transfected with the siRNAs and protein expression levels were analyzed by Western blotting with anti-GFP antibody.

We started with RNAi experiments, by first checking the efficiency of RNAi knock-down. For this purpose, we transfected BAC-expressing chTOG-GFP,

Kif18A-GFP, MCAK-GFP and EB1-GFP mES cell lines with the siRNA oligos and analyzed the protein expression levels by anti-GFP antibody after 48 hours. Our results showed that MCAK was almost completely knocked out and we could obtain more than 80% knocking down for chTOG and Kif18A. In EB1 there was still some protein left in cells, but knocking down efficiency was still more than 50-60% (Figure 4.3).

Then we imaged the TUBB-GFP labeled mES cells after siRNA transfections and we have observed some phenotypical changes in their spindle morphologies (Figure 4.4). In the siLUC transfected control cells, we have seen bipolar diamond shaped spindles. However, in the sichTOG cells, both the spindle size decreased quite a lot and also the fluorescence intensity of the GFP signal coming from TUBB-GFP diminished. This shows that the knockdown of a MT polymerase results in a decrease of tubulin incorporation into the spindle MTs and therefore affects both the size and MT intensity of mitotic spindles. On the other hand, siKif18A showed its effect in an opposite way, it caused an increase in the spindle length, generating bent banana shaped spindles. Because the antagonism between TOG and kinesin-8 families is shown in other systems (Brouhard et al., 2008; Varga et al, 2009), this outcome was not surprising. Although chTOG and Kif18A knockdowns showed some changes in the spindle morphology, we could not observe any effect of siEB1 or siMCAK. The mitotic spindle preserved its integrity in the absence of these two proteins.

The co-depletion experiments with siEB1 and other three MAPs gave quite interesting results. The double knock-down of EB1 with chTOG could partially rescue the minispindle phenotype of sichTOG giving longer and more tubulin-rich spindles. The morphological problems with siKif18A cells still continued in EB1 knockdown, so it could not totally or partially rescue the long spindles. It did not cause any change in siMCAK spindles, the double knockdown of two inefficient proteins EB1 and MCAK did not affect the spindle.

### Mitotic Spindle Phenotypes

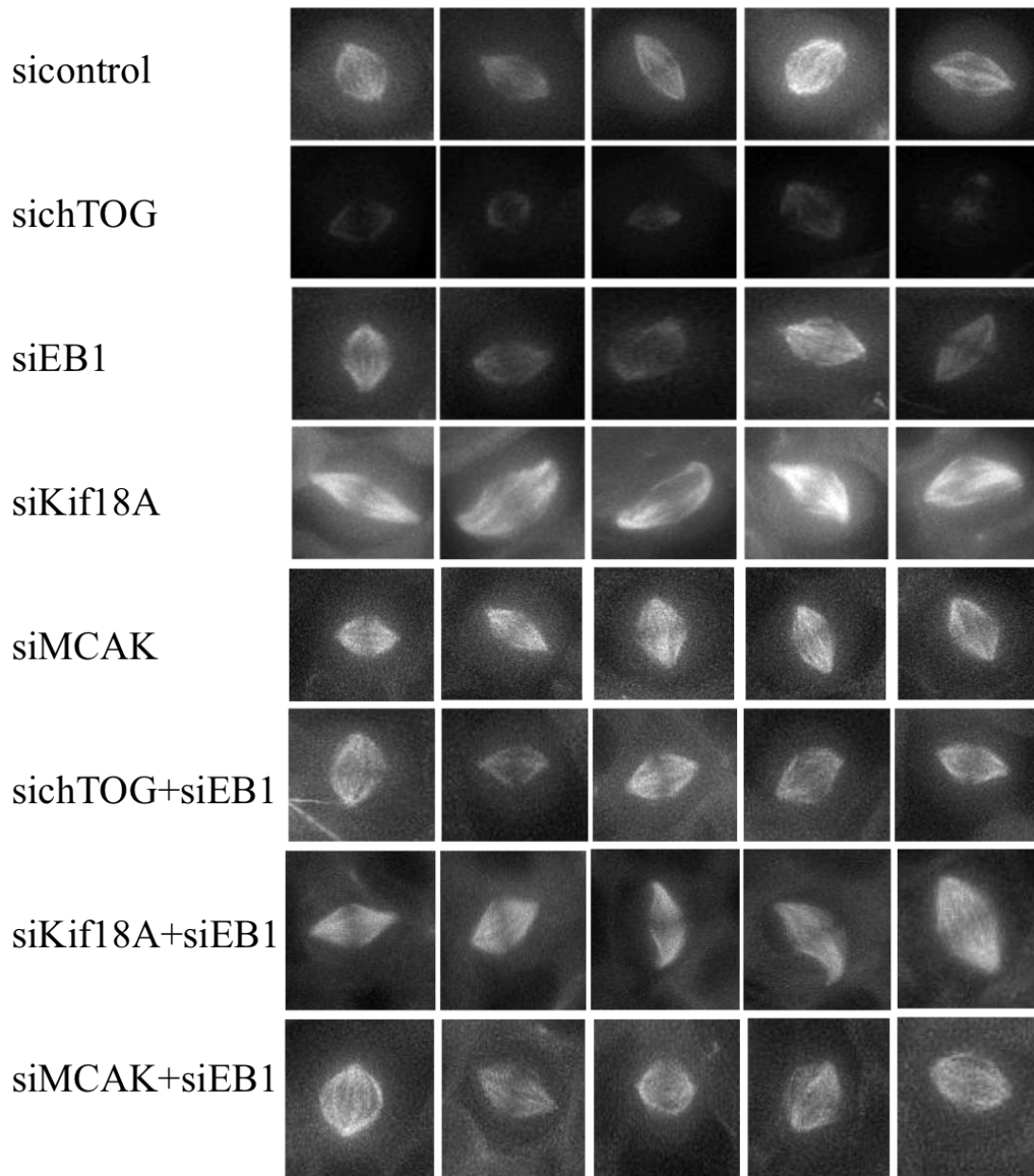


**Figure 4.4: Spindle morphologies after single and double gene knock-downs.** siRNA treatments were carried out in 8-well imaging chambers and after 48 hours of transfection, TUBB-GFP cells were imaged under 60X for 12 hours. Representative spindles were chosen from 3 experiments. In control cells, the mitotic spindle has a bipolar diamond-shaped structure. In sichTOG cells, the intensity of microtubules in spindle decreases significantly and they have a shorter spindle size and width. siEB1 and siMCAK cells do not show any prominent phenotype, they look more or less like control cells. Kif18A depletion causes longer and banana-shaped spindles. In the co-depletion experiments of sichTOG, siKif18A and siMCAK with siEB1, EB1 co-depletion partially rescues the minispindle phenotype of sichTOG cells whereas it does not lead to any change in siKif18A or siMCAK.



Phenotypical changes were clear in the spindle morphologies after RNAi but we wanted to quantitatively analyze them to better understand any relationship among them. For this reason we measure the lengths and widths of spindles as defining the length (L) as the distance from pole to pole and width (W) as the wideness of spindle microtubules (Figure 4.5). First we have analyzed the spindle length. Mitotic spindle is a subcellular machine that uses microtubule-based force generators and a network of regulators first to assemble itself and then to mediate the chromosome segregation (Goshima and Scholey, 2010). Therefore, the changes in the microtubule dynamics directly affect the microtubule length and consequently the spindle length in mitosis.

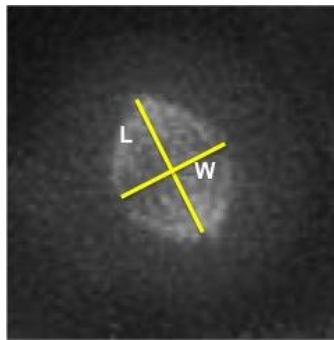


**Figure 4.5: Spindle length (L) and width (W).** Spindle length is measured as the distance from pole-to-pole and spindle width as the width of the metaphase plate after chromosome alignment.

We have measured the spindle length as the distance from pole to pole. After collecting ~50 cells from 3 independent experiments (N=3) and having ~15-20 cells from each experiment, we first analyzed whether our independent measurements were consistent with each other or not. For this reason we have first carried out the Chi-squared test for consistency between experiments. We first took the arithmetic averages of each single and double siRNA conditions and also calculated their standard deviations and standard error of means. Then we have calculated the weighted mean of these three experiments (Figure 4.6).

When we take the  $P > 0.05$  our chi-squared value at  $Df 2 (N-1)$  was 5.991. So any value, which is lower than this, will indicate that the variation between samples was insignificant, but when it is higher than this then our samples are from different pools. According to our calculations, chi-squared values were; sicontrol:

5.583, sichTOG: 0.86, siEB1:2.81, sichTOG\_siEB1:3.13, siKif18A:12.95, siKif18A\_siEB1:45.46, siMCAK:1.62, siMCAK\_siEB1:4.15. These results indicated that siKif18A and siKif18A\_siEB1 experiments were fluctuating more than acceptable levels among each other.

Afterwards, we have confirmed our chi-squared results with another test called ANOVA. ANOVA is a very commonly used version of F-test and functions to test the variation between samples. If our samples can also pass this test, then we can pool the individual measurements and analyze them accordingly.

After one-way ANOVA-test assuming that samples were unpaired they had a Gaussian distribution. We compared the three independent experiments to each other and obtained a P-value showing the overall consistency of experiments. For 95% confidence level, we took  $P > 0.05$  and p values were: sicontrol: 0.0434, sichTOG: 0.6621, siEB1:0.3095, sichTOG\_siEB1:0.3423, siKif18A:0.0053, siKif18A\_siEB1:0.0001, siMCAK:0.6233, siMCAK\_siEB1:0.1621. These results were also supporting the outcomes of chi-squared test showing the high level of inconsistency in siKif18A and siKif18A\_siEB1 experiments. The P value of sicontrol sample was around the border with its 0.0434 value and all the other remaining experiments were consistent within each other.

After confirming that most of the experiments were carried out in a right way, we have pooled the data from 3 independent experiments and performed the one-way ANOVA test with Tukey's multiple comparisons. Our results show that the spindle length of siLuc-transfected cells was  $11.927 \pm 0.464$  (mean  $\pm$  SD; n=48). On the other hand, we have observed a sharp reduction in sichTOG cells to  $9.852 \pm 0.256$  (mean  $\pm$  SD; n=58) showing a very significant change compared to control group  $p < 0.0001$  (ANOVA, Tukey's test). As being consistent with the previous studies, we did not see any difference in the siEB1 group with an average of  $11.335 \pm 0.305$  (mean  $\pm$  SD; n=52) and  $p = 0.3322$  to control. As a known catastrophe-inducing factor and a predicted microtubule depolymerase, the depletion of Kif18A increased the spindle length and caused a banana-shaped

morphology. In this group, the length was increased to  $13.428 \pm 0.703$  in average (mean  $\pm$  SD; n=52) and  $p < 0.0001$  to control.

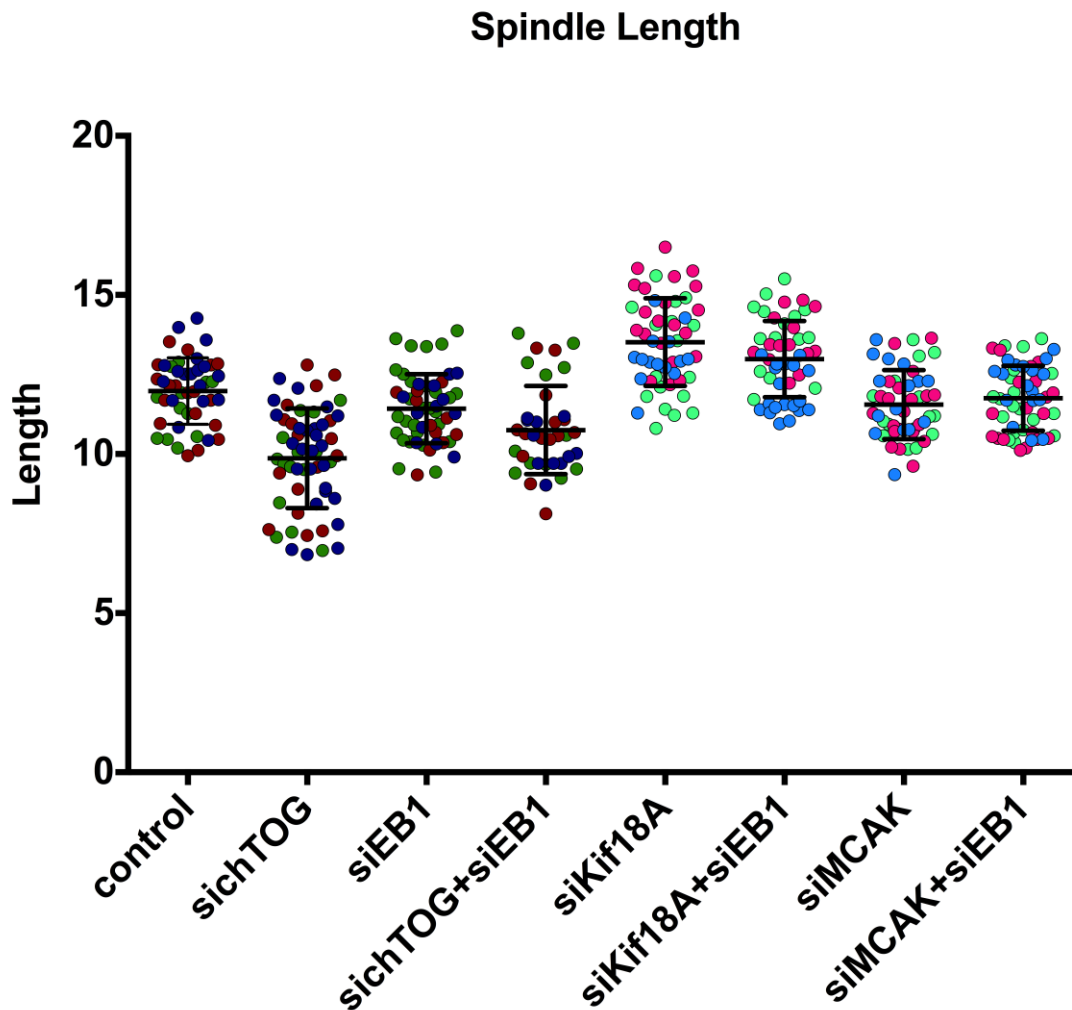


**Figure 4.6: Changes in the spindle length after gene knock-downs.** Average spindle lengths for each RNAi condition were: siLuc  $11.927 \pm 0.464$  (mean  $\pm$  SD; n=48), sichTOG  $9.852 \pm 0.256$  (mean  $\pm$  SD; n=58), siEB1  $11.335 \pm 0.305$  (mean  $\pm$  SD; n=52), siKif18A  $13.428 \pm 0.703$  (mean  $\pm$  SD; n=52), siMCAK  $11.57 \pm 0.186$  (mean  $\pm$  SD; n=50), sichTOG-siEB1  $10.733 \pm 0.43$  (mean  $\pm$  SD; n=37), siKif18A-siEB1  $13.069 \pm 0.961$  (mean  $\pm$  SD; n=48), siMCAK-siEB1  $11.768 \pm 0.326$  (mean  $\pm$  SD; n=54). There were significant changes between the control group and sichTOG and control-siKif18A with a  $p < 0.0001$  by ANOVA. sichTOG-siEB1 has p values 0.0168 to sichTOG, 0.1873 to siEB1 and 0.002 to control groups by ANOVA.

While the single depletions of chTOG, EB1 and Kif18A gave consistent results in spindle length phenotypes with the other systems (Goshima et al., 2005), the co-depletions of these genes elucidated their in vivo behaviors much more in detail. In sichTOG-siEB1 group, the mini spindle phenotype in sichTOG was partially rescued by the siEB1 double knock down. Here we have measured the length as

10.733 ± 0.43 (mean ± SD; n=37) and when we look at the ANOVA results of sichTOG-siEB1 to control, sichTOG and siEB1 we see that there is a significant change from sichTOG to sichTOG-siEB1 p=0.0168 and to control p=0.002. On the contrary, the difference between siEB1 and sichTOG-siEB1 was not significant at all p=0.1873. This analysis confirms that siEB1 partially rescues the decrease in spindle length after sichTOG treatment.

When we co-transfect the mES cells with siKif18A and siEB1 we have seen that there was not a significant change in siKif18A phenotype. The mean spindle length was measured as 13.069 ± 0.961 (mean ± SD; n=48) and it was statistically significant from the control and siEB1 groups, P=0.0018 and P<0.0001, respectively, but ANOVA test gave a P=0.3746 showing no change in spindle length after siEB1 transfection.

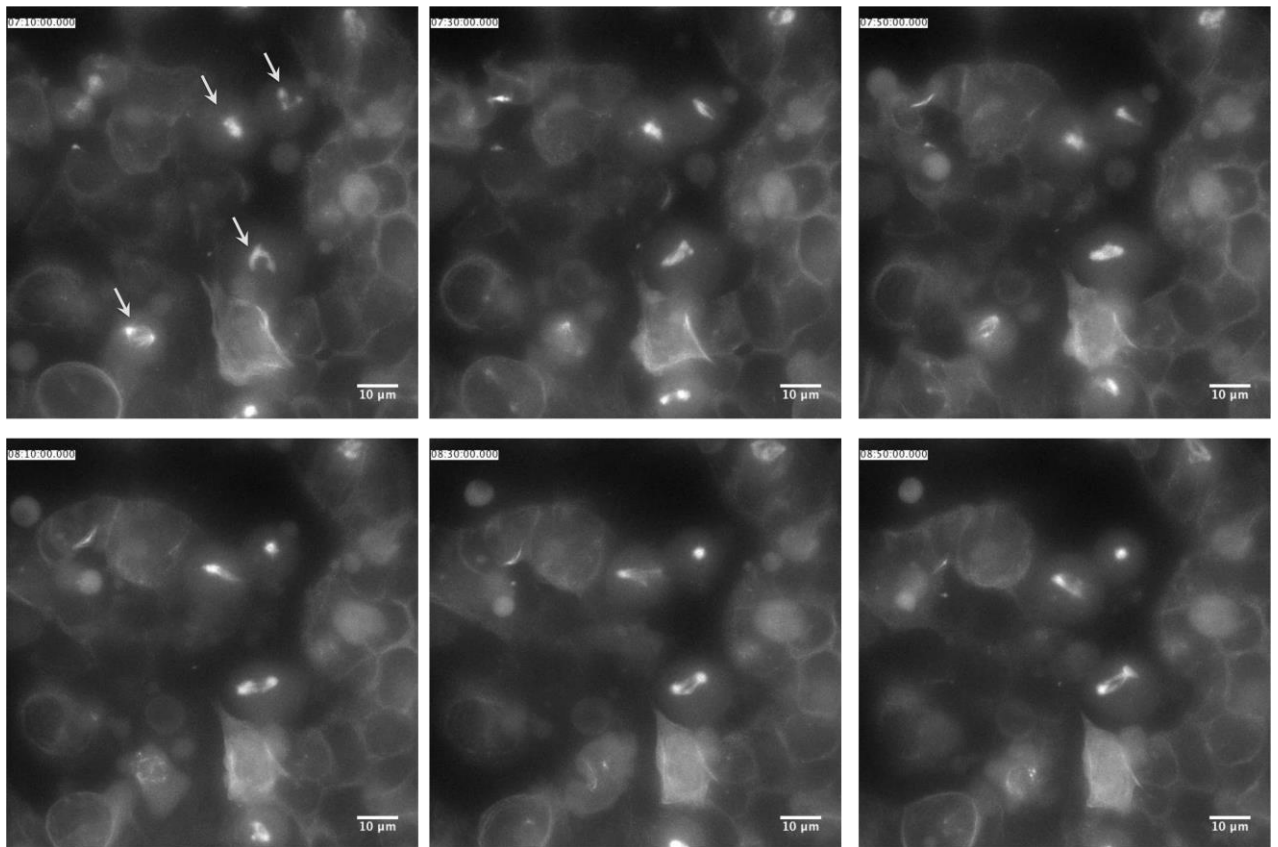


**Figure 4.7: Spindle assembly defects in sichTOG\_siKif18A cells.** TUBB-GFP expressing mES cells were transfected with the same amount of siRNA against chTOG and Kif18A genes. After 48 hours, they were imaged under 60X microscope. In this figure we see the screen-shots from a representative movie. Images were chosen from the movie between 07:10-08:50 hours in every 20 minutes. In the first image, 4 seen that are in mitosis are shown by white arrows. At 08:10, the

cell at the lower left corner undergoes a catastrophic mitosis while other 3 cells still try to generate a bipolar spindle.

We obtained an interesting and also little bit surprising result from sichTOG-siKif18A group. Although the antagonistic functions of these two MT-binding proteins are known, their co-depletion did not rescue their effects on the microtubule dynamics and consequently on the spindle length but rather severely disrupted the whole spindle assembly.

We then moved on to analyze the width of metaphase spindle under the given siRNA conditions. We have measured the spindle width in the control group as  $6.830 \pm 1.041$  (mean  $\pm$  SD; n=48). In siRNA-treated experimental groups it was,  $6.081 \pm 0.79$  (mean  $\pm$  SD; n=58) for sichTOG,  $6.537 \pm 0.68$  (mean  $\pm$  SD; n=52) for siEB1,  $6.225 \pm 0.76$  (mean  $\pm$  SD; n=37) for sichTOG\_siEB1,  $6.859 \pm 1.16$  (mean  $\pm$  SD; n=52) for siKif18A,  $6.223 \pm 0.84$  (mean  $\pm$  SD; n=49) for siKif18A\_siEB1,  $6.667 \pm 0.84$  (mean  $\pm$  SD; n=51) for siMCAK and  $6.224 \pm 0.8$  (mean  $\pm$  SD; n=55) for siMCAK\_siEB1. Then we have analyzed these values in ANOVA whether they are significantly different from each other or not. ANOVA results of multiple comparisons show that sichTOG strongly influences the length of the spindle width by having a P value of 0.0004 compared to control group. Interestingly, siEB1 knockdown itself could not decrease the spindle width too much however it has an additive effect on siKif18A by causing a sharp decline in siKif18A\_siEB1 co-depleted cells with a P value of 0.0079 when siKif18A and siKif18A\_siEB1 conditions are compared to siMCAK did not cause any change in spindle width either as in spindle length.

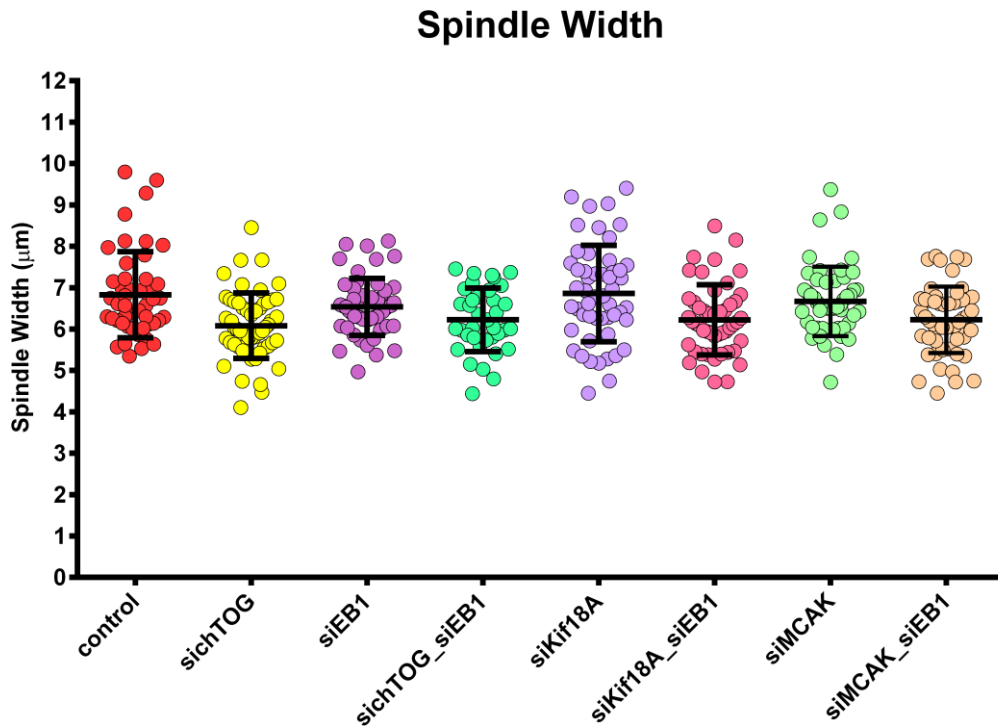


**Figure 4.8: Spindle width after gene knockdowns.** The average lengths of spindle widths were measured as: control group  $6.830 \pm 1.041$  (mean  $\pm$  SD;  $n=48$ ), sichTOG  $6.081 \pm 0.79$  (mean  $\pm$  SD;  $n=58$ ), siEB1  $6.537 \pm 0.68$  (mean  $\pm$  SD;  $n=52$ ) sichTOG\_siEB1  $6.225 \pm 0.76$  (mean  $\pm$  SD;  $n=37$ ) siKif18A  $6.859 \pm 1.16$  (mean  $\pm$  SD;  $n=52$ ), siKif18A\_siEB1  $6.223 \pm 0.84$  (mean  $\pm$  SD;  $n=49$ ), siMCAK  $6.667 \pm 0.84$  (mean  $\pm$  SD;  $n=51$ ) and siMCAK\_siEB1  $6.224 \pm 0.8$  (mean  $\pm$  SD;  $n=55$ ) sichTOG condition is significantly different from the control group with a p value of 0.0004 while cells in the other conditions remain mostly unaffected.

After measuring the lengths and widths of the metaphase spindle, we wanted to compare them with each other to conclude about the morphology of the spindle. For this purpose we have taken the ratio of the length to width  $1.78 \pm 0.22$  (mean  $\pm$  SD;  $n=48$ ). In siRNA-treated experimental groups it was,  $1.637 \pm 0.26$  (mean  $\pm$  SD;  $n=58$ ) for sichTOG,  $1.766 \pm 0.24$  (mean  $\pm$  SD;  $n=52$ ) for siEB1,  $1.743 \pm 0.23$  (mean  $\pm$  SD;  $n=37$ ) for sichTOG\_siEB1,  $2.027 \pm 0.41$  (mean  $\pm$  SD;  $n=52$ ) for siKif18A,  $2.219 \pm 0.32$  (mean  $\pm$  SD;  $n=49$ ) for siKif18A\_siEB1,  $1.753 \pm 0.22$  (mean  $\pm$  SD;  $n=51$ ) for siMCAK and  $1.922 \pm 0.32$  (mean  $\pm$  SD;  $n=55$ ) for siMCAK\_siEB1. According to ANOVA analysis, there are statistically meaningful changes in siKif18A and siKif18A\_siEB1 compared to control group, having P values 0.0007 and 0.0001, respectively. One important result is that sichTOG did not change the overall morphology of the mitotic spindle, although it causes a significant decline in both spindle length and width. These cells could probably preserve their spindle morphologies by proportional shortening of length and width.

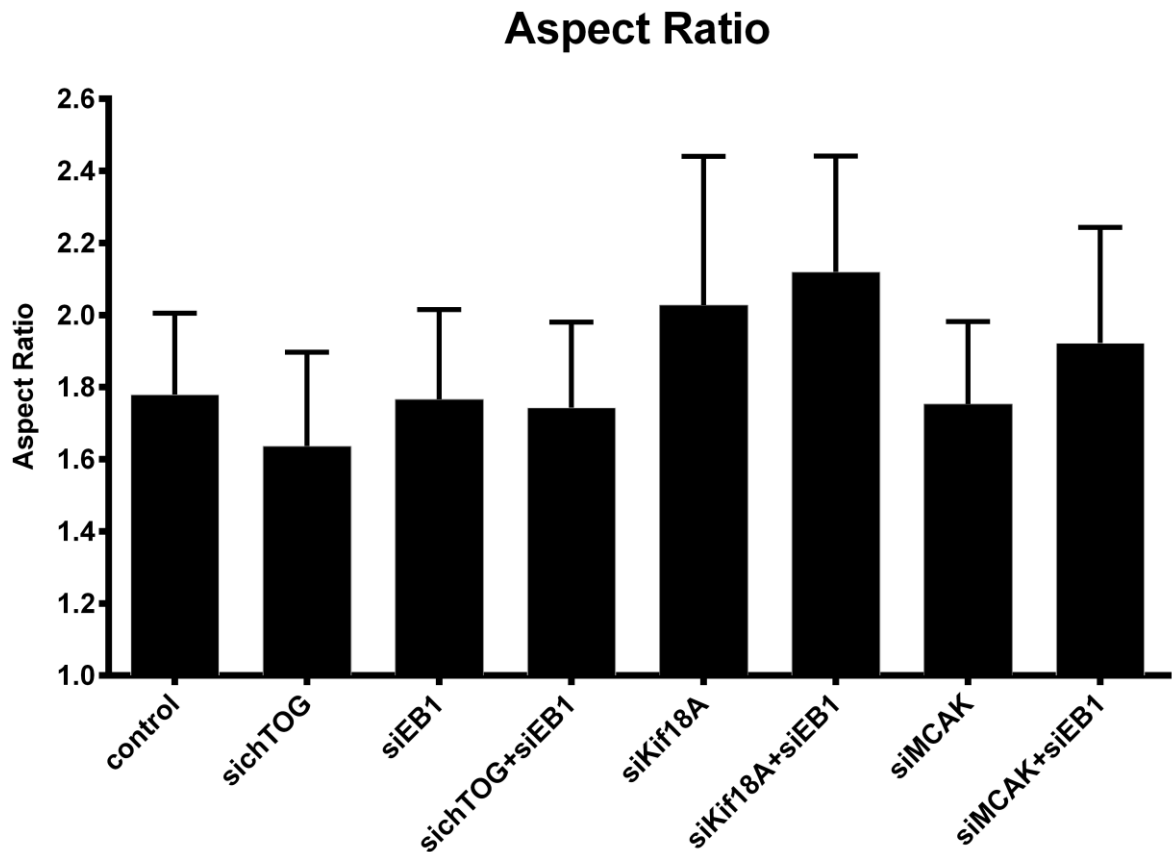


**Figure 4.9: Aspect ratio of ES cells after RNAi treatment.** Aspect ratio was described and calculated as the L/W. In control group the average ratio was  $1.78 \pm 0.22$  (mean  $\pm$  SD; n=48). In siRNA-treated experimental groups it was,  $1.637 \pm 0.26$  (mean  $\pm$  SD; n=58) for sichTOG,  $1.766 \pm 0.24$  (mean  $\pm$  SD; n=52) for siEB1,  $1.743 \pm 0.23$  (mean  $\pm$  SD; n=37) for sichTOG\_siEB1,  $2.027 \pm 0.41$  (mean  $\pm$  SD; n=52) for siKif18A,  $2.219 \pm 0.32$  (mean  $\pm$  SD; n=49) for siKif18A\_siEB1,  $1.753 \pm 0.22$  (mean  $\pm$  SD; n=51) for siMCAK and  $1.922 \pm 0.32$  (mean  $\pm$  SD; n=55) for siMCAK\_siEB1. In siKif18A and siKif18A\_siEB1 groups, the overall spindle morphology has changed compared to control group, having P values of 0.0007 and 0.0001, respectively by ANOVA analysis. In the other conditions, we did not observe a significant change.

Accurate chromosome segregation relies on the precise regulation of mitotic progression. This regulation basically involves control over the timing of mitosis and spindle assembly checkpoint (SAC) which sends the signal for the segregation of sister chromatids after the completion of all chromosome-microtubule attachments (Meraldi et al., 2004). After analyzing the changes in spindle morphologies of mES cells in different gene knock-downs, we wanted to relate it to how these changes influence the progress of mitosis in terms of metaphase alignment time and chromosome segregation errors.

In this part we have used a stably labeled H2A-GFP mES cell line and repeated the siRNA experiments in these cells. By imaging the cells at a 2min/frame rate, we have collected the movies and afterwards we first calculated the amount of time that a cell spends between nuclear envelope breakdown (NEB) until anaphase onset.

The metaphase alignment time for control cells was  $21.68 \pm 3.379$  (mean  $\pm$  SD; n=76). In siRNA-treated experimental groups it was,  $25.12 \pm 11.98$  (mean  $\pm$  SD; n=50) for sichTOG,  $22.55 \pm 7.89$  (mean  $\pm$  SD; n=76) for siEB1,  $27.47 \pm 16.16$  (mean  $\pm$  SD; n=95) for sichTOG\_siEB1,  $32.59 \pm 17.57$  (mean  $\pm$  SD; n=101) for siKif18A,  $33.14 \pm 24.84$  (mean  $\pm$  SD; n=84) for siKif18A\_siEB1 and  $47.98 \pm 34.04$  (mean  $\pm$  SD; n=84) for sichTOG\_siKif18A.

These results were implying that chTOG and EB1 did not affect the alignment time having P values  $> 0.05$  by ANOVA compared to control group. On the other hand, siKif18A increases the time for chromosome alignment more than 50% and the co-depletion of Kif18A with EB1 did not change this outcome. In both conditions the P value was 0.005 as compared to control showing a quite significant increase. A very surprising result came from the siKif18A\_sichTOG double knock-down. The P value of siKif18A\_sichTOG was less than 0.0001 showing an extremely sharp change. As described in TUBB-GFP cells, this knock-down was producing severe spindle assembly defects. As supporting this result, we have found that the metaphase alignment time was almost doubled in this co-depletion, indicating that a delay in the spindle assembly automatically affects the chromosome alignment and therefore mitotic progression.



## Metaphase Alignment Time

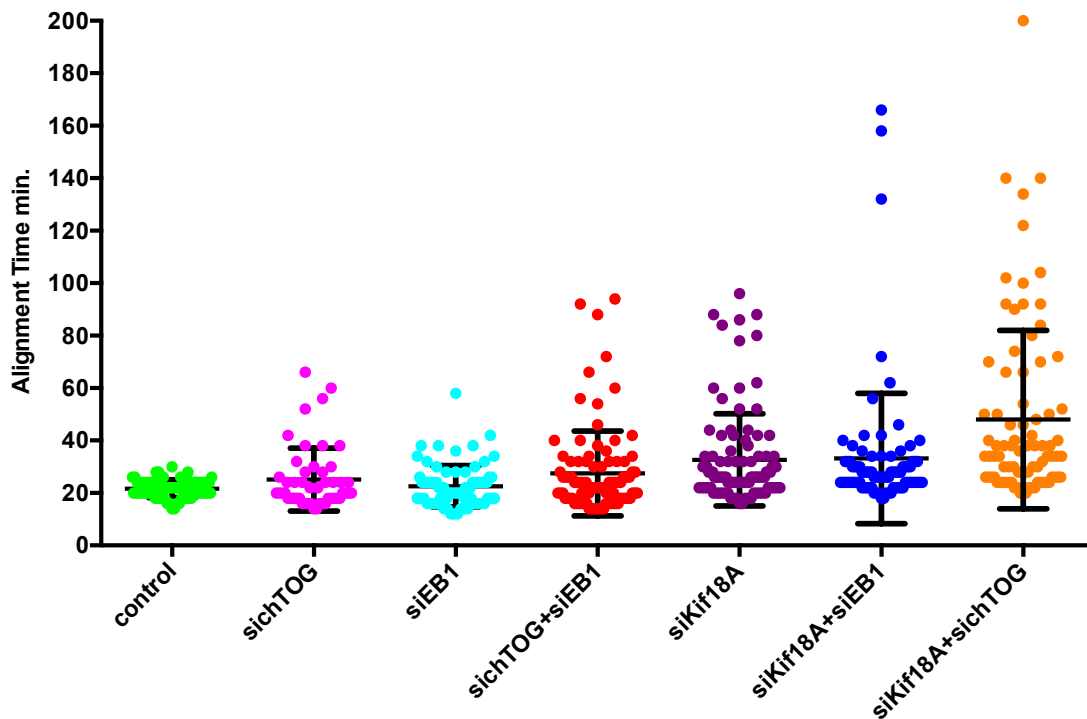


**Figure 4.10: Metaphase alignment time between NEBD and Anaphase-onset.** The metaphase alignment time for control cells was  $21.68 \pm 3.379$  (mean  $\pm$  SD;  $n=76$ ). In siRNA-treated cells,  $25.12 \pm 11.98$  (mean  $\pm$  SD;  $n=50$ ) for sichTOG,  $22.55 \pm 7.89$  (mean  $\pm$  SD;  $n=76$ ) for siEB1,  $27.47 \pm 16.16$  (mean  $\pm$  SD;  $n=95$ ) for sichTOG\_siEB1,  $32.59 \pm 17.57$  (mean  $\pm$  SD;  $n=101$ ) for siKif18A,  $33.14 \pm 24.84$  (mean  $\pm$  SD;  $n=84$ ) for siKif18A\_siEB1 and  $47.98 \pm 34.04$  (mean  $\pm$  SD;  $n=84$ ) sichTOG\_siKif18A. There are significant changes siKif18A and siKif18A-siEB1 to the control group with a  $p$  value 0.005 and between control and siKif18A-sichTOG groups with a  $p < 0.0001$ , by ANOVA.

Chromosome segregation is actually the most important part of a proper mitosis because any defect in it directly changes the genomic content of the daughter cells and increases the susceptibility for cancer formation or cell death. Therefore we wanted to compare the number of chromosome defects either lagging chromosomes or chromosome bridges.

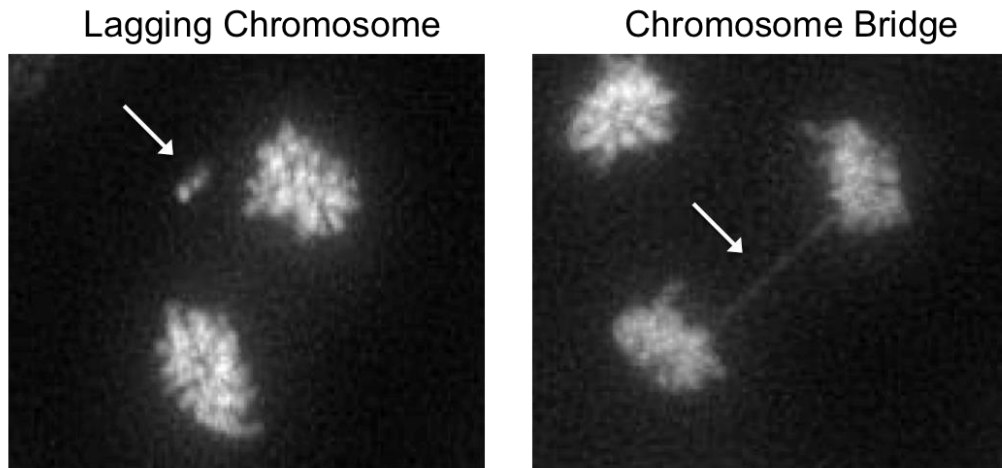


**Figure 4.11: Lagging chromosomes and chromosome bridge errors in cell division.** Anaphase lagging chromosomes are identified as single, kinetochore-positive chromosomes that lag between the two masses of segregating chromosomes during anaphase. Chromosome bridges on the other hand span the chromosomes in anaphase that are mainly caused by condensation or cohesion defects or by dicentric chromosomes pulled to opposite poles.

Our results showed that the error rate of chromosome segregation is  $3.5\% \pm 1.8$  (mean  $\pm$  SD;  $n=3$ ) (Figure 4.10). In RNAi treated groups chromosome errors were really high; in sichTOG  $28.34 \pm 8.12$  (mean  $\pm$  SD;  $n=3$ ), siEB1  $22.26 \pm 2.735$  (mean  $\pm$  SD;  $n=3$ ), siKif18A  $27.76\% \pm 7.501$  (mean  $\pm$  SD;  $n=3$ ). In double knock-downs we see that again EB1 and chTOG codepletion decreases the error rate little bit to  $17.22\% \pm 4.028$  (mean  $\pm$  SD;  $n=3$ ) but it does not cause a statistically significant change  $P > 0.05$  by ANOVA from sichTOG phenotype. siEB1 leads to an additional effect on siKif18A phenotype by increasing the error rate to  $32.27\% \pm 6.645$  (mean  $\pm$  SD;  $n=3$ ). As in parallel with spindle assembly and metaphase timing, we observed an additional effect of chTOG and Kif18A depletions in cells,  $34.23\% \pm 5.998$  (mean  $\pm$  SD;  $n=3$ ) of the cells have a defective chromosome in their daughter cells when these two antagonistic proteins are degraded.

## Chromosome Segregation Errors

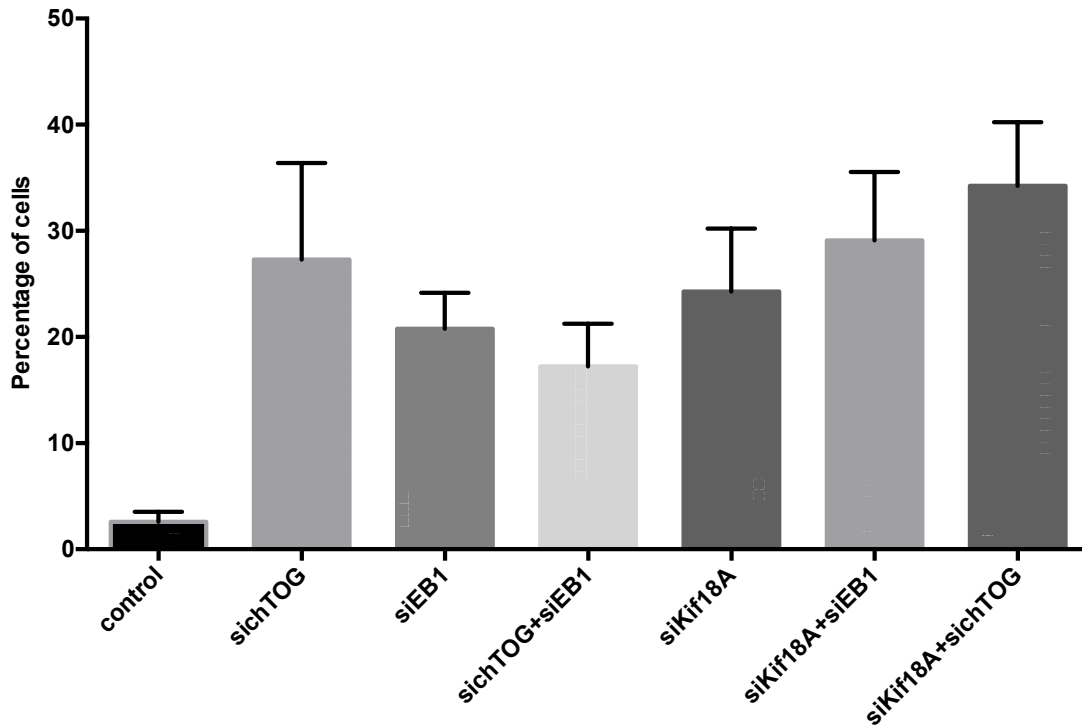


**Figure 4.12: Percentage of chromosome segregation errors in ES cells after RNAi treatments.** The error rate of chromosome segregation is  $3.5\% \pm 1.8$  (mean  $\pm$  SD;  $n=3$ ). In RNAi treated groups; in sichTOG  $28.34 \pm 8.12$  (mean  $\pm$  SD;  $n=3$ ), siEB1  $22.26 \pm 2.735$  (mean  $\pm$  SD;  $n=3$ ), siKif18A  $27.76\% \pm 7.501$  (mean  $\pm$  SD;  $n=3$ ). In the double knock-downs of EB1 and chTOG  $17.22\% \pm 4.028$  (mean  $\pm$  SD;  $n=3$ ) siKif18A\_siEB1  $32.27\% \pm 6.645$  (mean  $\pm$  SD;  $n=3$ ) and in chTOG and Kif18A co-depletion  $34.23\% \pm 5.998$  (mean  $\pm$  SD;  $n=3$ ). All of the experimental groups show significant difference from the control group by ANOVA as  $p < 0.0001$ .

## Discussion

The mitotic spindle is a subcellular apparatus that is built up to segregate chromosomes accurately during cell division. The shape of the mitotic spindle is a good model for studying scaling inside the cell. The control of spindle assembly is very crucial in terms of the on time mitotic progression and proper chromosome segregation. In our studies, we analyzed how defects in the spindle assembly machinery and therefore in its morphology affects the outcome of mitosis. For this purpose, we have knocked down the MAP genes, chTOG, Kif18A, EB1 and MCAK and observed their effects on spindle morphology, metaphase alignment timing and chromosome segregation errors.

In our studies, we have found that chTOG and Kif18A influence the spindle length and MCAK and EB1 do not affect it too much. From the previous studies we know that members of the TOG protein family are highly conserved MT polymerases (Brouhard et al., 2008) and loss of their function generally leads to spindle shortening (Kinoshita et al., 2002). In another study, XMAP215 has been shown to contribute to spindle length regulation via its MT nucleation activity (Groen et al., 2009). On the other hand, this family of proteins also has MT destabilization activity (Shirasu-Hiza et al., 2003) depending on the available free tubulin levels (Brouhard et al., 2008), and this leads to longer cytoplasmic MTs in the budding yeast Stu2 mutant (Van Breugel et al., 2003). Besides the catalytic control of chTOG on the MT +end, EB1 is a master regulator of MT +end dynamics because it autonomously tracks the growing +ends of MTs and it also functions as a recruiter of additional +end tracking proteins and promotes MT growth (Akhmanova & Steinmetz; 2008, Bieling et al. 2007, Rogers et al. 2002). EB1 depletion leads to the formation of shorter spindles in *Drosophila* S2 cells (Goshima et al. 2005), but it does not affect the spindle size in mammalian HeLa cells (Ferreira et al., 2013). How does EB1 promote MT growth was remaining as an open question (Komarova et al. 2009) but in a very recent study it has been shown that EB1 synergistically affects the enzymatic activity of XMAP215 and such an interplay between these two molecules causes a 4-fold increase in the MT growth rates (Zanic et al., 2013). However EB1 itself does not also promote

the growth, Zanic and co-workers have also shown that EB1 itself has an ability to bump the catastrophe frequency.

This simultaneous promotion of growth and catastrophe by EB1 may explain the rescue of chTOG minispindle phenotype by the codepletion with EB1. In only sichTOG condition, the enzyme catalyzing MT growth is lost and this itself causes a severe defect in polymerization of MTs. In only EB1 depletion, on the other hand, we lose the synergistic effect of EB1 on chTOG and this leads to a decrease in MT growth rates. Additionally catastrophe frequencies are expected to be decreased in this condition as well. In the end, these opposing effects cancel out each other and we can not see a change in spindle size. In the double knockdown of chTOG and EB1, decrease in growth rates was the same as in only sichTOG condition but now we expect to see a decrease in the catastrophe frequency of MTs, because EB1 is absent in cells. A decrease in the catastrophe frequency will give the cells a chance to elongate their spindles and therefore to be able to rescue their minispindle phenotypes.

Kinesin-8 family of motor proteins are quite important regulators of spindle size because it has both MT-destabilizing and plus end-directed MT translocating activities (Gupta et al. 2006, Howard & Hyman 2007, Varga et al. 2006). Their depletion in fission yeast or animal cells leads to spindle lengthening associated with an increase in spindle MT plus end growth (Garcia et al. 2002, Goshima & Vale 2003, West et al. 2002), on the other hand their overexpression shortens spindles (Goshima et al. 2005). In vitro studies implicated that kinesin-8 preferentially destabilizes MT plus ends but compared to kinesin-13 its depolymerization activity is very weak, so the accumulation of multiple molecules at the ends of an MT is required to trigger processive depolymerization. This accumulation facilitated by the processive MT-translocating activity leading to MT length-dependent depolymerizing activity, an excellent mechanism for maintaining spindle MTs at a constant length (Varga et al., 2006; Varga et al., 2009). The depletion of mammalian kinesin-8 homolog Kif18A caused an increase in the human HeLa cells as we have seen in our mouse ES cells. We have further shown that EB1 co-depletion did not affect the

elongation of spindle most probably due to the opposing roles of EB1 on the growth and catastrophe of MTs that is mentioned before.

Kinesin-13 motors use ATP hydrolysis to depolymerize MTs rather than to walk along them (Helenius et al., 2006). The motors localize to kinetochores, centrosomes, and spindle MTs, where they depolymerize MT plus and minus ends to coordinate poleward flux and Pac-Man kinetochore motility (Desai et al. 1999, Kwon et al. 2004). Although kinesin-13 motors are primarily involved in the chromosome capturing and k-fiber shortening in anaphase, it has been shown that their depletion causes an increase in spindle length in *Drosophila* S2 cells (Goshima et al., 2005). However in mammalian HeLa cells, depletion of MCAK did not grossly affect the formation of bipolar mitotic spindles (Zhu et al., 2005) In our RNAi studies the siMCAK treatment did not produce any clear phenotype in the spindle morphology and its co-depletion with EB1 did not change this as well. So we confirmed that in mammalian cells MCAK does not seem to be important for spindle size and morphology.

Again in our co-depletion studies, we have knocked-down the antagonistic genes chTOG and Kif18A to see whether they can rescue their effects in the spindle phenotype. We have observed that in this double RNAi knock-down the spindle assembly was almost disrupted, many of the cells were failing to assemble a bipolar spindle. As supporting this result, we have also seen delays in the metaphase alignment times and high number of errors in the chromosome segregation during anaphase. All of these results imply that although these two proteins chTOG and Kif18A work in opposite ways, ES cells cannot tolerate their absence at the same time. Because timing is crucial in mitosis, to be able to assemble the spindle and to capture the chromosomes on time, MT dynamics has to be very well controlled and maintained. Despite the fact that Klp67A and Msp, *Drosophila* homologs of Kif18A and chTOG, could rescue the spindle morphology in the double knockdown in *Drosophila* S2 cells (Goshima et al., 2005), we could not confirm this result in the mammalian ES cell model. The reason for this might be the strictly controlled timing in ES cell mitosis, the loss

of two MT +end regulators might prevent the building up of the spindle on time by decreasing the dynamic behavior of MTs and therefore both assembly and chromosome capture might be affected seriously by this condition.

The spindle length is the distance between two poles and the spindle width is the width of the microtubules, perpendicular to the spindle axis, at the center of the spindle where the chromosomes are positioned (Hara and Kimura, 2013). Previous studies suggested a tight link between spindle length and spindle width. Mechanical manipulation of in vitro–reconstructed metaphase spindles using *Xenopus* egg extract or in vivo mitotic spindles in mammalian Ptk2 cells demonstrated that the aspect ratio of the spindle, which is the ratio of the width to the length, remained constant after the manipulation or compression of the spindle (Dumont and Mitchison, 2009; Itabashi et al., 2009). These observations suggested that the spindle self-organizes itself to maintain a constant aspect ratio between the spindle length and spindle width.

In our RNAi studies, we wanted to understand whether this ratio is conserved or not after the depletion of MAPs. We could only observe a significant change in the widths of sichTOG cells. This decrease was in parallel with the shortening of their spindle lengths and finally led to a constant aspect ratio, meaning that the diamond shape of the spindle was preserved even if chTOG is not present in the cell. The only exceptions were the siKif18A and siKif18A\_siEB1 cells. Although their spindle widths did not fluctuate too much in these conditions, aspect ratios increased as a result of the increase in their spindle lengths. This can be explained by the squeezing and expansion of chromosomes (Hara and Kimura, 2013). Chromosomes can be squeezed or expanded into certain volumes and the width of the metaphase plate and therefore spindle microtubules can be adjusted accordingly to keep the aspect ratio as constant as possible. However, there has to be certain limits during these adjustments are being done because chromosomes possess their own volumes and the metaphase plate volume cannot be lower than this. On the other hand, too much expansion of the metaphase plate will be prevented by the tension on the kinetochore microtubules, which are acting as attractive forces on chromosomes. Therefore

cells in siKif18A condition might have already reached their maximum spindle width and this could prevent the restoration of their diamond shape by giving higher aspect ratios.

We next examined the roles of MT tip-tracking proteins on the progression and robustness of mitosis. Kif18A depletion elevated the rate of chromosome alignment failure and led to a mitotic arrest. This might be related to an increase in kinetochore oscillation levels in siKif18A cells (Wordeman et al., 2007; Stumpff et al., 2008), that is important for chromosome alignment and therefore metaphase timing. Similar results have also observed in *Drosophila* S2 cells, the depletion of kinesin-8 homolog Klp67A regulates the chromosome congression by its MT-depolymerising motor activity at kinetochores, but not along the spindle (Savoian and Glover, 2009). In our RNAi experiments we have also observed similar results and additionally we have found that the co-depletion of Kif18A with EB1 increases both the metaphase alignment time as well as the chromosome segregation error rates. These results altogether show that although EB1 itself does not have a very prominent effect on timing it can compensate the absence of Kif18A to a certain degree.

siChTOG and siEB1 did not affect the timing of chromosome alignment showing that they are either not important for chromosome congression, they are not involved in the control of SAC or their depletion can be compensated by other proteins during mitosis. However the first possibility does not seem correct because in the absence of these two proteins we see an increase in the unaligned chromosome numbers. This indicates that both chTOG and EB1 are actually important for chromosome capturing. Most probably the absence of both chTOG and EB1 did not affect the spindle assembly checkpoint so the cells could move on the mitosis without the proper congression and alignment of chromosomes.



## **5. Generation of an ES Cell Model to Study the Spatio-temporal Determinants of Neuronal Morphology**

Cell polarity and symmetry breaking is one of the key processes in different cell types. Neurons are highly polarized cells and mechanisms that establish and maintain these highly specialized cells have been intensively studied for years. To study these mechanisms different model systems have been utilized. They are basically neuronal cell lines, primary neuronal cultures and mouse models used in morphological studies. In this chapter, I will introduce you a new ES cell based differentiation and morphology model, which brings the advantages of all of the previously mentioned systems; high resolution imaging capacity of neuron cultures, control over development in mouse models and easy genetic manipulation and culturing of neuronal cell lines. We have generated Tet-induced shRNA cell lines for chTOG, Kif18A and MCAK that are also stably expressing TUBB-GFP. These labeled cells were mixed with unlabeled wild-type mES cells before differentiation at 1:1000ratio and then they were differentiated into mouse cortical cells and spinal motor neurons. Our results showed that, all of the three genes could be successfully knocked-down by shRNA after 48 hours of Tet induction. After mixing the labeled and unlabeled cells, single neurons could be imaged at high resolution and their skeletons could be generated afterwards. The shRNA studies in chTOG showed that, the knock-down of this gene in early differentiation interferes with the differentiation process.

## Introduction

Neurons are highly polarized cells commonly possessing two types of cellular processes, usually a single axon and several dendrites whose structural and functional properties are distinct. Axons are involved in the convey of information away from the neuronal cell body on the other hand dendrites receive information from outside of the cell and transmit it towards the cell body. In summary, axons form presynaptic structures, whereas dendrites are generally postsynaptic. Up to date, most of our knowledge of the specification of axons and dendrites during the early stages of neuronal differentiation comes from cell culture studies of dissociated, differentiating neurons (Bradke and Dotti, 2000; Craig and Banker, 1994). In two of these early studies have shown that embryonic hippocampal pyramidal neurons (Dotti and Banker, 1987) and embryonic cerebellar neurons (Ferreira et al., 1989) initially extend two or more processes that have bipotential to differentiate into axons or dendrites (Figure 5.1, Stage 2). These bipotential processes grow slowly until one of them is destined to become the axon (Figure 5.1, Stage 3). Right afterwards, the axonal process starts to extend at a faster rate while the others slow down and then at later stages they differentiate into dendrites (Figure 5.1, Stage 4&5). The distinguishing features of a neurite that becomes the axon is that its growth cone enlarges (Figure 5.1, Stage 3).

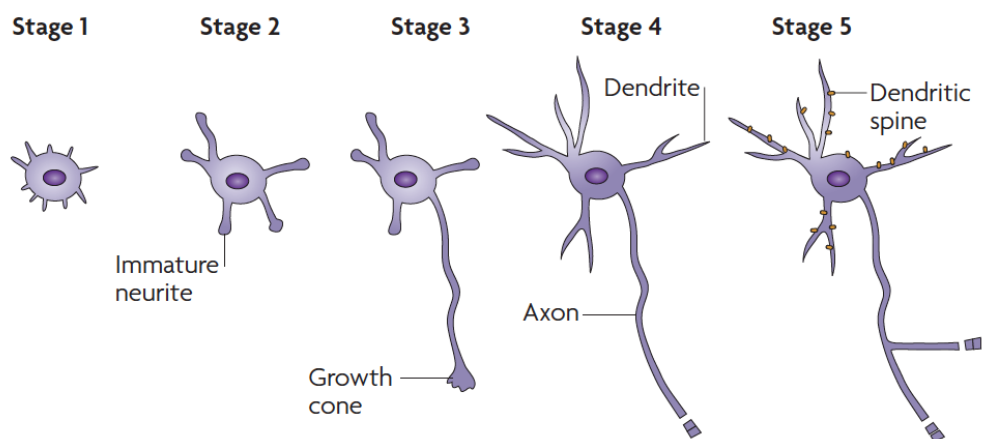


**Figure 5.1: Stages of polarization in neuron cultures.** The neuronal polarization in cultured rat embryonic hippocampal neurons starts shortly after plating, the neurons form small protrusion veils and a few spikes (stage 1). These truncated protrusions develop into several immature neurites (stage 2). One neurite then starts to break the initial morphological symmetry, growing at a rapid rate, and immediately establishing the polarity (stage 3). Thereafter, the remaining neurites elongate and acquire the characteristics of dendrites (stage 4). Seven days after plating, neurons form synaptic contacts through dendritic spines and axon terminals, and establish a neuronal network (stage 5). Adapted from Arimura and Kaibuchi, 2008.

To study the morphological determinants and polarity factors, different model systems have been developed so far. These models can be basically divided in three groups: Primary neuron cultures, neuronal cell lines and mouse models. Primary neuron cultures are maybe the most widely used model, due to their easy imaging and differentiation. These cultures are mainly generated from the cortical or spinal tissues of either embryonic or post-natal rodents. They are good for imaging because they grow as 2D on slides. However their genetic manipulation is very difficult due to the fact that neurons do not divide. This makes the nucleofection necessary to introduce the desired DNA into the nuclei of neurons. Secondly, these cells are terminally differentiated and they do not resemble the embryonic development processes.

Second widely used model is neuronal cell lines. These lines are generated from the neuronal cancer tissues like neuroblastomas, chordomas etc. Many neuronal cell lines are being currently used such as SH-SY5Y, NT-2 and PC12. It is quite easy to maintain these cell lines in culture because they grow continuously due to their tumorigenic character. They also grow as 2D as the primary cultures

making them suitable for imaging. On the other hand, they do not possess a stable genetic background due to their cancerous behavior. These cells gain or lose genetic material in each cell cycle and this makes it impossible to be sure about their genetic background. Furthermore, there might be some difficulties in reproducing the results in these cells, because as the DNA content changes their response to differentiation protocols also changes.

Mouse models have become quite popular in recent years because of many technological improvements carried out in the generation of transgenic mouse and in the genetic manipulation of mouse embryos in the uterus (Tabata and Nakajima, 2001). These improvements facilitated the genetic manipulation and therefore labeling and the control over embryonic development. So they were eliminating the downsides of primary neuron cultures. The use of an in vivo system was also supporting the development and differentiation of neurons in their own microenvironment, so it was not necessary to make them adapt to in vitro culture conditions.

## Results

We started to generate the ES cell model for neuronal differentiation and morphology by setting up an inducible gene silencing system. For this purpose we have used a Tet-responsive induction of shRNA, which has also given temporal gene silencing control during embryogenesis and development of neurons. In this system, we have used 2 different plasmids, pcDNA6/TR and Block-IT H1/TO shRNA vectors. The pcDNA6/TR plasmid has been used to express the Tetracycline-repressor protein. Tet-R protein produced by pcDNA6/TR plasmid binds to the Tet. In its original vector, Tet-R protein expression was controlled by the CMV promoter. Because we know that CMV promoter gets inactivated a while after transfection we have changed the expression promoter with SV40. This promoter was also controlling the selective marker, which is Blasticidin. By regulating both marker and Tet-R protein expressions by the same promoter we aimed to select and maintain the Tet-R positive cells in later passages. Tet-R protein was involved in the repression of target promoter. In our case, it was H1 promoter, which is used to induce shRNA expression. The TATA sequences in the H1 promoter were flanked with 2 Tetracycline-response elements (TetO<sub>2</sub>). These elements had sequences that are specific for Tet-R recognition and under normal cell culture conditions they were repressing the gene expression. Upon addition of Tetracycline or Doxycycline, Tet-R proteins interact with these small molecules and this interaction breaks the protein-DNA binding. After the dissociation of Tet-R from TetO<sub>2</sub>, RNA polymerase can start transcribing the gene of interest and therefore the express is turned on (Figure 5.2).

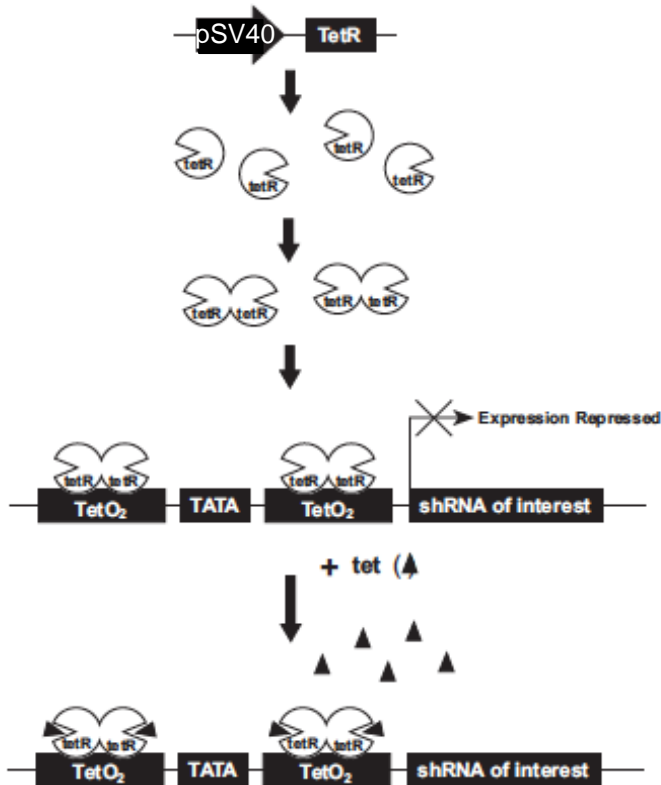


**Figure 5.2: The Tet-inducible gene expression system.** In the absence of tetracycline, the Tet repressor expressed from the pcDNA6/TR plasmid forms a homodimer that binds with extremely high affinity to each TetO<sub>2</sub> sequence in the H1 promoter of the shRNA expression vector. Binding of the Tet repressor homodimers to the TetO<sub>2</sub> sequences represses transcription of the shRNA of interest. Upon addition, tetracycline binds with high affinity to each Tet repressor homodimer in a 1:1 stoichiometry and causes a conformational change in the repressor that renders it unable to bind the Tet operator. The Tet repressor:tetracycline complex then dissociates from the Tet operator and allows induction of transcription of the shRNA of interest, resulting in target gene knockdown (adapted from [http://tools.lifetechnologies.com/content/sfs/manuals/blockit\\_h1entryvector\\_man.pdf](http://tools.lifetechnologies.com/content/sfs/manuals/blockit_h1entryvector_man.pdf)).

Our first step was to transfect the TUBB-GFP cells with pcDNA6/TR plasmid. After the selection with Blasticidin we isolated 5 different clones of Tet-R expressing cells. Then we checked the Tet-R expression levels by Western Blotting (Figure 5.3). Out of the 5 clones, clones 2,3 and 5 have shown higher expression of Tet-R than 1 and 4. As a negative control we used the untransfected wild-type ES cells and they did not show any Tet-R expression. TUBB antibody was the loading control for equal protein loading. Among the 3 clones, we have chosen the clone 5 and continued our shRNA transfections with these cells.

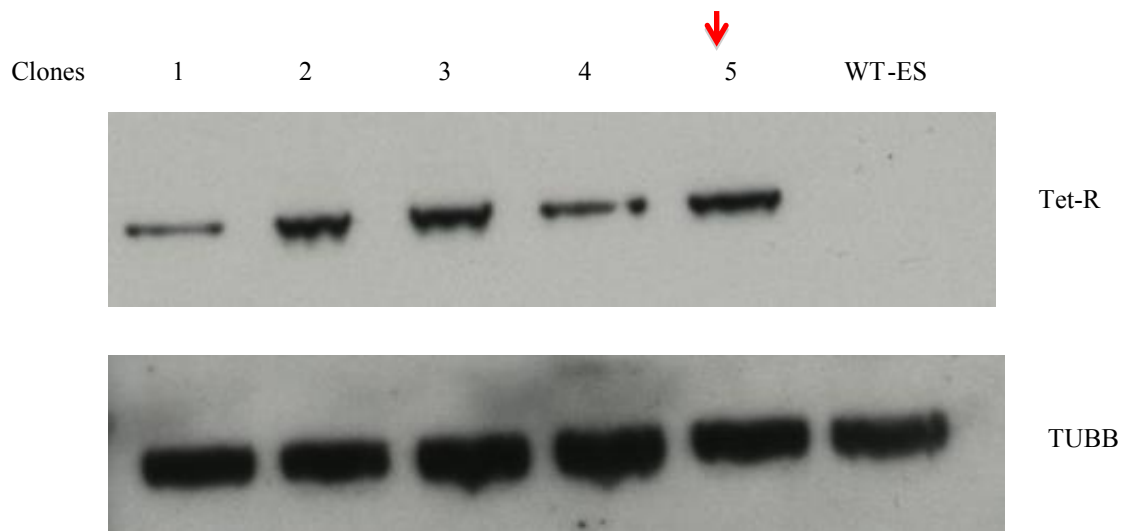


**Figure 5.3: The control of Tet-R expression in different stable clones.** 5 different clones were collected after pcDNA6/TR stable transfection and antibiotic marker selection and the expression levels of Tet-repressor protein (Tet-R) were analyzed by Western Blotting. The clone number 5 was found as expressing the highest levels of Tet-R and therefore selected as the Tet-R clone for the following shRNA plasmid transfections.

Then these cells were transfected for shRNA plasmids containing sequences against Kif18A, MCAK and chTOG. After the selection with Zeocin, cells were expanded in number and stored in liquid nitrogen for later uses. We checked the efficiency of shRNA by Western Blotting after inducing the shRNA expression with Tetracycline. The induced cells were collected at before induction and after 24 and 48 hours of induction. The protein lysates were resolved in SDS-PAGE and blotted onto membranes. The Western blot results show that at 24 hours we can still see plenty of target proteins in cells, especially Kif18A and MCAK are still at the same amount as in uninduced cells (Figure 5.4). Only chTOG starts being degraded before 24 hours. However at 48 hours, the cell degraded almost all of the chTOG and 75% of MCAK and Kif18A started being degraded at this time point. So these results altogether imply that shRNA plasmids work and at least 48 hours is required for the proper gene silencing of target proteins.

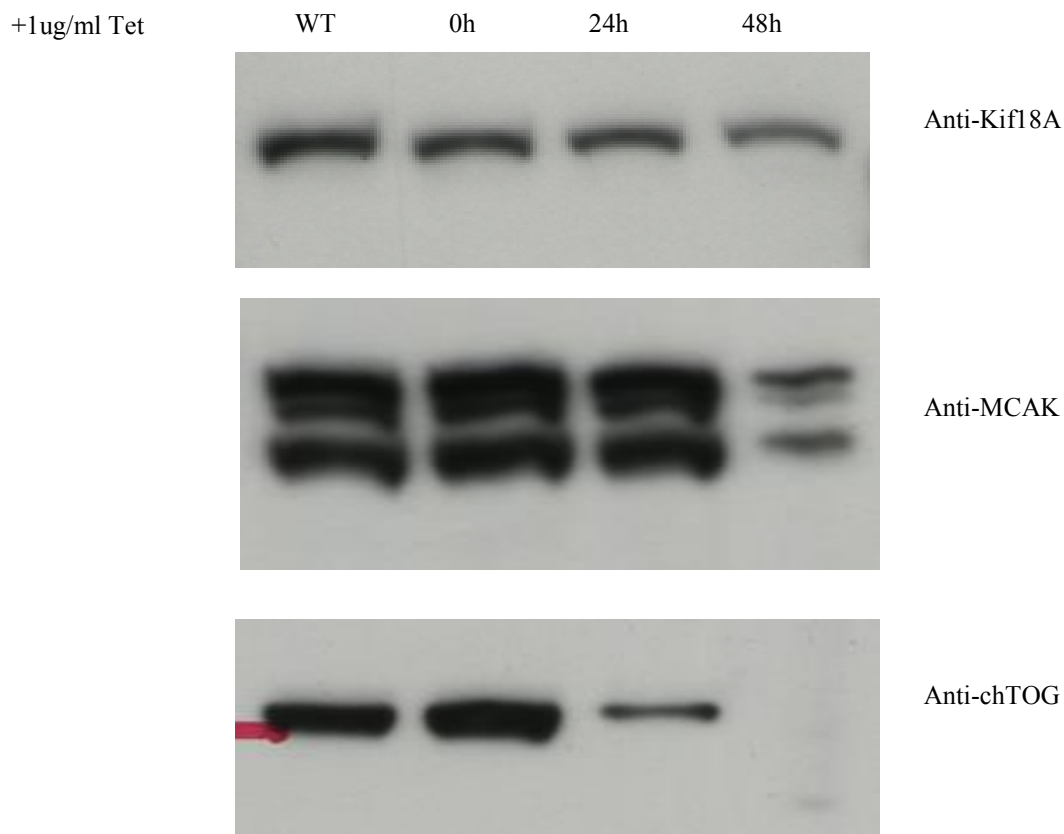


**Figure 5.4: The depletion of MAPs in stable cell lines after Tet-induction.** mES cell lines expressing shRNA's against Kif18A, MCAK and chTOG genes are induced by Tetracycline and the protein lysates are collected at 0, 24 and 48 h time points. The amount of remaining proteins after Tet induction is analyzed by Western blotting by antibodies against each of these genes.

After the generation of the inducible gene silencing system in ES cells, we next differentiated them into cortical cells. To be able to draw the skeleton of single neurons, we mixed our shRNA expressing TUBB-GFP labeled cells with WT-ES cells. After the cortical patterning facilitated by cyclopamine induction, we put the cells onto poly-D lysine-laminin coated coverslips and grown them for a week. After this final maturation step, we fixed the cells and stained them with antibodies against GFP, Tau and TBR1. First we checked the specificity of GFP and Tau antibodies whether they are really labeling the shRNA expressing cells (GFP) and mature neurons (Tau). In the GFP panel of the figure 5.5, we see 4 neuronal cells and a few glial or undifferentiated cells in the left corner. These undifferentiated cells are not stained by the Tau as seen in the Tau panel and one neuron shown by the arrow has not been recognized by the GFP antibody indicating that this cell is an unlabeled wild-type cell.



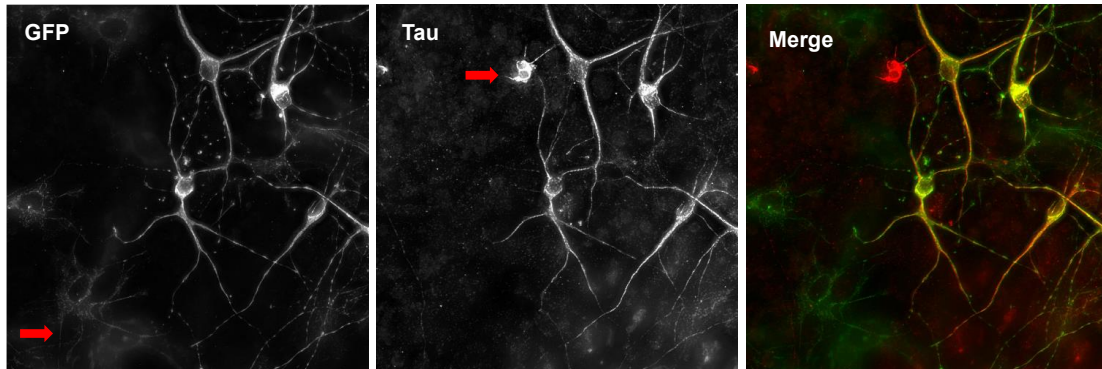
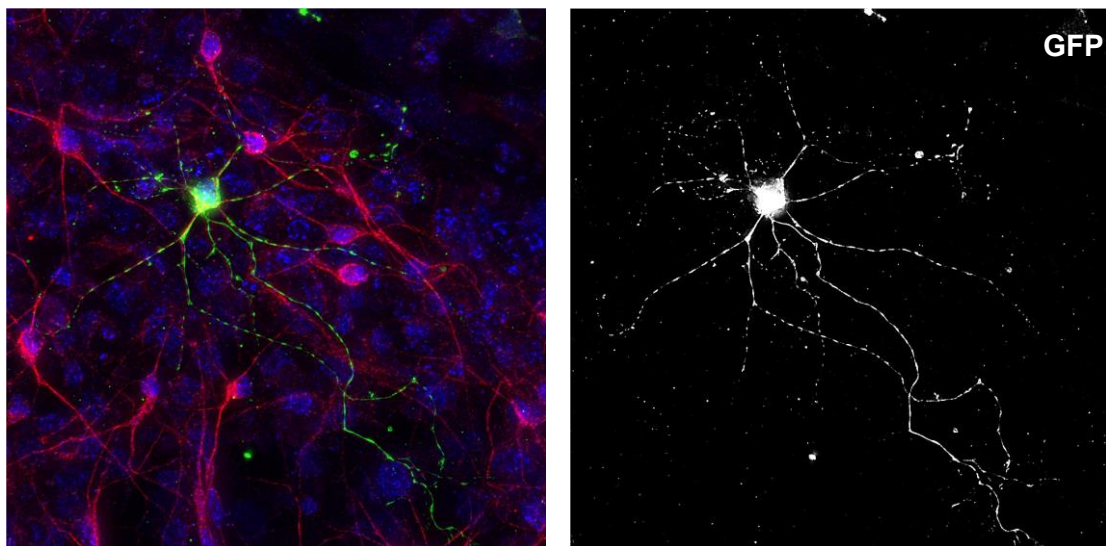


**Figure 5.5: The specificity of GFP and Tau markers.** GFP panel shows the labeled cells and Tau panel shows the mature neurons. Red arrow in GFP panel indicates the Tau(-) GFP labeled cells, probably astrocytes. Red arrow in the Tau panel marks a mature neuron, which is GFP (-). The merge panel shows the specificity of GFP and Tau antibodies.

We next wanted to pick up single neurons out of this neuron pool. The 1:1000 ratio of GFP labeled:unlabeled ES cell gave quite good results, many single neurons could be imaged. In Figure 5.6, we can see one of such cortical neurons, which is positive for GFP, Tau and TBR1. In the first panel, we can see many other Tau+ neurons around the GFP+ neuron and it is really difficult to draw their morphologies depending on the Tau signal. However in the GFP panel, a single neuron beautifully shows up with its neurites.



Green: TUBB-GFP (Labeled Cells)  
 Red: Tau (Mature Neuron)  
 Blue: TBR1 (Neuronal Cells)

**Figure 5.6: The cellular morphology of cortical neurons.** A mixture of GFP-labeled and unlabeled mES cells is differentiated into cortical cells and then fixed and stained with the indicated antibodies. A single mature GFP-expressing cortical neuron could be imaged among other mature cortical cells.

Cortical differentiation of mES cells was successful but we also wanted to confirm this method in larger neuron types such as motor neurons. For this purpose, we differentiated the mES cells into Spinal Motor Neurons (SMN) and after fixation, stained them with dendritic marker MAP2 (Figure 5.7). We have chosen to specifically focus on their dendritic morphology because they have very long axons and it was really difficult to get high-resolution images of the entire neuron. The skeletons of SMN dendrites have been drawn in the Simple Neurite Tracer plug-in of ImageJ. In an ongoing project we have collected the skeletons of many of such neuron dendrites and analyzed them quantitatively by the dimension of fraction method developed in our laboratory by my colleagues Sujoy Ganguly and Hugo Bowne-Anderson. According to this method, we have found 3 different morphological classes in SMNs (unpresented data) and further analyses are still being carried on.

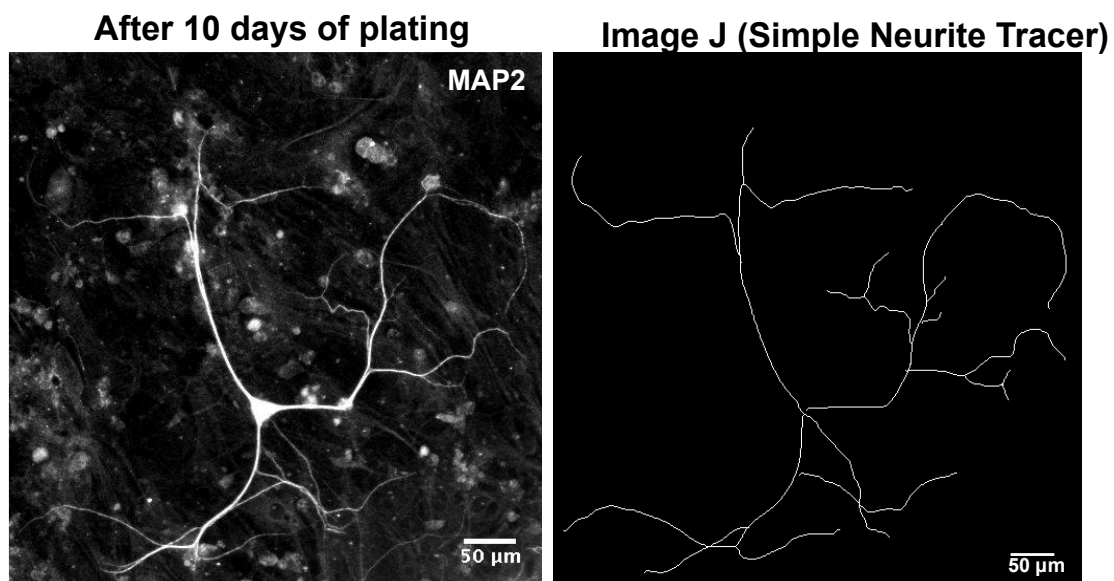


**Figure 5.7: The dendritic morphology of SMNs.** ES cells are differentiated into the Spinal Motor Neurons and fixed and then stained with MAP2 antibody. You see the raw image of the neuron on the left and the skeleton of its dendrites on the right.

Next we wanted to elucidate how the depletions of MAPs affect the neuronal differentiation. We carried out the RNAi experiment with shchTOG cell line and induced the shRNA gene expression at the first day of cortical neuron differentiation. After fixation and staining of the cells with GFP and Tau markers we have observed that GFP and Tau signals do not overlap with each other (Figure 5.8). In Figure 5.8, you see two representative images of the experiment.

Red arrows indicate the cell populations that are undifferentiated. They are positive for GFP signal, which means that these cells are depleted from chTOG and they do not express the mature neuron marker Tau. These cells are also found as cell clusters rather than flat, which is a property of stem cells. On the other hand, cells shown by green arrows are unlabeled ones, which do not express the GFP marker and they are positive for Tau. This result indicates that chTOG is essential for neuronal differentiation and in the absence of it; cells are somehow kept at the pluripotent stage without differentiation.

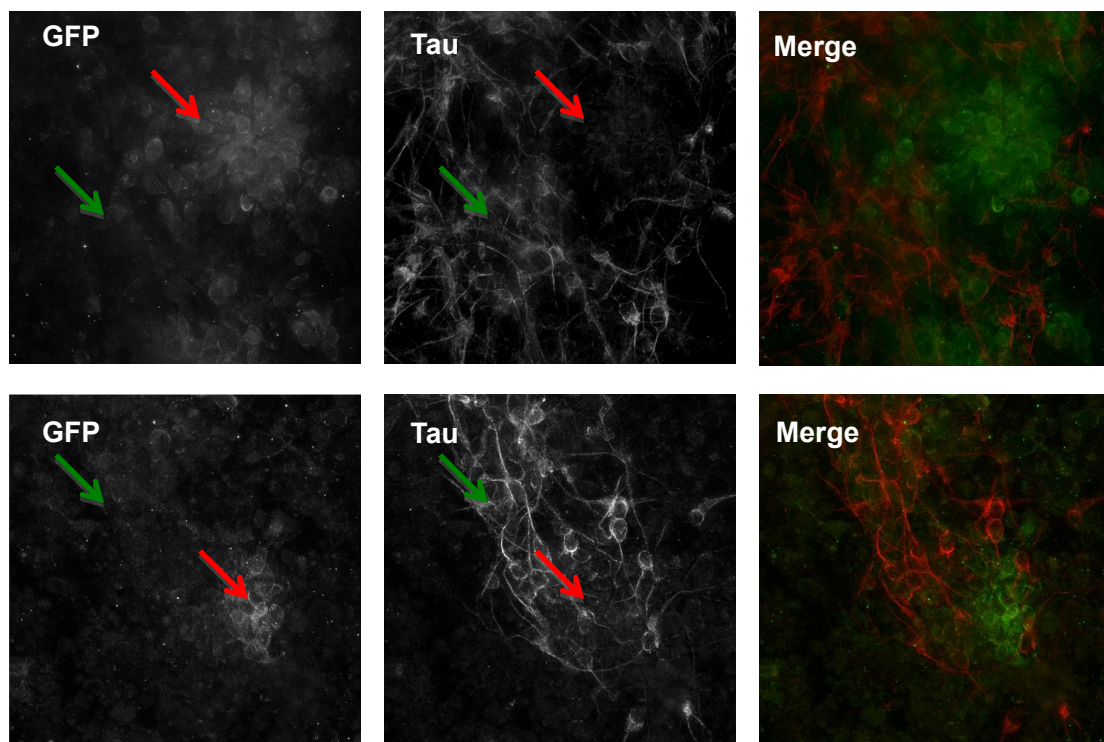


**Figure 5.8: Depletion of chTOG impairs the neuronal differentiation.** ES cells expressing sh chTOG are induced with Tetracycline before initiation of differentiation and then they are differentiated into cortical neurons. Differentiated cells are fixed and then stained with GFP and Tau antibodies. Two representative images of the experiment are shown. Red arrows show GFP(+) and Tau (-) cells and green arrows show GFP(-) and Tau (+) cells. You can see the chTOG depleted cells do not express the mature neuron marker or vice versa.

## Discussion

Cell culture experiments, both primary and neuronal cell lines suffer from the disadvantage that the embryonic context is lost or disrupted and, therefore, might not exactly reflect events *in vivo*. There are well-documented examples in embryos where neuritogenesis begins with the emergence of a single neurite that becomes the axon and later emerging neurites become dendrites (Jacobson, 1991; Roberts, 1988). Despite this caveat, primary neuronal cell cultures have been used extensively to investigate the molecular mechanisms underlying neuronal polarity and a number of key polarity molecules have been identified (Wiggin et al., 2005; Chilton and Gordon-Weeks, 2007). On the other hand, mouse models are expensive and laborious to generate and maintain afterwards and they are quite disadvantageous during imaging if high-resolution data are required for further analyses. In our study, we wanted to preserve the developmental processes of naïve neurons and also wanted to develop a method, which allows us to visualize the single neurons at high resolution to be able to pick-up their morphologies.

In this study, we generated a new inducible ES cell based model to study the molecular determinants of cellular morphologies, in our case particularly in neurons. Although ES cells are quite advantageous in term of their pluripotency and easy genetic manipulation, they can be quite unsatisfactory when high-resolution data is required for analysis. This was because during differentiation the cell density should be kept at a constant level to provide a proper microenvironment to differentiating cells. This is absolutely important for a successful differentiation experiment, because cells are not only reacting to the substances that are added into the medium but they also respond to the ones that are secreted by neighboring cells. For this reason we had to keep the initial cell number at a certain level but in this case the morphologies of differentiated neurons would be very difficult to draw.

We solved this problem by labeling the shRNA expressing cells with a TUBB-GFP BAC construct and then mixing these cells with unlabeled wild-type mES cells.

Tubulin was chosen as a marker because it is ubiquitously expressed in all cell types and it is the main component of cellular cytoskeleton and localizes in a homogenous manner in the cell. After mixing labeled and unlabeled cells at 1:1000 ratios, many single neurons could be imaged under the microscope. Because both cortical and SMNs were plated onto laminin-polyD-lysine coverslips at later stages of differentiation, they grow as 2D on these substrates and this makes them much more suitable for imaging.

Another advantage of this ES cell based system is to be able to control the development of neurons starting from the very early stages of their differentiation. By introducing the Tet-inducible shRNA expression system, we can knock-down the desired genes within 48 hours after induction and this gives an opportunity for researchers to dissect the effects of genes in different developmental stages (Neukirchen et al., 2011). In recent years, in utero electroporation method has been developed to genetically control the neural precursor cells in the mouse brain (Pacary and Guillemot, 2014). This method has advantages over the neuron cultures because it enables the genetic modification before differentiation is completed and does it in the microenvironment of neurons to preserve their tissue-specific behaviors, such as migration. But here they are still in the brain and the imaging of them requires highly advanced microscopy systems such as 2-photon microscopes and even using this system single-molecule localization or tracking experiments are very difficult to set-up in brain tissues. However in our model, differentiating neurons grow as monolayers on the laminin and poly-D lysine coated surfaces and it is theoretically much easier to do single molecule experiments with them once they are labeled with appropriate markers.

In our preliminary knock-down experiments carried out in shchTOG cell line, we have observed that the differentiation of neurons was severely damaged by chTOG depletion (Figure 5.8). Many of the GFP<sup>+</sup> shchTOG cells were negative for mature neuron marker Tau and they were forming small clumps that are mainly found in ES cells. On the other hand, wild-type ES cells differentiate normally, we can see them in the same image as GFP<sup>-</sup> and Tau<sup>+</sup> cells. This result indicates that

tetracycline induction and gene knock-down work quite effectively and in this way we can interfere with the differentiation of ES cells.

In our future work, we want to use this model to understand the functions of Kif18A, MCAK and chTOG in neuronal morphology, especially in the dendrites of SMNs and cortical neurons. We want to deplete each of these genes at different stages of their patterning and to analyze the dendritic morphologies after their differentiation process is completed. By this way, we hope to reveal the roles of these microtubule end-tracking proteins in the generation of cellular architectures.

## 6. Summary

In this study we have generated a non-invasive live-cell imaging method for ES cells for the first time and afterwards we have analyzed the effects of +TIP-binding MAPs in the spindle morphology and mitotic progression using this method. Our RNAi studies with chTOG, EB1, Kif18A and MCAK showed that chTOG is important for spindle assembly and its absence causes mini-spindle phenotype. On the other hand, the knock-down of Kif18A produces longer spindles indicating that this protein is involved in the control of spindle length. Moreover, EB1 and MCAK knockdown did not show a clear difference in the spindle morphology. We have found an interesting result from the co-depletions of chTOG and EB1. Although chTOG reduces the spindle length and EB1 did not change it, the co-depletion of these two genes partially rescued the mini-spindle phenotype of sichTOG. This result further supports the view of the catastrophic activity of EB1 at the MT +ends and shows that the synergy between chTOG and EB1 depends on the presence of chTOG in the cell. Therefore we hypothesize that in the absence of chTOG, EB1 works as a catastrophe factor to initiate the depolymerization of MTs.

Another surprising result that we have found was the additive effects of chTOG and Kif18A co-depletion in the spindle assembly and mitotic progression. Although the antagonistic functions of these two genes in the spindle length have been previously shown in *Drosophila* S2 cells, we have found that the simultaneous knockdown of chTOG and Kif18A did not rescue their mini-spindle and long spindle phenotypes. On the contrary, we observed that in the absence of these two genes, the spindle assembly mechanism was severely disrupted. We have also seen a similar kind of abnormality in the mitotic progression and chromosome segregation. Double knock-down of chTOG and Kif18A led to increased metaphase alignment times and high levels of chromosome segregation errors.

In the last part, we have generated an inducible neuronal morphology model in ES cells to be able to analyze the effects of genes in the generation neuronal morphology at different developmental stages. For this purpose, we have labeled the shRNA expressing cell lines with GFP-TUBB and by mixing them with unlabeled cells before differentiation we could generate the skeletons of neurons. Our results show that the Tet-induction system works efficiently, although there are some fluctuations between different genes, and the knock-down of chTOG at the early stages of differentiation interferes with the neuronal development. We will continue to our experiments with different MAP genes and by knocking them down at early and late stages of neuronal differentiation.



## 7. Bibliography

Akhmanova A. and Steinmetz MO. Tracking the ends: a dynamic protein network controls the fate of microtubule tips. *Nature reviews Molecular cell biology*, 2008. 9(4):309-322.

Akhmanova A. and Steinmetz MO. Microtubule+ TIPs at a glance. *Journal of cell science*, 2010.123(20):3415-3419.

Al-Bassam J., Kim H., Brouhard G., van Oijen A., Harrison SC., Chang F. CLASP promotes microtubule rescue by recruiting tubulin dimers to the microtubule. *Developmental cell*, 2010.19(2): 245-258.

Al-Bassam J. and Chang F. Regulation of microtubule dynamics by TOG-domain proteins XMAP215/Dis1 and CLASP. *Trends in cell biology*, 2011. 21(10):604-614.

Amos LA. and Klug A. Arrangement of subunits in flagellar microtubules. *Journal of cell science*, 1974.14(3):523-549.

Andrews PD., Ovechkina Y., Morrice N., Wagenbach M., Duncan K., Wordeman L., Swedlow JR. Aurora B regulates MCAK at the mitotic centromere. *Developmental cell*, 2004.6(2):253-268.

Artus J. and Hadjantonakis AK. Live imaging genetically-encoded fluorescent proteins in embryonic stem cells using confocal microscopy. *Modern Research and Educational Topics in Microscopy*, 2007. A.Mendez-Vilas and J. Diaz (Eds):190-202

Askham JM., Vaughan KT., Goodson HV., Morrison EE. Evidence that an interaction between EB1 and p150Glued is required for the formation and

maintenance of a radial microtubule array anchored at the centrosome. *Molecular biology of the cell*, 2002.13(10): 3627-3645.

Avilion AA., Nicolis SK., Pevny LH., Perez L., Vivian N., Lovell-Badge R. Multipotent cell lineages in early mouse development depend on SOX2 function. *Genes Dev*, 2003. 17(1): 126-40.

Audebert S., Koulakoff A., Berwald-Netter Y., Gros F., Denoulet P., Eddé B. Developmental regulation of polyglutamylated alpha-and beta-tubulin in mouse brain neurons. *Journal of cell science*, 1994.107(8):2313-2322.

Babinet C. and Cohen-Tannoudji M. Genome engineering via homologous recombination in mouse embryonic stem (ES) cells: an amazingly versatile tool for the study of mammalian biology. *An Acad Bras Cienc*, 2001. 73(3): 365-83.

Banerjee ASOK., Roach MC., Wall KA., Lopata MA., Cleveland DW., Luduena RF. A monoclonal antibody against the type II isotype of beta-tubulin. Preparation of isotypically altered tubulin. *Journal of Biological Chemistry*, 1988.263(6):3029-3034.

Beddington RS., Morgernstern J., Land H, Hogan, A. An in situ transgenic enzyme marker for the midgestation mouse embryo and the visualization of inner cell mass clones during early organogenesis. *Development*, 1989. 106(1): 37-46.

Bieling P., Kandels-Lewis S., Telley IA., van Dijk J., Janke C., Surrey, T. CLIP-170 tracks growing microtubule ends by dynamically recognizing composite EB1/tubulin-binding sites. *The Journal of cell biology*, 2008.183(7): 1223-1233.

Bradke F., Dotti CG. Establishment of neuronal polarity: lessons from cultured hippocampal neurons. *Curr. Opin. Neurobiol.*, 2000. 10:574–81.

Bringmann H., Cowan CR., Kong J., Hyman AA. LET-99, GOA-1/GPA-16, and GPR-1/2 are required for aster-positioned cytokinesis. *Curr Biol.*, 2007. 17:185-91.

Brittle AL. and Ohkura H. Mini spindles, the XMAP215 homologue, suppresses pausing of interphase microtubules in *Drosophila*. *The EMBO journal*, 2005.24(7): 1387-1396.

Brouhard GJ., Stear JH., Noetzel TL., Al-Bassam J., Kinoshita K., Harrison SC., ... Hyman AA. XMAP215 is a processive microtubule polymerase. *Cell*, 2008. 132(1): 79-88.

Brunner D., and Nurse P. CLIP170-like tip1p spatially organizes microtubular dynamics in fission yeast. *Cell*, 2000. 102:695-704.

Buey RM., Mohan R., Leslie K., Walzthoeni T., Missimer JH., Menzel A., ... Steinmetz MO. Insights into EB1 structure and the role of its C-terminal domain for discriminating microtubule tips from the lattice. *Molecular biology of the cell*, 2011.22(16):2912-2923.

Burgoyne RD., Cambray-Deakin MA., Lewis SA., Sarkar SRIJATA., Cowan NJ. Differential distribution of beta-tubulin isotypes in cerebellum. *The EMBO journal*, 1988.7(8): 2311.

Burns RG.  $\alpha$ -,  $\beta$ -, and  $\gamma$ -tubulins: Sequence comparisons and structural constraints. *Cell motility and the cytoskeleton*, 1991. 20(3): 181-189.

Busch KE. and Brunner D. The microtubule plus end-tracking proteins mal3p and tip1p cooperate for cell-end targeting of interphase microtubules. *Current biology*, 2004.14(7): 548-559.

Capecchi MR. Gene targeting in mice: functional analysis of the mammalian genome for the twenty-first century. *Nat Rev Genet.*, 2005. 6(6): 507-12.

Caspi O., Itzhaki I., Kehat I., Gepstein A., Arbel G., Huber I., ... Gepstein L. In vitro electrophysiological drug testing using human embryonic stem cell derived cardiomyocytes. *Stem cells and development*, 2009.18(1):161-172.

Cederquist GY., Luchniak A., Tischfield MA., Peeva M., Song Y., Menezes MP., ... Engle EC. An inherited TUBB2B mutation alters a kinesin-binding site and causes polymicrogyria, CFEOM and axon dysinnervation. *Human molecular genetics*, 2012.ddd393.

Charrasse S., Schroeder M., Gauthier-Rouviere C., Ango F., Cassimeris L., Gard D. L., Larroque C. The TOGp protein is a new human microtubule-associated protein homologous to the *Xenopus* XMAP215. *Journal of Cell Science*, 1998.111(10): 1371-1383.

Cheeseman IM. and Desai A. Molecular architecture of the kinetochore-microtubule interface. *Nature Reviews Molecular Cell Biology*, 2008.9:33-46.

Chilton JK. And Gordon-Weeks PR. Role of microtubules and MAPs during neuritogenesis. In *Intracellular mechanisms for neuritogenesis*, 2007. (pp. 57-88). Springer US.

Chiron S., Bobkova A., Zhou H., Yaffe MP. CLASP regulates mitochondrial distribution in *Schizosaccharomyces pombe*. *The Journal of cell biology*, 2008.182(1):41-49.

Chrétien D., Metoz F., Verde F., Karsenti E., and Wade R. H. Lattice defects in microtubules: protofilament numbers vary within individual microtubules. *The Journal of cell biology*, 1992.117(5):1031-1040.

Chung S., Andersson T., Sonntag KC., Björklund L., Isacson O., Kim KS. Analysis of different promoter systems for efficient transgene expression in mouse embryonic stem cell lines. *Stem Cells*. 2002. 20(2):139-45.

Craig AM., Banker G. Neuronal polarity. *Annu. Rev. Neurosci.*, 1994.17:267-310.  
Cullen CF., Deák P., Glover DM., Ohkura H. mini spindles A Gene Encoding a Conserved Microtubule-Associated Protein Required for the Integrity of the Mitotic Spindle in *Drosophila*. *The Journal of cell biology*, 1999.146(5): 1005-1018.

Dammermann A., Desai A., Oegema K. The minus end in sight. *Current biology*, 2003.13(15):R614-R624.

De Groot CO., Jelesarov I., Damberger FF., Bjelić S., Schärer MA., Bhavesh NS., ... Steinmetz MO. Molecular insights into mammalian end-binding protein heterodimerization. *Journal of Biological Chemistry*, 2010.285(8):5802-5814.

Delhaise F., Bralion V., Schuurbiens N., Dessy, F. Establishment of an embryonic stem cell line from 8-cell stage mouse embryos. *Eur J Morphol*, 1996. 34(4): 237-43.

Desai A., Verma S., Mitchison TJ., Walczak, CE. Kin I kinesins are microtubule-destabilizing enzymes. *Cell*, 1999. 96(1):69-78.

De Zeeuw CI., Hoogenraad CC., Goedknecht E., Hertzberg E., Neubauer A., Grosveld F., Galjart N. CLIP-115, a novel brain-specific cytoplasmic linker protein, mediates the localization of dendritic lamellar bodies. *Neuron*, 1997. 19(6): 1187-1199.

Díaz-Valencia JD., Morelli MM., Bailey M., Zhang D., Sharp DJ., Ross JL. Drosophila Katanin-60 Depolymerizes and Severs at Microtubule Defects. *Biophysical journal*, 2011.100(10):2440-2449.

Ding L. Poser I., Paszkowski-Rogacz M., Buchholz F. From RNAi screens to molecular function in embryonic stem cells. *Stem Cell Reviews and Reports*, 2012. 8(1):32-42.

Dixit R., Barnett B., Lazarus JE., Tokito M., Goldman YE., Holzbaur EL. Microtubule plus-end tracking by CLIP-170 requires EB1. *Proceedings of the National Academy of Sciences*, 2009.106(2):492-497.

Domogatskaya A., Rodin S., Boutaud A., Tryggvason K. Laminin-511 but not -332, -111, or -411 enables mouse embryonic stem cell self-renewal in vitro. *Stem Cells*, 2008. 26(11):2800-2809.

Donaldson DD., Wongtli GG., Moreau J., Stahli M., Rogersi, D. Inhibition of pluripotential embryonic stem cell differentiation by purified polypeptides. *Nature*, 1988. 336(6200):15.

Dotti CG. and Banker GA. Experimentally induced alteration in the polarity of developing neurons. *Nature*, 1987.330:254–56.

Downing KH. and Nogales E. Tubulin structure: insights into microtubule properties and functions. *Current opinion in structural biology*, 1998.8(6): 785-791.

Drechsel DN. and Kirschner MW. The minimum GTP cap required to stabilize microtubules. *Current Biology*, 1994.4(12):1053-1061.

Dumont J., Petri S., Pellegrin F., Terret ME., Bohnsack MT., et al. A centriole- and RanGTP-independent spindle assembly pathway in meiosis I of vertebrate oocytes. *J. Cell Biol.*, 2007.176:295–305.

Dumont S. and Mitchison TJ. Force and length in the mitotic spindle. *Current Biology*, 2009.19(17):R749-R761.

Efimov A., Kharitonov A., Efimova N., Loncarek J., Miller PM., Andreyeva N., ... Kaverina I. Asymmetric CLASP-Dependent Nucleation of Noncentrosomal Microtubules at the trans-Golgi Network. *Developmental cell*, 2007.12(6):917-930.

Eilken HM., Nishikawa SI., and Schroeder T. Continuous single-cell imaging of blood generation from haemogenic endothelium. *Nature*, 2009.457(7231): 896-900.

Emre N., Coleman R., and Ding S. A chemical approach to stem cell biology. *Curr Opin Chem Biol*, 2007. 1(3):252-258.

Evans MJ. and Kaufman MH. Establishment in culture of pluripotential cells from mouse embryos. *Nature*, 1981. 292(5819):154-156.

Evans L., Mitchison T., Kirschner, M. Influence of the centrosome on the structure of nucleated microtubules. *The Journal of cell biology*, 1985.100(4):1185-1191.

Ferreira A., Busciglio J., and Caceres A. Microtubule formation and neurite growth in cerebellar macroneurons which develop in vitro: Evidence for the involvement of the microtubule-associated proteins, MAP-1a, HMW-MAP2 and Tau. *Brain Res. Dev. Brain Res.*, 1989.49: 215–228.

Ferreira JG., Pereira AJ., Akhmanova A., Maiato H. Aurora B spatially regulates EB3 phosphorylation to coordinate daughter cell adhesion with cytokinesis. *The Journal of cell biology*, 2013.201(5):709-724.

Gaertig J. and Wloga D. Ciliary tubulin and its post-translational modifications. *Current topics in developmental biology*, 2008.85: 83-113.

Garcia MA., Koonrugsa N., Toda T. Two kinesin-like Kin I family proteins in fission yeast regulate the establishment of metaphase and the onset of anaphase A. *Current biology*, 2002. 12(8):610-621.

Gard DL. and Kirschner MW. A microtubule-associated protein from *Xenopus* eggs that specifically promotes assembly at the plus-end. *The Journal of cell biology*, 1987.105(5):2203-2215.

Gardner MK., Zanic M., Gell C., Bormuth V., Howard J. Depolymerizing kinesins Kip3 and MCAK shape cellular microtubule architecture by differential control of catastrophe. *Cell*, 2011. 147:1092-1103.

Gardner MK., Zanic M., Howard J. Microtubule catastrophe and rescue. *Current opinion in cell biology*, 2013.25(1): 14-22.

Gergely F., Draviam VM., Raff JW. The ch-TOG/XMAP215 protein is essential for spindle pole organization in human somatic cells. *Genes & development*, 2003.17(3):336-341.

Godinho SA., Kwon M., Pellman D. Centrosomes and cancer: how cancer cells divide with too many centrosomes. *Cancer Metastasis Rev.*, 2009. 28(1-2):85-98.

Goshima G., Wollman R., Stuurman N., Scholey JM., Vale RD. Length control of the metaphase spindle. *Current biology*, 2005.15(22):1979-1988.

Goshima G., Wollman R., Goodwin SS., Zhang N., Scholey JM., Vale RD., Stuurman N. Genes required for mitotic spindle assembly in *Drosophila* S2 cells. *Science*, 2007.316(5823): 417-421.

Goshima G. and Scholey JM. Control of mitotic spindle length. *Annual review of cell and developmental biology*, 2010.26:21-57.

Groen AC., Maresca TJ., Gatlin JC., Salmon ED., Mitchison TJ. Functional overlap of microtubule assembly factors in chromatin-promoted spindle assembly. *Molecular biology of the cell*, 2009.20(11):2766-2773.

Guo Y., Kim C., Mao Y. New insights into the mechanism for chromosome alignment in metaphase. *Int Rev Cell Mol Biol.*, 2013.303:237-62.

Gupta KK., Paulson BA., Folker ES., Charlebois B., Hunt AJ. and Goodson HV. Minimal plus-end tracking unit of the cytoplasmic linker protein CLIP-170. *J. Biol. Chem.*, 2009. 284:6735-6742.

Gupta ML., Carvalho P., Roof DM., Pellman D. Plus end-specific depolymerase activity of Kip3, a kinesin-8 protein, explains its role in positioning the yeast mitotic spindle. *Nat Cell Biol.*, 2006.8:913-923.



Hara Y. and Kimura A. An allometric relationship between mitotic spindle width, spindle length, and ploidy in *Caenorhabditis elegans* embryos. *Molecular biology of the cell*, 2013.24(9): 1411-1419.

Helenius J., Brouhard G., Kalaidzidis Y., Diez S., Howard, J. The depolymerizing kinesin MCAK uses lattice diffusion to rapidly target microtubule ends. *Nature*, 2006.441(7089):115-119.

Helmke KJ., Heald R., Wilbur JD. Interplay between spindle architecture and function. *Int Rev Cell Mol Biol*, 2013.306:83-125.

Homma N., Takei Y., Tanaka Y., Nakata T., Terada S., Kikkawa M., ... Hirokawa N. Kinesin superfamily protein 2A (KIF2A) functions in suppression of collateral branch extension. *Cell*, 2003. 114: 229-239.

Honnappa S., Gouveia SM., Weisbrich A., Damberger FF., Bhavesh NS., Jawhari H., ... Steinmetz MO. An EB1-binding motif acts as a microtubule tip localization signal. *Cell*, 2009. 138(2): 366-376.

Hoogenraad CC., Akhmanova A., Grosveld F., De Zeeuw CI., Galjart N. Functional analysis of CLIP-115 and its binding to microtubules. *Journal of cell science*, 2000.113(12): 2285-2297.

Houghtaling BR., Yang G., Matov A., Danuser G., Kapoor TM. Op18 reveals the contribution of nonkinetochore microtubules to the dynamic organization of the vertebrate meiotic spindle. *Proc Natl Acad Sci U S A*, 2009. 106(36):15338-43.

Howard J. and Hyman AA. Microtubule polymerases and depolymerases. *Current opinion in cell biology*, 2007.19(1): 31-35.

Hübner K., Fuhrmann G., Christenson LK., Kehler J., Reinbold R., De La Fuente R., ... Schöler HR. Derivation of oocytes from mouse embryonic stem cells. *Science*, 2003. 300(5623): 1251-6.

Hunter AW., Caplow M., Coy DL., Hancock WO., Diez S., Wordeman L., Howard J. The kinesin-related protein MCAK is a microtubule depolymerase that forms an ATP-hydrolyzing complex at microtubule ends. *Molecular cell*, 2003.11(2): 445-457.

Hutchins JR., Toyoda Y., Hegemann B., et al. Systematic analysis of human protein complexes identifies chromosome segregation proteins. *Science*, 2010.328(5978): 593-599.

Hyman AA., Salser S., Drechsel DN., Unwin N., Mitchison, TJ. Role of GTP hydrolysis in microtubule dynamics: information from a slowly hydrolyzable analogue, GMPCPP. *Molecular biology of the cell*, 1992.3(10):1155-1167.

Jacobson L. and Sapolsky R. The Role of the Hippocampus in Feedback Regulation of the Hypothalamic-Pituitary-Adrenocortical Axis\*. *Endocrine reviews*, 1991. 12(2): 118-134.

Janke C., Rogowski K., Wloga D., Regnard C., Kajava AV., Strub JM., ... Eddé B. Tubulin polyglutamylase enzymes are members of the TTL domain protein family. *Science*, 2005.308(5729): 1758-1762.

Janke C. and Bulinski JC. Post-translational regulation of the microtubule cytoskeleton: mechanisms and functions. *Nature reviews Molecular cell biology*, 2011. 12(12):773-786.

Jiang J., Chan YS., Loh YH., Cai J., Tong GQ., Lim CA., ... Ng HH. A core Klf circuitry regulates self-renewal of embryonic stem cells. *Nature cell biology*, 2008.10(3):353-360.

Keller G. Embryonic stem cell differentiation: emergence of a new era in biology and medicine. *Genes & Development*, 2005.19 (10): 1129-1155.

Kikkawa M., Ishikawa T., Nakata T., Wakabayashi T., Hirokawa N. Direct visualization of the microtubule lattice seam both in vitro and in vivo. *The Journal of cell biology*, 1994.127(6):1965-1971.

Kinoshita K., Noetzel TL., Arnal I., Drechsel DN., Hyman AA. Global and local control of microtubule destabilization promoted by a catastrophe kinesin MCAK/XKCM1. *Journal of Muscle Research & Cell Motility*, 2006.27(2):107-114.

Kittler R., Pelletier L., Ma C., et al. RNA interference rescue by bacterial artificial chromosome transgenesis in mammalian tissue culture cells. *Proceedings of the National Academy of Sciences of the United States of America*, 2005.102(7): 2396-2401.

Kodama A., Karakesisoglou I., Wong E., Vaezi A., Fuchs, E. ACF7: an essential integrator of microtubule dynamics. *Cell*, 2003. 115(3): 343-354.

Komarova YA., Akhmanova AS., Kojima S., Galjart N., and Borisy GG. Cytoplasmic linker proteins promote microtubule rescue in vivo. *J. Cell Biol.*, 2002. 159:589-599.

Komarova Y., De Groot CO., Grigoriev I., Gouveia SM., Munteanu EL., Schober JM., ... Akhmanova A. Mammalian end binding proteins control persistent microtubule growth. *The Journal of cell biology*, 2009.184(5): 691-706.

Kwon M., Morales-Mulia S., Brust-Mascher I., Rogers GC., Sharp DJ., Scholey, JM. The chromokinesin, KLP3A, drives mitotic spindle pole separation during prometaphase and anaphase and facilitates chromatid motility. *Molecular biology of the cell*, 2004.15(1):219-233.

Lawson JL. And Salas, RE. Microtubules: greater than the sum of the parts. *Biochemical Society transactions*, 2013.41(6):1736-1744.

Leandro-García LJ., Leskelä S., Jara C., Gréen H., Åvall-Lundqvist E., Wheeler H. E., ... Rodríguez-Antona C. Regulatory polymorphisms in  $\beta$ -tubulin IIa are associated with paclitaxel-induced peripheral neuropathy. *Clinical Cancer Research*, 2012.18(16):4441-4448.

Lee SH., Lumelsky N., Studer L., Auerbach JM., McKay RD. Efficient generation of midbrain and hindbrain neurons from mouse embryonic stem cells. *Nat Biotechnol*, 2000. 18(6): 675-9.

Lee T., Langford KJ., Askham JM., Brüning-Richardson A., Morrison EE. MCAK associates with EB1. *Oncogene*, 2007.27(17): 2494-2500.

L'Hernault SW. and Rosenbaum JL. Chlamydomonas. alpha-tubulin is posttranslationally modified by acetylation on the epsilon-amino group of a lysine. *Biochemistry*, 1985.24(2): 473-478.

Li S., Lei L., Somerville CR., Gu Y. Cellulose synthase interactive protein 1 (CSI1) links microtubules and cellulose synthase complexes. *Proceedings of the National Academy of Sciences*, 2012.109(1):185-190.

Loh YH., Wu Q., Chew JL., Vega VB., Zhang W., Chen X., ... Ng HH. The Oct4 and Nanog transcription network regulates pluripotency in mouse embryonic stem cells. *Nature genetics*, 2006.38(4):431-440.

Louie RK., Bahmanyar S., Siemers KA., Votin V., Chang P., Stearns T., ... Barth AI. Adenomatous polyposis coli and EB1 localize in close proximity of the mother centriole and EB1 is a functional component of centrosomes. *Journal of cell science*, 2004.117(7):1117-1128.

Ludueña RF. and Banerjee A. The isotypes of tubulin. In *The Role of Microtubules in Cell Biology*, 2008. Neurobiology, and Oncology (pp. 123-175). Humana Press.

Maiato H., Khodjakov A., Rieder CL. Drosophila CLASP is required for the incorporation of microtubule subunits into fluxing kinetochore fibres. *Nature cell biology*, 2004.7(1):42-47.

Mandelkow EM., Schultheiss R., Rapp R., Müller M., Mandelkow E. On the surface lattice of microtubules: helix starts, protofilament number, seam, and handedness. *The Journal of cell biology*, 1986.102(3):1067-1073.

Manna T., Honnappa S., Steinmetz MO., Wilson L. Suppression of microtubule dynamic instability by the+ TIP protein EB1 and its modulation by the CAP-Gly domain of p150glued. *Biochemistry*, 2008.47(2): 779-786.

Margolis RL. and Wilson L. Opposite end assembly and disassembly of microtubules at steady state in vitro. *Cell*, 1978. 13(1):1-8.

Martin GR. Isolation of a pluripotent cell line from early mouse embryos cultured in medium conditioned by teratocarcinoma stem cells. *Proc Natl Acad Sci U S A*, 1981. 78(12): 7634-8.

McEwen BF, Heagle AB, Cassels GO, Buttle KF, Rieder CL. Kinetochore fiber maturation in PtK1 cells and its implications for the mechanisms of chromosome congression and anaphase onset. *J Cell Biol.*, 1997. 137(7):1567-80.

Megason S., and Fraser S. Imaging in systems biology. *Cell*, 2007. 130:784-795.

Miller PM., Folkmann AW., Maia AR., Efimova N., Efimov A., Kaverina, I. Golgi-derived CLASP-dependent microtubules control Golgi organization and polarized trafficking in motile cells. *Nature cell biology*, 2009.11(9): 1069-1080.

Mimori-Kiyosue Y., Shiina N., Tsukita, S.The dynamic behavior of the APC-binding protein EB1 on the distal ends of microtubules.*Current Biology*, 2000.10(14):865-868.

Mitchison T., Wühr M., Nguyen P., Ishihara K., Groen A., Field CM. Growth, interaction, and positioning of microtubule asters in extremely large vertebrate embryo cells. *Cytoskeleton*, 2012.69(10):738-750.

Mitsui K., Tokuzawa Y., Itoh H., Segawa K., Murakami M., Takahashi K., ... Yamanaka S. The homeoprotein Nanog is required for maintenance of pluripotency in mouse epiblast and ES cells. *Cell*, 2003. 113(5): 631-42.

Montenegro Gouveia S., Leslie K., Kapitein LC., Buey RM., Grigoriev I., Wagenbach M., ... Akhmanova A. In vitro reconstitution of the functional interplay between MCAK and EB3 at microtubule plus ends. *Current Biology*, 2010.20(19): 1717-1722.

Moores CA., Yu M., Guo J., Beraud C., Sakowicz R., Milligan RA. A mechanism for microtubule depolymerization by KinI kinesins. *Molecular cell*, 2002.9(4): 903-909.

Morrison EE., Wardleworth BN., Askham JM., Markham AF., Meredith DM. EB1, a protein which interacts with the APC tumour suppressor, is associated with the microtubule cytoskeleton throughout the cell cycle. *Oncogene*, 1998.17(26):3471-3477.

Moritz M. and Agard DA.  $\gamma$ -Tubulin complexes and microtubule nucleation. *Current opinion in structural biology*, 2001.11(2):174-181.

Muyrers JP., Zhang Y., and Stewart AF. Techniques: recombinogenic engineering—new options for cloning and manipulating DNA. *Trends in Biochemical Sciences*, 2001.26(5): 325–331.

Nagy A., Gertsenstein M., Vintersten K., Behringer R. *Manipulating the Mouse Embryo. A laboratory manual*. Third edition, 2003. Cold Spring Harbor Press.

Nakagawa H., Koyama K., Murata Y., Morito M., Akiyama T., Nakamura Y. EB3, a novel member of the EB1 family preferentially expressed in the central nervous system, binds to a CNS-specific APC homologue. *Oncogene*, 2000.19(2):210-216.

Nichols J., Evans EP. and Smith AG. Establishment of germ-line-competent embryonic stem (ES) cells using differentiation inhibiting activity. *Development*, 1990. 110(4): 1341-8.

Nichols J., Zevnik B., Anastassiadis K., Niwa H., Klewe-Nebenius D., Chambers I., ... Smith A. Formation of pluripotent stem cells in the mammalian embryo depends on the POU transcription factor Oct4. *Cell*, 1998. 95(3): 379-91.

Niederstrasser H., Salehi-Had H., Gan EC., Walczak C. and Nogales, E. XKCM1 acts on a single protofilament and requires the C terminus of tubulin. *J. Mol. Biol.*, 2002. 316: 817--828.

Niwa H. How is pluripotency determined and maintained? *Development*, 2007. 134(4): 635-46.

Noda Y., Sato-Yoshitake R., Kondo S., Nangaku M., Hirokawa N. KIF2 is a new microtubule-based anterograde motor that transports membranous organelles distinct from those carried by kinesin heavy chain or KIF3A/B. *The Journal of cell biology*, 1995.129(1):157-167.

O'Brien ET., Salmon ED., Walker RA., Erickson HP. Effects of magnesium on the dynamic instability of individual microtubules. *Biochemistry*, 1990.29(28):6648-6656.

Okabe S., Forsberg-Nilsson K., Spiro AC., Segal M., McKay RD. Development of neuronal precursor cells and functional postmitotic neurons from embryonic stem cells in vitro. *Mech Dev*, 1996. 59(1): 89-102.

Pacary E. and Guillemot F. In Utero Electroporation to Study Mouse Brain Development. In Brain Development, 2014. (pp. 285-293). Humana Press.

Perez F., Diamantopoulos GS., Stalder R., Kreis TE. CLIP-170 highlights growing microtubule ends in vivo. Cell, 1999. 96(4):517-527.

Peris L., Wagenbach M., Lafanechère L., Brocard J., Moore AT., Kozielski F., ... Andrieux A. Motor-dependent microtubule disassembly driven by tubulin tyrosination. The Journal of cell biology, 2009.185(7):1159-1166.

Poser I., Sarov M., Hutchins JR., Hériché JK., Toyoda Y., Pozniakovsky A., ... Hyman AA. BAC TransgeneOmics: a high-throughput method for exploration of protein function in mammals. Nature Methods, 2008.5(5): 409-415.

Raff EC., Fackenthal JD., Hutchens JA., Hoyle HD., Turner FR. Microtubule architecture specified by a  $\beta$ -tubulin isoform. Science, 1997.275(5296): 70-73.

Rankin KE. and Wordeman L. Long astral microtubules uncouple mitotic spindles from the cytokinetic furrow. The Journal of cell biology, 2010.190(1):35-43.

Rieger MA., Hoppe PS., Smejkal BM., Eitelhuber AC., Schroeder T. Hematopoietic cytokines can instruct lineage choice. Science, 2009.325(5937): 217-218.

Roberts A. The early development of neurons in Xenopus embryos revealed by transmitter immunocytochemistry for serotonin, GABA and glycine. Developmental Neurobiology of the Frog, 1988. New York, 191-205.

Rodin S., Domogatskaya A., Ström S., Hansson EM., Chien KR., Inzunza J., Hovatta O., Tryggvason K. Long-term self-renewal of human pluripotent stem cells on human recombinant laminin-511. Nature Biotechnology, 2010.28(6):611-615.

Rodionov V., Nadezhdina E., Borisy G. Centrosomal control of microtubule dynamics. Proceedings of the National Academy of Sciences, 1999.96(1):115-120.



Robertson EJ. Teratocarcinomas and embryonic stem cells. A practical approach, ed. H.B.D. Rickwood D. 1987: IRL Press.

Samejima I, Lourenço PC, Snaith HA, Sawin KE. Fission yeast mto2p regulates microtubule nucleation by the centrosomin-related protein mto1p. *Molecular biology of the cell*, 2005.16(6):3040-3051.

Sarov M, Schneider S, Pozniakovski A, et al. A recombineering pipeline for functional genomics applied to *Caenorhabditis elegans*. *Nature Methods*, 2006.3(10): 839-844.

Savoian MS. And Glover DM. *Drosophila* Klp67A binds prophase kinetochores to subsequently regulate congression and spindle length. *Journal of cell science*, 2010.123(5): 767-776.

Schroeder T. Long-term single-cell imaging of mammalian stem cells. *Nature methods*, 2011.8(4s): S30-S35.

Schroer TA. Dynactin. *Annu. Rev. Cell Dev. Biol.*, 2004. 20:759-779.

Shirasu-Hiza M, Coughlin P, Mitchison T. Identification of XMAP215 as a microtubule-destabilizing factor in *Xenopus* egg extract by biochemical purification. *The Journal of cell biology*, 2003.161(2):349-358.

Spiller DG, Wood CD, Rand DA, White MR. Measurement of single-cell dynamics. *Nature*, 2010.465(7299):736-745.

Straube A, Brill M, Oakley BR, Horio T, Steinberg G. Microtubule organization requires cell cycle-dependent nucleation at dispersed cytoplasmic sites: polar and perinuclear microtubule organizing centers in the plant pathogen *Ustilago maydis*. *Molecular biology of the cell*, 2003.14(2): 642-657.

Stumpff J., Dassow von G., Wagenbach M., Asbury CL., Wordeman L. The kinesin-8 motor Kif18A suppresses kinetochore movements to control mitotic chromosome alignment. *Dev Cell*, 2008. 14:252-262.

Su LK., Burrell M., Hill DE., Gyuris J., Brent R., Wiltshire R., ... Kinzler KW. APC binds to the novel protein EB1. *Cancer research*, 1995.55(14):2972-2977.

Su LK. and Qi Y. Characterization of Human MAPRE Genes and Their Proteins. *Genomics*, 2001.71(2):142-149.

Sukoyan MA., Vatolin SY., Golubitsa AN., Zhelezova AI., Semenova LA., Serov OL. Embryonic stem cells derived from morulae, inner cell mass, and blastocysts of mink: comparisons of their pluripotencies. *Mol Reprod Dev*, 1993. 36(2): 148-58.

Tabata H. and Nakajima K. Efficient in utero gene transfer system to the developing mouse brain using electroporation: visualization of neuronal migration in the developing cortex. *Neuroscience*, 2001.103(4):865-872.

Thomas KR. and Capecchi MR. Site-directed mutagenesis by gene targeting in mouse embryo-derived stem cells. *Cell*, 1987. 51(3): 503-12.

Tirnauer JS., Canman JC., Salmon ED., Mitchison TJ. EB1 targets to kinetochores with attached, polymerizing microtubules. *Molecular biology of the cell*, 2002.13(12):4308-4316.

Tischfield MA., Baris HN., Wu C., Rudolph G., Van Maldergem L., He W., ... Engle EC. Human TUBB3 Mutations Perturb Microtubule Dynamics, Kinesin Interactions, and Axon Guidance. *Cell*, 2010. 140(1):74-87.

van Breugel M., Drechsel D., Hyman A. Stu2p, the budding yeast member of the conserved Dis1/XMAP215 family of microtubule-associated proteins is a plus end-binding microtubule destabilizer. *The Journal of cell biology*, 2003.161(2):359-369.

Varga V., Helenius J., Tanaka K., Hyman AA., Tanaka TU., Howard J. Yeast kinesin-8 depolymerizes microtubules in a length dependent manner. *Nat Cell Biol.*, 2006.8:957-962.

Varga V., Leduc C., Bormuth V., Diez S., Howard J. Kinesin-8 motors act cooperatively to mediate length-dependent microtubule depolymerization. *Cell*, 2009. 138:1174-1183.

Vasquez RJ., Gard DL., Cassimeris L. XMAP from *Xenopus* eggs promotes rapid plus end assembly of microtubules and rapid microtubule polymer turnover. *The Journal of cell biology*, 1994.127(4):985-993.

Vitre B., Coquelle FM., Heichette C., Garnier C., Chrétien D., Arnal I. EB1 regulates microtubule dynamics and tubulin sheet closure in vitro. *Nature cell biology*, 2008.10(4):415-421.

Von Dassow G., Verbrugghe KJ., Miller AL., Sider JR., Bement WM. Action at a distance during cytokinesis. *J. Cell Biol.*, 2009. 187:831–45.

Voter WA., O'Brien ET., Erickson HP. Dilution-induced disassembly of microtubules: Relation to dynamic instability and the GTP cap. *Cell motility and the cytoskeleton*, 1991. 18(1):55-62.

Walker RA., O'brien ET., Pryer NK., Soboeiro MF., Voter WA., Erickson HP., Salmon ED. Dynamic instability of individual microtubules analyzed by video light microscopy: rate constants and transition frequencies. *The Journal of cell biology*, 1988.107(4):1437-1448.

Wang PJ. and Huffaker, TC. Stu2p: A microtubule-binding protein that is an essential component of the yeast spindle pole body. *The Journal of cell biology*, 1997.139(5):1271-1280.

West RR., Malmstrom T., McIntosh JR. Kinesins klp5+ and klp6+ are required for normal chromosome movement in mitosis. *Journal of cell science*, 2002.115(5):931-940.

Wichterle H. and Peljito M. Differentiation of mouse ES cells to spinal motor neurons. *Current protocols in stem cell biology*, 2008. 1:1-9.

Wiggin GR., Fawcett JP., Pawson T. Polarity proteins in axon specification and synaptogenesis. *Dev. Cell.*, 2005. 8:803–816.

Williams RL., Hilton DJ., Pease S., Willson TA., Stewart CL., Gearing DP., Gough NM. Myeloid leukaemia inhibitory factor maintains the developmental potential of embryonic stem cells. *Nature*, 1988. 336(6200): 684-7.

Winey M., Mamay CL., O'Toole ET., Mastronarde DN., Giddings TH., McDonald KL., McIntosh JR. Three-dimensional ultrastructural analysis of the *Saccharomyces cerevisiae* mitotic spindle. *J Cell Biol.*, 1995. 129 (6):1601-15.

Wordeman L. Microtubule-depolymerizing kinesins. *Current opinion in cell biology*, 2005.17(1):82-88.

Zanic M., Widlund PO., Hyman AA., Howard J. Synergy between XMAP215 and EB1 increases microtubule growth rates to physiological levels. *Nature cell biology*, 2013.15(6):688-693.

Zhang Y., Buchholz F., Muyrers JP., and Stewart, AF. A new logic for DNA engineering using recombination in *Escherichia coli*. *Nature Genetics*, 1998.20(2): 123–128.

Zheng Y., Wong ML., Alberts B., Mitchison T. Nucleation of microtubule assembly by a gamma-tubulin-containing ring complex. *Nature*, 1995.378(6557):578-583.

## **Erklärung entsprechend §5.5 der Promotionsordnung**

Hiermit versichere ich, dass ich die vorliegende Arbeit ohne unzulässige Hilfe Dritter und ohne Benutzung anderer als der angegebenen Hilfsmittel angefertigt habe; die aus fremden Quellen direkt oder indirekt übernommenen Gedanken sind als solche kenntlich gemacht. Die Arbeit wurde bisher weder im Inland noch im Ausland in gleicher oder ähnlicher Form einer anderen Prüfungsbehörde vorgelegt.

Die Dissertation wurde im Zeitraum vom 13.09.2010 bis 30.09.2014 verfasst und von Prof. Dr. Jonathon Howard am Max Planck Institute für Molekulare Zellbiologie und Genetik betreut.

Meine Person betreffend erkläre ich hiermit, dass keine früheren erfolglosen Promotionsverfahren stattgefunden haben.

Ich erkenne die Promotionsordnung der Fakultät für Mathematik und Naturwissenschaften, Technische Universität Dresden an.

Ozlem Demir  
30.09.2014